

Nested Reconfigurable Modules
for Multi-robot System

DISSERTATION

Shunsuke Nansai

Department of Advanced Multidisciplinary Engineering
Graduate School of Advanced Science and Technology
Tokyo Denki University

Supervisors:

Professor, Masami Iwase, Tokyo Denki University
Professor, Mohan Rajesh Elara, Singapore University of Technology and Design

March, 2015

Table of Contents

1	Introduction	1
1.1	Previous and Related Studies	1
1.2	Purpose: Nested Reconfigurability	4
1.2.1	Theo Jansen Linkage Mechanism	8
1.3	Summary of the Contents	8
1.4	Contribution	14
2	A Reconfigurable Jansen Leg with Multiple Gait Patterns	16
2.1	Reconfigurable linkages and design	16
2.1.1	Walking machines and leg linkages	18
2.2	Position analysis of a Theo Jansen linkage	19
2.2.1	The bilateration matrix	20
2.2.2	Bilateration-based system of equations	22
2.2.3	Equations of velocity and acceleration	24
2.3	Beyond the standard Theo Jansen linkage: New gait patterns	25
2.3.1	Tracing the coupler curve of a Jansen leg	25
2.3.2	Finding the new gait patterns	27
2.4	Characterization of leg transformation	32
2.5	Implementation of a reconfigurable Jansen leg	34
2.5.1	Extendable links	37
2.5.2	Base system	37
2.6	Experimental results	39
2.6.1	Generation of gait patterns	39
2.6.2	Leg transformation	43
2.7	Conclusions	43

3	Speed Control of Jansen Linkage Mechanism for Exquisite Tasks	44
3.1	Trajectory Design for Constant Speed Control of Toes	44
3.2	Numerical Simulation	45
3.3	Application of Proposed Method	47
3.4	Conclusion	48
4	An Approach to Gait Synchronization and Transition for Reconfigurable Walking Platforms	49
4.1	Specification of the Reconfigurable Jansen Platform	49
4.2	Design of The Trajectory Generator	52
4.3	Synchronization	54
4.4	Static Stability Analysis of the Realized Gaits	56
4.5	Characterization of Gait Transition	58
4.5.1	Gait Transition I - <i>Static gait transition</i> -	58
4.5.2	Gait Transition II - <i>Dynamic gait transition</i> -	60
4.6	Stability Analysis of Gait Transition	61
4.7	Conclusion	65
5	Dynamic Modeling and Nonlinear Position Control of a Quadruped Robot with Theo Jansen Linkage Mechanisms	66
5.1	Free-Fall Model	66
5.1.1	Dynamic Model of Jansen Linkage Mechanism	67
5.1.2	Dynamic Model of Gear System	72
5.1.3	System Integration	76
5.2	Plant Model	78
5.2.1	Contact with the Ground	78
5.2.2	Collision with the Ground	80
5.3	Control System Design	80
5.3.1	Approximate Model	80
5.3.2	Transformation of Dynamic Model	81
5.3.3	Control System based on Energy Control	83
5.4	Numerical Simulations	85

5.5	Conclusion	89
6	Conclusion	91
6.1	A Reconfigurable Jansen Leg with Multiple Gait Patterns	92
6.2	Speed Control of Jansen Linkage Mechanism for Exquisite Tasks	93
6.3	An Approach to Gait Synchronization and Transition for Reconfigurable Walking Platforms	94
6.4	Dynamic Modeling and Nonlinear Position Control of a Quadruped Robot with Theo Jansen Linkage Mechanisms	94
	Reference	95

List of Tables

2.1	Identified foot trajectory patterns of interest for nested reconfiguration applications	29
2.2	Numerical analysis of experiment results	39
4.1	The identified novel gait patterns	50
4.2	The switching angles of support leg and idling leg	54
4.3	Initial states of each leg for the synchronization (\mathbf{n} : count of loop of PHASE, $\boldsymbol{\eta} = (\boldsymbol{\theta}_A - \boldsymbol{\theta}_B + 2\boldsymbol{\pi})/3$)	55
4.4	Results of the static stability analysis of the synchronization	57
4.5	The initial and final state of the idling leg in the Transformation in Walking. ($f(\boldsymbol{\theta}, \boldsymbol{l})$: Length of $\overline{P_1P_8}$)	61
4.6	Results of the static stability analysis of the gait transition II - <i>Dynamic gait transition</i> -	64
5.1	Physical parameters of the Theo Jansen linkage mechanism. ($\zeta, \xi = 1, \dots, 8$)	68
5.2	Kinematic parameters of the Theo Jansen linkage mechanism	69
5.3	The lengths of links adopted for the Theo Jansen linkage mechanism of this study	69
5.4	Physical parameters of the gear system.	73

List of Figures

1.1	Conceptual depiction of intra-reconfigurability	2
1.2	Conceptual depiction of inter-reconfigurability	3
1.3	Concept of nested reconfigurability	5
1.4	Prototype of a reconfigurable Jansen leg that extends the capabilities of the original design, while maintaining its mechanical simplicity during normal operation. This linkage, that switches from a pin-jointed Grübler kinematic chain to a five degree-of-freedom mechanism with slider joints in the reconfiguration process, not only produces different useful gait patterns but also generates behaviors beyond locomotion.	11
1.5	Legged robots based on one degree-of-freedom reconfigurable planar leg mechanisms may operate in environments and tasks of high complexity while maintaining simple control schemes. This four-legged robot is based on reconfigurable Jansen legs capable of generating up to six different gait cycles.	13
2.1	The Jansen leg, a one degree-of-freedom planar linkage of eight links, seven revolute joints —one of them involving there binary links, and three independent loops.	21
2.2	The bilateration problem.	22
2.3	Top: Possible locations of point P_8 , the foot, in all assembly modes of a standard Jansen leg. The lowest sampled curve corresponds to the trajectory used in walking platforms. Bottom: Traced foot trajectory of a standard Jansen leg. The green path corresponds to the assembly mode family given by $A_{1,2,3} > 0$, $A_{1,3,4} > 0$, $A_{1,3,6} < 0$, and $A_{6,5,7} < 0$. In the red path, $A_{1,2,3} < 0$, $A_{1,3,4} > 0$, $A_{1,3,6} < 0$, and $A_{6,5,7} < 0$	26

2.4	Transformation from digitigrade locomotion ($d_{5,7} : +20\%$) to step climbing ($d_{3,6} : +16\%$). Left: Some steps of a simulation of the leg transformation, the binary links of variable dimension and the vertical movement of the grounded revolute joint centers are highlighted in cyan and light green. The corresponding foot trajectories are also depicted —digitigrade locomotion in black and step climbing in blue. Right-top: The lowest values of $P_{8,y}$ for each of the foot trajectories in the transformation are connected by an arrow. These values are used to determine the initial and final input angles, θ_A and θ_B respectively, in the transformation process. Right-bottom: The evolution of $P_{1,y}$ from $t = t_o$ to $t = t_f$	31
2.5	Flowchart of the proposed method for leg transformation (see text for details).	35
2.6	A fully-functional reconfigurable Jansen leg with four linear actuators suitable for the transformation procedure presented in section 2.4(link combinations presented in column “single link” of Table 2.1) (center). Zoomed areas present the base system (center-right) and links of variable dimension —extendable links (center-left). Details of these designs can be observed in the corresponding exploded views —base system (bottom) and extendable links (top).	36
2.7	Prototypes of the base system (right) and extendable links (left).	38
2.8	Comparison between the simulated leg trajectory (in gray) and the average experimental trajectory (in red) obtained after ten cycles of the input joint (curves depicted in black) for the gait patterns plantigrade locomotion (standard trajectory of a Jansen leg), digitigrade locomotion, obstacle avoidance, step climbing, and drilling motion.	40
2.9	Comparison between the simulated speed at the foot point (in black) — <i>i. e.</i> , magnitude (Euclidean norm) of equation (2.14)— and the average experimental speed (in red) computed from the average experimental trajectory (Fig. 2.8) for the gait patterns plantigrade locomotion (standard trajectory of a Jansen leg), digitigrade locomotion, obstacle avoidance, step climbing, and drilling motion.	41

2.10	Experimental transformation process from plantigrade locomotion to step climbing ($d_{5,7} : +20\%$). Top: Snapshots of the experiment. A green marker, circled by a red line, located in the foot point is tracked. The green and red trajectories represent the plantigrade locomotion pattern and the step climbing pattern, respectively. The white line represents an estimated ground, it is computed because the prototype is tilted due to an inclination in the base system. The small red circle represents the origin of the reference frame. Bottom-left: Zoomed view of the tracked trajectories. Bottom-right: Rotated experimental leg trajectories in which the ground line is parallel to the x-axis of the reference frame. The resulting curve during the transformation process is shown in blue.	42
3.1	The time variation of the angle of the driving link.	46
3.2	The time variation of the angular velocity of the driving link.	46
3.3	The time variation of the norm of the velocity vector of the toe.	46
3.4	The trajectory of the norm of the velocity vector of the toe.	47
4.1	Walking patterns in quadruped robots	52
4.2	The switching angles of support leg and idling leg. The red and green curves represent the sections of the support leg and idling leg, respectively.	54
4.3	The simulation result of the synchronization for the stable walking (left). Red leg : Left-Fore leg. Green leg : Left-Back. Blue leg : Right-Fore. Purple leg : Right-Back. The generated trajectories for the driving link (right-top). The gait pattern of “Obstacle avoidance” (right-bottom).	56
4.4	The transformation from “Obstacle avoidance” to “Jam avoidance” by Static Transformation. Top: Some steps of the transformation. The binary links of variable dimension are highlighted in orange-red and dark-blue. Bottom: The generated trajectories for the driving link.	59

4.5	The transformation from “Obstacle avoidance” to “Jam avoidance” by Transformation in Walking. Left: Some steps of the transformation. The binary links of variable dimension are highlighted in orange-red and dark-blue. Right-Top: The generated trajectories for the driving link. Right-Bottom: The foot trajectory of leg “Left-Fore”. The green and red line represents the trajectory of the idling leg and the support leg, respectively. The blue line represents the foot trajectory under the transformation. . . .	61
4.6	The variety of the supporting leg polygon of the quadruped robot. The gray area represents the static stability zone.	62
4.7	The positional relationship between a line on the 2 legs in opposing corner and the COG which is relevant to the static stability. If the COG exists in side of the support leg than the line, the robot is static stable.	62
4.8	The variety of combination of the gait pattern. “A” within circle and “B” within square represents a gait pattern A and a gait pattern B, respectively.	63
5.1	Schematic diagram of the quadruped robot composed of four Jansen linkage mechanisms and five gears which is driven by only one input to the bright yellow gear. The red, sky blue, green, and purple represent Left-Fore, Right-Fore, Left-Back, and Right-Back respectively.	67
5.2	Schematic diagram of the Theo Jansen linkage mechanism with all parameters defined. The solid lines $l_{ij1}, l_{ij2}, l_{ij3}, l_{ij5}, l_{ij6}, l_{ij7}$ are the links; the two blue triangular parts are treated as the mass components; the dashed lines connect the gravity center of the mass and the corners of the triangle parts.	68
5.3	Schematic diagram of the gear system with parameters defined. The black-margined gear represents the driving gear, and the other gears represent the driven gears.	74
5.4	Time evolutions of x -coordinate (top) and y -coordinate (middle) of the robot’s toes, and the trajectory of the feet (bottom).	86
5.5	Time evolution of the angles of the driving gear (top) and driven gears (bottom).	87
5.6	Trajectory of robot’s position.	87

5.7	Time evolution of x-coordinate of the robot.	87
5.8	Time evolutions of the kinetic energy E_k and the potential energy E_p . . .	88
5.9	Time evolutions of the values of the Lyapunov's function V and its differential \dot{V}	88
5.10	Time evolution of the input torque u	88
5.11	The snapshots of walking towards the target position based on the energy-based position control.	89

1 . Introduction

A robot is capable of autonomous mobile, and by changing its morphologies in response to various environments/tasks it is expected to work on fixed environment/task such as production line and building maintenance system as well as highly uncertain situation such as rescues and planetary explorations. A reconfigurable robot is a representative example of a robot which is able to work well in such situation, and can maximize adaptability of a system via wide variety of morphology changing in response to the environments/tasks. From such reasons, the reconfigurable robot has been studied since 1970s. In these studies, categories of reconfigurability research in robotics are divided into two broad classes: Intra-reconfigurability and Inter-reconfigurability.

1.1 Previous and Related Studies

Intra-reconfigurable robot is while itself is independent robot, and is capable of changing their own morphologies involving mechanical parts, actuators and sensor morphologies as well as power and controller. Intra-reconfigurability has been studied generally around mobility, adaptability, sensors and computing. Intra-reconfigurability for mobility improves the flexibility of traversing over variety of terrains and spaces such as land, air and water. For example, a robot might transform into a wheeled type on the plane, or into a sphere type on the slope. Thus, intra-reconfigurability provides highly adaptability in response to local environments/tasks through morphology changing. Fig. 1.1 depicts the concept of intra-reconfigurability.

[1] has proposed a reconfigurable platform based on OPEN-R. The proposed platform has been capable of reconfiguring from legged type into wheeled type easily. [2] has developed AZIMUT which is a mobile robotic platform combining wheels and legs. [3] has developed a versatile amphibious robot based on an eccentric paddle mechanism (ePad-

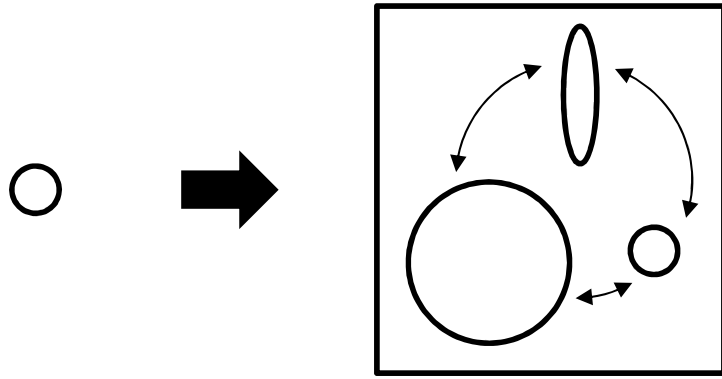


Fig. – 1.1 Conceptual depiction of intra-reconfigurability

dle). And, the ePaddle concept by gait sequence and five kind of gait patterns have been proposed. [4] has proposed an ankle rehabilitation robot allowing desirable ankle/leg motion, and being capable of reconfiguring from motion (ROM)/strengthening exercise device into balance/proprioception exercise device. [5] has developed a Black Ghost Knife Fish robot with wiggly fins. And by a reconfiguration approach, a new evolution for fin/body of a underwater robot has been derived. [6] has developed a wheeled reconfigurable mobile robot. [7] with a focus on planetary surface vehicles, has presented a methodology for determining optimal design of reconfigurable system. [7] has also proposed metrics for assessing the impact of reconfigurability.

From above literatures, intra-reconfigurability can provide highly adaptability in response to several limited environment/task, but the adaptability corresponding to unknown environments/tasks is always finite.

Inter-reconfigurable robot organizes more complex morphology system through assembly, disassembly and organized cooperation motion between homogeneous/heterogeneous intelligent modules. Inter-reconfigurability consists of optimization of module/software configuration and communication path, task planning and reciprocal recognition, and by utilizing these it is capable of realizing specialized robot corresponding to a variety of environment, task and situation. Thus, inter-reconfigurability provides highly redundancy corresponding to the module configuration and failures, also provides highly flexibility according to the environments and the tasks. Fig. 1.2 depicts the concept of inter-reconfigurable robot.

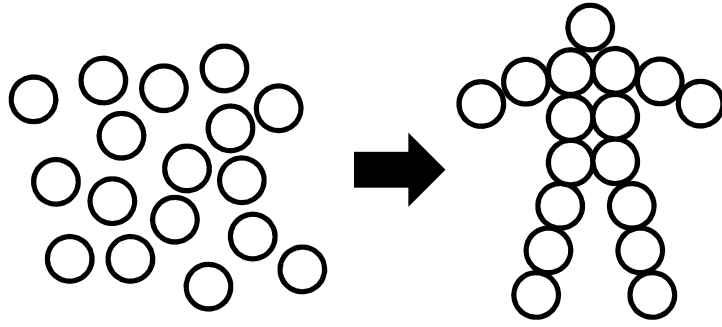


Fig. – 1.2 Conceptual depiction of inter-reconfigurability

[8] has demonstrated PolyBot which is one of the modular reconfigurable robot. The module of the PolyBot consists of a joint with 1-DOF and two docking parts, and the PolyBot has realized a snake-like robot and a roop-shape robot through assembly of some modules. [9] has introduced a programmable Inter-Reconfigurable robot, and has demonstrated how the robot can self-organize into a global structure by executing a common graph grammar. Also this study has presented a challenge to the grammatical method. [10] has presented SuperBot, a deployable multifunctional Inter-Reconfigurable robotic system. And, 6 types of prototype modules have been built and have demonstrated that SuperBot is flexible and powerful system via preliminary experiments. [11] has presented a programmable modular robotic system named Miche by using self- disassembly approach. Each module has been allowed to connect and communicate with its immediate neighbors. This study has demonstrated their hypothesis that making shapes by disassembly is robust. [12] has presented Inter-Reconfigurable robot named swarm-bot which is composed by autonomous mobile robot s-bot, and has discussed the self-assembling capabilities of the robot. S-bots can either act independently or self-assemble into a swarm-bot by using their grippers. This study has demonstrated self-assembly with s-bots.

From above literatures, inter-reconfigurability provides highly redundancy and flexibility corresponding to unknown environments/tasks by configuring a new morphologies through assembly, disassembly and organizing of some individual modules, but has a disadvantage that it is difficult to possess optimal mechanisms corresponding to limited environments/tasks.

1.2 Purpose: Nested Reconfigurability

This study aims to formulate a concept of nested reconfiguration which possesses both intra- and inter- reconfiguration, and to develop a robot capable of achieving wide-ranging tasks in highly uncertain environments through providing the nested reconfiguration. Nested reconfigurable robot consists of modular robots capable of changing their morphologies individually and assembly/disassembly/organizing system to configure a optimal morphology in response to the given environments/tasks. Also, it has advantages of both intra- and inter-reconfigurable robot, and provides higher adaptability and flexibility corresponding to the given environments/tasks.

Fig. 1.3 depicts the concept of nested reconfigurability. From Fig. 1.3, characteristics of nested reconfigurability are to configure new reconfigurable morphology by changing morphology of an individual reconfigurable robot (intra-reconfiguration), and assembling/disassembling the individual reconfigurable robots (inter-reconfiguration). Thus, by providing a new reconfigurability via reconfiguration of other reconfigurability, that is, by nesting the reconfigurability, the resilience and flexibility of the system can be maximized in various environments/tasks.

Individual modules must possess own controller, sensors, actuators, power, and docking system for nested reconfigurable robot to involve both intra- and inter-reconfigurability. A number of issues have to be addressed to implement nested reconfigurable robot. These issues falls into two broad issues: hardware issues and software issues. The hardware issues involve following topics:

- Development of intra-reconfigurable modular robot capable of maintaining component assembly while changing its morphology.
- Development of docking system for homogeneous/heterogeneous intra-reconfigurable modules.
- Development of mechanisms capable of sensory reconfiguration and sharing.
- Optimization of the torque-power-size tradeoff of the actuators.
- Development of energy efficiency systems and mechanisms for energy sharing.

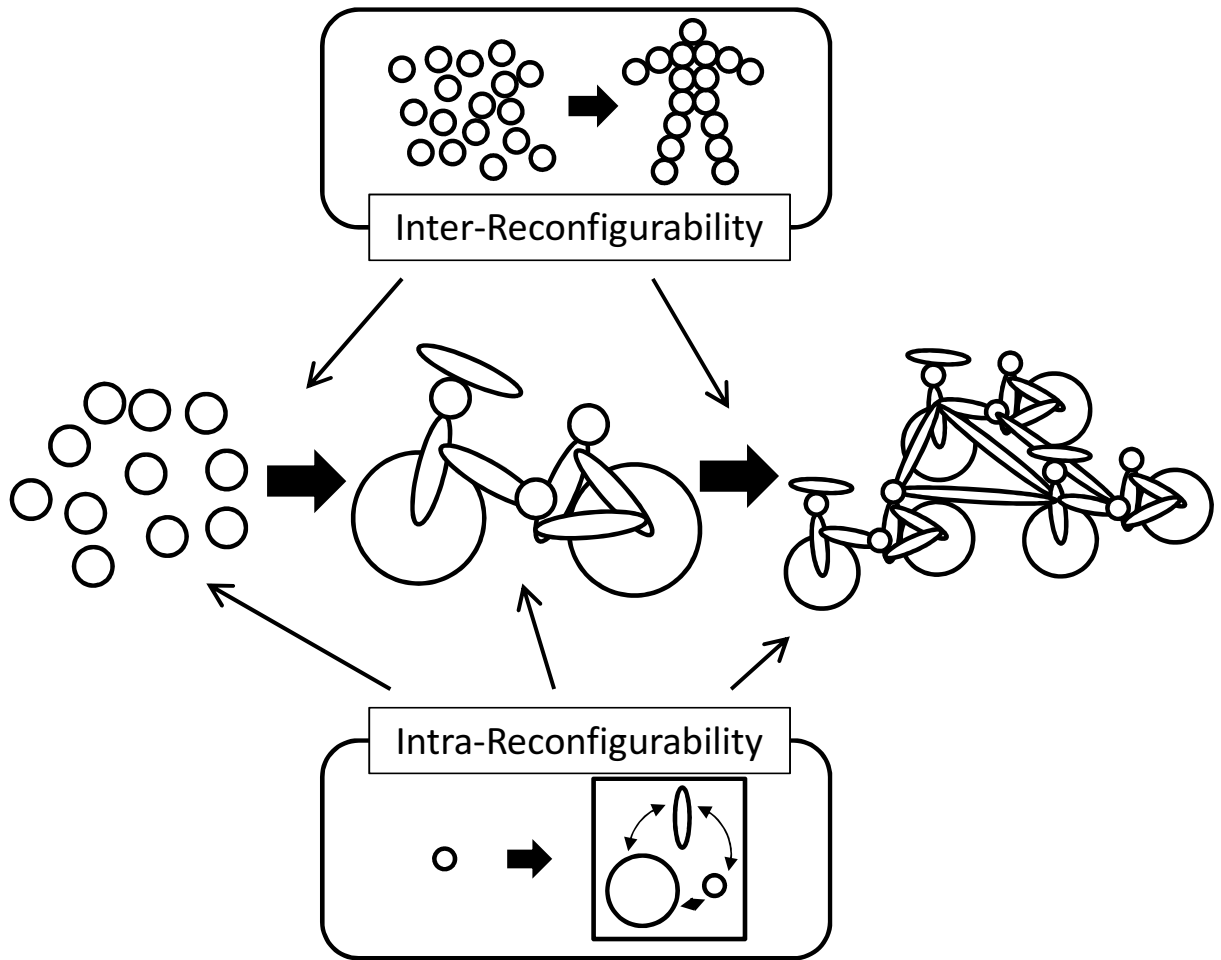


Fig. – 1.3 Concept of nested reconfigurability

The software issues involve following topics:

- Establishment of an algorithm optimizing intra- and inter-reconfiguration in response to the environments/tasks/failures.
- Establishment of an assembly/disassembly algorithm realizing both inter- and intra-reconfiguration.
- Formulation of communication framework for messaging both within individual component robotic module as well as between robotic modules.
- Design of control system for both individual component robotic modules as well as between robotic modules.
- Optimization of computational and energy loads through energy and sensory shar-

ing.

These issues have been addressed for either intra- or inter-reconfigurability, but there are no studies for nested reconfigurability. This study supposes a multi-legged robot which is required highly adaptability and flexibility in response to a various environments/tasks as a pioneer of nested reconfigurability.

Legged robots have always been a preferred choice for a variety of applications like search and rescue given their versatile and rugged locomotion capabilities. The choice of legged mechanisms often responds to design requirements such as the ability to move through irregular terrains or to increase stability, maneuverability or energy efficiency. However, any valid gait reconfiguration –*i.e.*, a useful change of walking pattern– in these legged robots poses numerous opportunities as well as research challenges. Legged animals coordinate a wide range of components and systems to walk adaptively and efficiently under a variety of speeds, terrains and task goals including chasing, courtship and stealth.

The robotics literature shows a variety of design strategies to generate different gait patterns in legged robots, including, to name a few: structural combination of rigid and tensile structural elements [13], morphological computation [14], oscillator controller with pneumatic actuators [15] and biomimetic adaptations based on ground contact timing [16] or using sensorimotor coordination [17]. Alternatively, walking platforms based on one degree-of-freedom reconfigurable planar leg mechanisms, that are capable of generating multiple useful gaits, while maintaining simple control schemes can also be proposed. For example, in [18], a reconfigurable Jansen leg that varies its hardware morphology to produce a wide set of novel gaits by parametric changes of its components and sub-assemblies was discussed. To ensure safe locomotion across a difficult terrain, a robot must be able to stably switch between gaits either at rest or in motion. Literature points a number of efforts to this end, [19] proposes an approach based on acyclic feed forward motion patterns that allow a robot to switch from one gait to another. [20] applies nonlinear oscillators to model Central Pattern Generators (CPGs) that is able to initiate/stop locomotion; generate different gaits, and to easily select and switch between the different gaits according to the speed and/or the behavioral context. [21] attempts to induce a quadruped robot to walk and switch gaits dynamically on irregular terrain and run on flat terrain by using a nervous system model.

In addition to this, many studies about the multi-legged robot are exist. Sebastian et al. [22] presented their efforts in developing a six legged, bio-inspired, and energy efficient robot (SpaceClimber 1) for extraterrestrial surface exploration, particularly for mobility in lunar craters. Estremera et al. [23] elaborated the development of crab and turning gaits for a hexapod robot, SILO-6, on a natural terrain containing uneven ground and forbidden zones as well as an application to humanitarian demining. Moro et al. [24] proposed an approach to directly map a range of gaits of a horse to a quadruped robot with an intention of generating a more life-like locomotion cycle. This work also presented the use of kinematic motion primitives in generating valid and stable walking, trotting, and galloping gaits that were tested on a compliant quadruped robot. In these works, the robots developed were generally effective in mimicking the gait cycles of their biological counterparts, but they suffered from high payload-to-machine-load ratio and high energy consumption.

Several approaches were studied in developing energy efficient walking machines. [25] presented a set of rules towards improving energy efficiency in statically stable walking robots by comparing two legged, namely mammal and insect, configurations on a hexapod robotic platform. [26] applied minimization criteria for optimizing energy consumption in a hexapod robot over every half a locomotion cycle, especially while walking on uneven terrains. [27] put forward two different approaches to determine optimal feet forces and joint torques for six legged robots towards minimizing energy consumption. Even though many literatures have contributed for the multi-legged robot, still it has been providing a number of challenges to researchers. And, since these multi-legged robots install some actuators on each leg, and realize the locomotion by controlling these motions, the control system must always involve complexity.

On the other hand, since nested reconfigurable robot developed in this study possesses a intra-reconfigurable legged module, and this intra-reconfigurable legged module builds basic systems of nested reconfigurable system, it is required to be able to drive with simple motion. That is, since the developed intra-reconfigurable module is required to be able to be driven with the lowest possible actuator, the complexity for walking should be involved into mechanical system.

1.2.1 Theo Jansen Linkage Mechanism

As such mechanism, Theo Jansen, a Dutch kinetic artist, has invented the Jansen linkage mechanism [28]. The Jansen linkage mechanism is a linkage mechanism which is capable the walking locomotion by 1 DOF, and can drive by 1 DOF even if some legs are coupled. Some literatures have reported about the Jansen linkage mechanism. Giesbrecht et al. have shown analysis of the kinematics of the Jansen linkage mechanism [29], derivation of the dynamics [30], optimization of the driving torque [31], and optimization of link lengths for a gait pattern [32]. Moldvan et al. have proposed a new type walking robot design with the Jansen linkage mechanism [33], and have shown analysis of the kinematics utilizing CAD [34], optimal design of the new type robot [35], derivation of forward kinematic equation [36], and gait synthesis utilizing Freudestein method [37].

However, since the Jansen linkage mechanism is one of closed linkage, it have only one gait pattern. Thus, it have a disadvantage that it is the low adaptability for environments. For such problem, Komoda et al. have realized gait patterns for climbing and stepping by adding cyclic motions or up-down motions at the center joint to the normal motion of the driving link [38,39]. This method is valid for climbing a single step, but for example, in case of which new gaits are needed for terrains such as mud, the additional motions have to be continued.

This study proposes a reconfigurable Jansen linkage mechanism as the intra-reconfigurable module robot. The reconfigurable Jansen linkage mechanism is the Jansen linkage mechanism which have actuators at links and which is capable to depict various gait patterns by changing the link length utilizing one of the features of the closed link mechanism in which different gait patterns can be depicted according to the link length combination. The reconfigurable Jansen linkage mechanism is utilized as the intra-reconfigurable module robot possessing both reconfigurable mechanism and docking mechanism. And, legged nested reconfigurable robot is realized by assembling these.

1.3 Summary of the Contents

In particular, firstly, development of the reconfigurable Jansen linkage mechanism is reported as intra-reconfigurable module. Also, a useful application case of a control

method of the developed reconfigurable Jansen linkage mechanism is proposed. And, it is shown that the most basic nested reconfigurable robot can be implemented by assembling these. In addition, a control system of a walking robot with Jansen linkage mechanism capable of driving with 1-DOF is designed. In development of reconfigurable Jansen linkage mechanism, firstly, forward kinematics of Jansen linkage mechanism is derived, and some interesting gait patterns are explored. Secondly, a gait transition method of the explored gait patterns is proposed, and repeatability and possibility of both the gait patterns and the gait transition method are demonstrated through experiments. As an application case of control method of reconfigurable Jansen linkage mechanism, constant speed control of the toe is proposed by utilizing the derived forward kinematics. A relation between the toe speed and the driving link speed is formulated by utilizing the derived forward kinematics, and by utilizing it, the angle variation of the driving link realizing the constant speed of the toe is derived. And, it is verified that the constant speed locomotion of the toe can be realized by the derived angle variation via a numerical simulation.

In development of the multi-legged nested reconfigurable robot, the multi-legged robot assembling the developed reconfigurable Jansen linkage mechanisms is developed. And, synchronization realizing the walking which is most basic locomotion strategy for the multi-legged robot is presented. Also, two types of gait transition methods for the explored gait patterns are presented, furthermore, it is verified that the walking and the gait transitions with stable are realized by the presented synchronization and gait transition methods via numerical simulations. In design of the control system of a walking robot with Jansen linkage mechanism capable of driving with 1-DOF, the position control system of the multi-legged nested reconfigurable robot with Jansen linkage mechanism capable of driving with 1-DOF which is supposed to be designed in our future work is designed based on the energy control. Also, it is verified that the position can be controlled by the designed control system.

This study is organized from six chapters: Chapter 2 shows both the development of the reconfigurable Jansen linkage mechanism as the intra-reconfigurable module, and its effectiveness through experiments. Chapter 3 reports the speed control of the toe of the Jansen linkage mechanism. The synchronization and the gait transition methods for the multi-legged nested reconfigurable robot are shown in Chapter 4. In Chapter 5, the

position control system for the more developed multi-legged robot with the Jansen linkage mechanism is designed. Chapter 6 concludes this study.

Chapter 2: A Reconfigurable Jansen Leg with Multiple Gait Patterns

Chapter 2 reports a reconfigurable approach to robotic legged locomotion that produces a wide variety of gait curves, opening new possibilities for innovative applications. The main departure from the state of the art in this area is that large solution spaces are generated using a one degree-of-freedom planar linkage, producing gait variance via parametric changes of link lengths. Our ultimate aim is to build robots that can entirely redesign their morphologies according to changes in the environment and to reflect their learning of new abilities. Chapter 2 represents an initial step towards robots that self-design themselves. We envision robots equipped with reconfigurable legs to generate a large number of locomotion capabilities during their deployment. Alternatively, for tasks that require single-purpose mechanisms, our approach can be used as a design approach to explore and select optimal yet feasible configurations that can be used to build specialized walking robots.

In particular, a novel reconfigurable Theo Jansen linkage that produces a wide variety of gait cycles is reported (Fig. 1.4). The standard Theo Jansen linkage is a popular closed kinematic chain suitable for developing legged robots, such pin-jointed planar linkage operates with only one actuator —*i.e.*, it is a Grübler kinematic chain. The proposed design extends the capabilities of the original mechanism, while maintaining its mechanical simplicity during normal operation, generating different useful gait patterns and behaviors beyond locomotion.

The main challenges in designing a reconfigurable version of a Theo Jansen linkage include the development of efficient approaches to trace foot trajectories —*i.e.* coupler curves, the definition of the novelty and utility of the resulting foot trajectories, the development of heuristics to guide the reconfiguration process, and the non-trivial process of implementing theoretical designs generated analytically into physical mechanisms. All these aspects are handled in Chapter 2, concluding with experimental results using a prototype fabricated with a minimum amount of off-the-shelf parts. The reconfigurable Theo Jansen linkage herein presented is an initial design and implementation of a four-legged robot for testing different reconfiguration scenarios and control strategies for limb

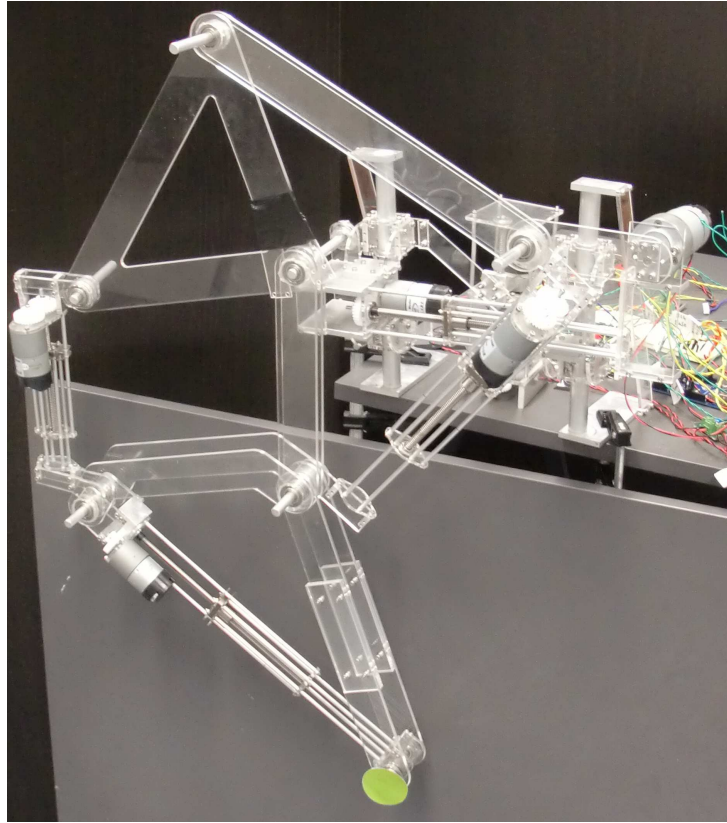


Fig. – 1.4 Prototype of a reconfigurable Jansen leg that extends the capabilities of the original design, while maintaining its mechanical simplicity during normal operation. This linkage, that switches from a pin-jointed Grübler kinematic chain to a five degree-of-freedom mechanism with slider joints in the reconfiguration process, not only produces different useful gait patterns but also generates behaviors beyond locomotion.

specialization and graceful degradation.

Chapter 3: Speed Control of Jansen Linkage Mechanism for Exquisite Tasks

Chapter 3 generates the angle trajectory of the driving link capable of the constant speed control of the toe of the Jansen linkage mechanism. In order to achieve it, the forward kinematics of the Jansen linkage mechanism which boils down to the problem of the Bilateralon is analyzed. In fact, it is proven that the norm of the toe speed bears a proportionate relationship to the angular velocity of the driving link. And, the angle trajectory of the driving link capable of the constant speed control of the toe of the Jansen linkage mechanism is generated by utilizing the relationship. It is verified that the constant speed control of the toe of the Jansen linkage mechanism is realized by the generated trajectory via a numerical simulation.

Chapter 3 is presented as one of useful application case of the control methods for the Jansen linkage mechanism. By applying this method, the speed of either the horizontal or the vertical direction can be controlled as well as the norm of the toe speed. For example, in the case of the multi-legged robot with the Jansen linkage mechanisms, since the feeding speeds of the toes can be controlled arbitrarily, we can take an advantage that it is become easy to consider the stability of the robot. Also, it seems that the method is useful for the robot design as well. Because, the robot capable of maintaining a constant toe speeds can be designed by designing non-circular gears based on the derived relational expression. By taking such design, all toe speed is maintained constant even if the robot is designed with 1-DOF.

Chapter 4: An Approach to Gait Synchronization and Transition for Reconfigurable Walking Platforms

In Chapter 4, we present a method for the generation of input joint trajectories to properly synchronize the movement of quadruped robots with reconfigurable legs. The approach is exemplified in a four-legged robot with reconfigurable Jansen legs capable of generating up to six useful different gait cycles. The proposed technique is validated through simulated results that show the platform's stability across its six feasible walking patterns and during gait transition phases, thus considerably extending the capabilities of the non-reconfigurable design.

A fundamental problem of the gait reconfiguration solutions based on reconfigurable

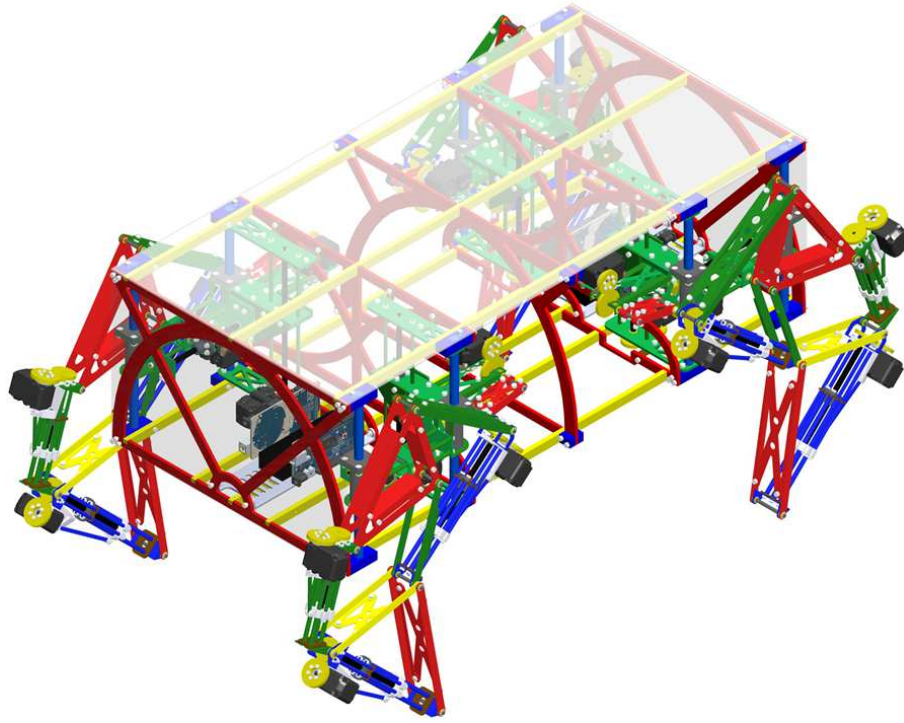


Fig. – 1.5 Legged robots based on one degree-of-freedom reconfigurable planar leg mechanisms may operate in environments and tasks of high complexity while maintaining simple control schemes. This four-legged robot is based on reconfigurable Jansen legs capable of generating up to six different gait cycles.

legged robots is to reach stability both in motion and rest, as well as while transforming from one configuration to another with the minimum number of legs, while the complete range of walking patterns is available. In Chapter 4, we discuss a method for the proper generation of input joint trajectories to synchronize the different gait cycles and gait transitions of quadruped robots with one degree-of-freedom reconfigurable legs. In order to exemplify our approach, we focus on a four-legged robot with reconfigurable Jansen legs (Fig. 1.5). Theoretically, such walking platform is capable of generating up to six useful different walking patterns, resulting from the different gait cycles of a reconfigurable Jansen leg. It will be shown how, by using the proposed technique, all these feasible patterns can be successfully attained. In this way, the capabilities of a quadruped robot based on standard non-reconfigurable Jansen legs are considerably extended.

Chapter 5: Dynamic Modeling and Nonlinear Position Control of a Quadruped Robot with Theo Jansen Linkage Mechanisms

In Chapter 5, we perform dynamic modeling and analysis on a four-legged robot composed of the Theo Jansen mechanisms which is never done in the literature. The projection method is applied to derive the dynamic model because of its powerfulness in modeling such complicated system. Then a position control strategy is proposed based on energy control. Finally, numerical simulations validate the efficacy of the designed controller.

Lagrange's method [40–42] is famous for deriving dynamic models. However, sometimes it is very difficult to build the dynamic model of a linkage mechanism, such as the Theo Jansen linkage, by using Lagrange's method because the forward kinematics of the system is very complicated. In Chapter 5, the projection method [43–45] is applied to derive the complete dynamic model of a four-legged robot composed of the Theo Jansen mechanisms. In comparison with the conventional approaches, Lagrange's, Gibbs-Appel, and Kane's for example, projection method has been observed to be more intuitive in nature and compact [43, 44, 46]. By using this method, the complicated linkage mechanism can be assumed as a simple holonomic system and the model is derived by focusing on constraints of the system as well as the holonomic system [46]. The dynamic model of the whole system can be derived by separating the system into a few sub-systems and then integrating the dynamic models of these sub-systems [47]. Considering these advantages, the projection method is chosen to build the dynamic model for the four-legged robot.

Chapter 6: Conclusion

Chapter 6 concludes this study. This study involving the purpose of this study and the research contents in each Chapter is summarized. The results of each Chapter are discussed, and it is verified that the purpose of this study is achieved.

1.4 Contribution

This study aims to formulate the concept of nested reconfiguration which possesses both intra- and inter- reconfiguration, and to develop the robot capable of achieving wide-ranging tasks in highly uncertain environments through providing the nested reconfiguration, and has studied following research topics: development of intra-reconfigurable

module robot possessing both the reconfigurable mechanisms and docking system, speed control of toe of the Jansen linkage mechanism, development of the multi-legged nested reconfigurable robot, and the position control of the multi-legged robot with the Jansen linkage mechanisms.

Through these studies, the concept of nested reconfiguration which possesses both intra- and inter-reconfiguration has been formulated. And application of nested reconfigurability and its design and control strategy have been proposed.

2 . A Reconfigurable Jansen Leg with Multiple Gait Patterns

Legged robots are able to move across irregular terrains and those based on one degree-of-freedom planar linkages can be energy efficient, but are often constrained by a limited range of gaits which can limit their locomotion capabilities considerably. This chapter reports the design of a novel reconfigurable Theo Jansen linkage that produces a wide variety of gait cycles, opening new possibilities for innovative applications. The suggested mechanism switches from a pin-jointed Grübler kinematic chain to a five degree-of-freedom mechanism with slider joints during the reconfiguration process. It is shown that such reconfigurable linkage significantly extend the capabilities of the original design, while maintaining its mechanical simplicity during normal operation, to not only produce different useful gait patterns but also to realize behaviors beyond locomotion. Experiments with an implemented prototype are presented and their results validate the proposed approach.

2.1 Reconfigurable linkages and design

A linkage can be modeled in general as a system of geometrical constraints, that is, a group of geometrical elements —*e.g.*, points, lines, circles, polygons— subject to geometrical measures —*e.g.*, angles, lengths, areas, volumes— and geometrical relations —*e.g.*, ratios, congruences, tangencies, contacts. In the design and mechanics of this kind of mechanisms, such system of geometrical constraints has been historically considered as invariable. However, given the advances in the last century in, principally, the analysis and synthesis of mechanisms, the computer-aided design (CAD) systems, and the techniques for rapid prototyping, researchers and inventors have started to conceive and study

linkages whose geometrical elements, measures, and/or relations can vary in some state of their operation. These kinematic chains are called reconfigurable linkages, a current main trend in mechanisms and machine science as evidenced by the multiple references that can be found in the literature since the mid-1990s —see, for instance, [48–50] and the references therein.

Reconfigurable linkages are a clear example of transformers, that is, products that transform into different systems or according to different states. In [51], following a combined inductive and deductive approach, principles and facilitators for innovation in design through transformation are proposed. A transformation principle constitutes a guideline that by itself creates a change. A transformation facilitator is defined as a design construct that helps or aids in generating mechanical modifications but whose implementation does not create transformation singly. A total of three transformation principles are suggested, namely, expand/collapse, expose/cover, and fuse/divide. Respect to the transformation facilitators, twenty are discussed; they include ideas such as, just to name some, common core structure, composite, function sharing, and inflate. The reconfigurable Theo Jansen linkage proposed in this work is based on the expand/collapse principle and uses the concept of telescope —manipulate an object along an axis to create an elongation, planar spread, or enclosure to alter its function— as facilitator; a basic approach through which the original design becomes versatile.

Linkage design has been historically considered as a synonym of kinematic synthesis or the problem of finding a suitable linkage —type, number of links, and dimensions— for a given movement or task. Kinematic synthesis is normally divided into three categories, namely, motion generation —also called rigid body guidance, function generation, and point-path generation [52, 53]. In motion generation, some locations (position and orientation) that represent the desired movement are known. In function generation, the goal is to coordinate an output crank rotation (or slide) with a specific input crank rotation (or slide). Finally, in point-path generation, the available information is similar to that of motion generation but in this case the orientation constraints correspond to don't-care conditions. Solutions approaches to these problems (in general, solutions to special instances) have been proposed by many researchers during the last two centuries; methods based on geometry [54, 55], numerical continuation [56, 57], optimization

techniques [58, 53, 59], resultant elimination tools [60], between others, have been proposed. An interesting historical review with references to classical works can be found in [61, Chapter 1]. For current trends and open problems in the field, the interested reader is addressed to [62].

Our work departs from the classical conception of linkage design as kinematic synthesis. This method was introduced by the German geometer Ludwig Burmester in the late 19th century. Burmester is in fact considered as the father of theoretical kinematics of mechanisms —the branch that studies the geometry of motion in general mechanisms [63]. He was probably the pioneer in the study of complex compound mechanisms [54], that is, kinematic chains with more than two independent loops in which at least one geometrical element is connected through kinematic pairs to more than two others [64]. In our reconfigurable linkage design approach, the objective is not to find the best linkage to accomplish a specific motion as in kinematic synthesis but to determine whether through simple changes in the topology or geometry of a given linkage, useful coupler curves or workspaces that improve the performance of the original design in specific cases, or completely modify its task, can be obtained. The mechanical implementation (practical engineering solution) of such transformations between discrete positions of the design space is a fundamental aspect of this methodology.

2.1.1 Walking machines and leg linkages

Since the beginning of the land transportation technology, numerous walking machines have been conceived and designed as an alternative to wheel vehicles because of their potential advantages in rough terrain. These benefits include, for example, higher speed, better fuel economy, greater mobility, better isolation from terrain irregularities, and less environmental damage [65]. A complete survey of the walking machines developed in the last decades can be found in [66]; where it is shown that different kinds of leg mechanisms have been proposed, systems that span from open planar kinematic chains to parallel architectures. In this work, we propose a reconfigurable leg mechanism based on a closed planar kinematic chain of one degree-of-freedom. This class of leg mechanisms has been selected because of its energy efficiency and simplicity of gait control.

A historical example of a walking machine based on one degree-of-freedom planar link-

ages is the mechanical system proposed by the Russian mathematician Pafnuty Chebyshev in 1850. The legs of this walking machine are based on a four-bar linkage designed by Chebyshev to approximate straight-line motion, details of this machine can be found in the volume 1 of the classical Artobolevsky’s handbook of mechanisms [67, pp. 406]. In more recent times, two one degree-of-freedom leg linkages, both invented in the last 25 years, have stood out, namely, the Klann mechanism and the Jansen linkage. The Klann mechanism, conceived by the Mechanical Engineer Joe Klann in 1994, is a Stephenson type III kinematic chain (a six-bar linkage) designed from the four-bar Burmester linkage developed in 1888 for harbor cranes [68]. The Jansen linkage corresponds to an eight-bar kinematic chain; it was created by Theo Jansen during his works of fusion of art and engineering, the history of the linkage development and invention is described in [28]. More details about this linkage are discussed later herein. For the development of our reconfigurable leg linkage, we opted for the Theo Jansen’s solution because of its higher potential of versatility, given the fact that the resulting coupler curve at the foot point is of higher degree than that of both the four-bar Chebyshev linkage and the six-bar Klann mechanism. An example of such versatility can be seen in the study of Komoda and Wagatsuma [38], in which an extension of the Theo Jansen linkage for climbing over bumps is proposed. This is perhaps the closer work to our approach.

2.2 Position analysis of a Theo Jansen linkage

The Theo Jansen linkage (“Jansen leg” is the term used in this chapter) is an eight-link one degree-of-freedom planar linkage, that is, a Grübler kinematic chain, designed by the Dutch kinetic sculptor Theo Jansen during the 1990s for emulating a smooth and elegant walking motion [28]. This linkage, depicted in Fig. 2.1, has three independent loops and consists of six binary links, one ternary link, and a coupler link with seven revolute joints. Since one of the revolute joints involves three binary links, the topology of this kinematic chain does not correspond to any of the sixteen topologies of standard one degree-of-freedom eight-bar linkages [69, Appendix D].

In a Jansen leg, according to the notation of Fig. 2.1, the centers of the revolute joints of the binary links define the line segments $\overline{P_1P_2}$, $\overline{P_1P_6}$, $\overline{P_2P_3}$, $\overline{P_3P_4}$, $\overline{P_3P_6}$, and $\overline{P_5P_7}$, those

for the ternary link define the triangle $\triangle P_1 P_4 P_5$, and those for the coupler link with point P_8 , the foot of a Jansen leg, define the triangle $\triangle P_6 P_7 P_8$. The position analysis problem for this linkage corresponds to, given the dimensions of every link, the position of the revolute joint centers P_1 and P_2 , and an angle θ for the input link, calculating all the feasible Cartesian locations of point P_8 . To this end, instead of using joint angles through independent loop-closure equations [70], we will use squared distances and bilateration matrices to compute the corresponding values of P_8 .

2.2.1 The bilateration matrix

The bilateration problem consists in finding the feasible locations of a point, say P_k , given its distances to two other points, say P_i and P_j , whose locations are known. Then, according to Fig. 2.2, the solution to this problem, in matrix form, can be expressed as:

$$\mathbf{p}_{i,k} = \mathbf{Z}_{i,j,k} \mathbf{p}_{i,j} \quad (2.1)$$

where $\mathbf{p}_{i,j} = \overrightarrow{P_i P_j}$ and

$$\mathbf{Z}_{i,j,k} = \frac{\mathbf{1}}{2 \mathbf{s}_{i,j}} \begin{bmatrix} s_{i,j} + s_{i,k} - s_{j,k} & -4 A_{i,j,k} \\ 4 A_{i,j,k} & s_{i,j} + s_{i,k} - s_{j,k} \end{bmatrix}$$

is called a *bilateration matrix*, with $s_{i,j} = d_{i,j}^2 = \|\mathbf{p}_{i,j}\|^2$, the squared distance between P_i and P_j , and

$$A_{i,j,k} = \pm \frac{1}{4} \sqrt{(s_{i,j} + s_{i,k} + s_{j,k})^2 - 2(s_{i,j}^2 + s_{i,k}^2 + s_{j,k}^2)}, \quad (2.2)$$

the oriented area of $\triangle P_i P_j P_k$ which is defined as positive if P_k is to the left of vector $\mathbf{p}_{i,j}$, and negative otherwise. It can be observed that the product of two bilateration matrices is commutative. Then, it is easy to prove that the set of bilateration matrices, *i.e.*, matrices of the form $\begin{pmatrix} a & -b \\ b & a \end{pmatrix}$, constitute a commutative group under the product and addition operations. Moreover, if $\mathbf{v} = \mathbf{Z}\mathbf{w}$, where \mathbf{Z} is a bilateration matrix, then $\|\mathbf{v}\|^2 = \det(\mathbf{Z}) \|\mathbf{w}\|^2$. The interested reader is addressed to [63] for a derivation of (2.1) and its properties.

It has been shown that by using bilateration matrices, the position analysis problem of linkages is greatly simplified –see, for instance, [71, 72]. This problem consists of finding

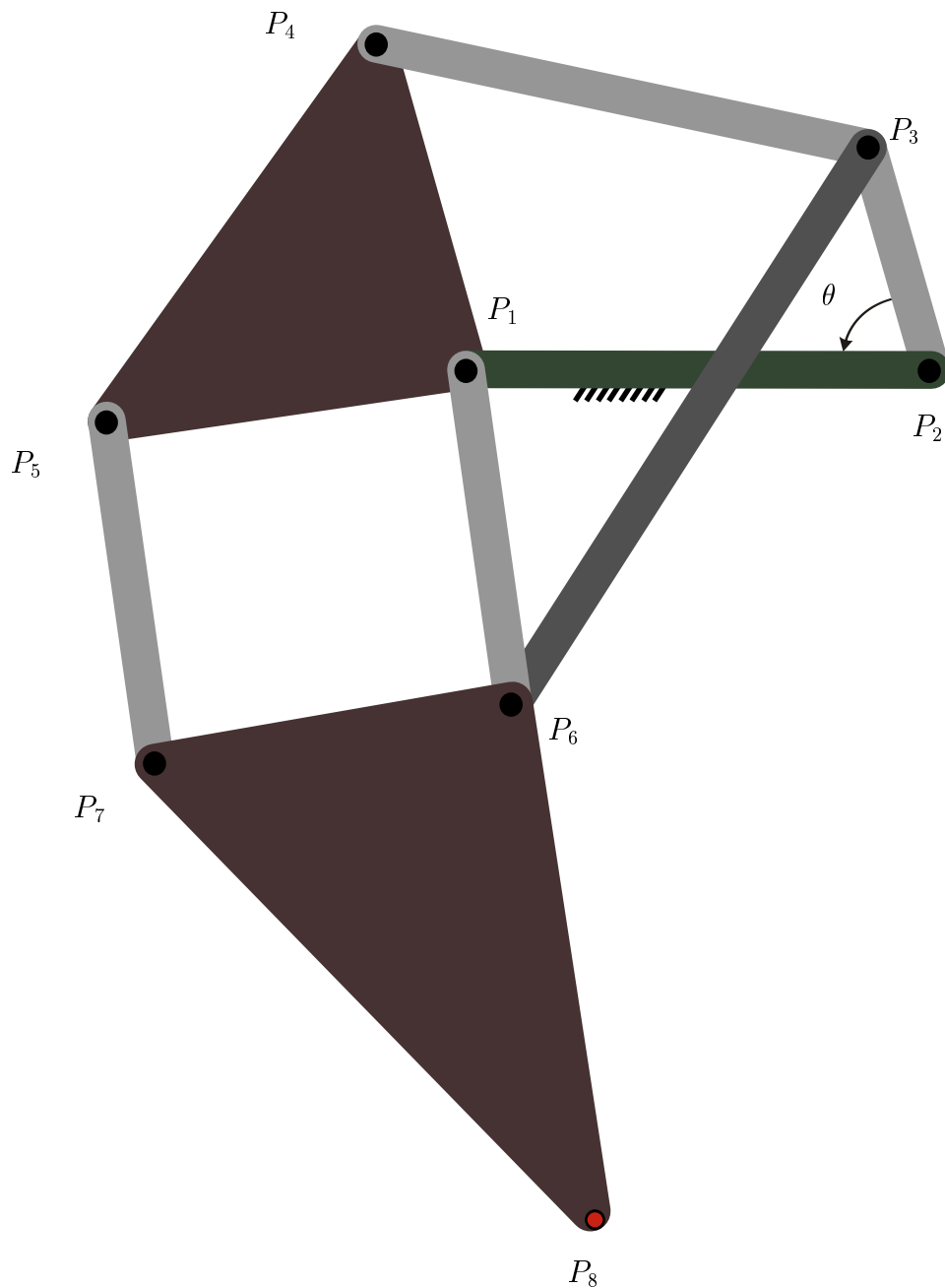


Fig. – 2.1 The Jansen leg, a one degree-of-freedom planar linkage of eight links, seven revolute joints —one of them involving there binary links, and three independent loops.

the feasible assembly modes that a kinematic chain can adopt. An assembly mode is a possible relative transformation between the links of a kinematic chain or linkage. When an assignment of positions and orientations is made for all links with respect to a given reference frame, an assembly mode is called a configuration. Next, we present how to apply the bilateration method for solving the position analysis problem of a Jansen leg.

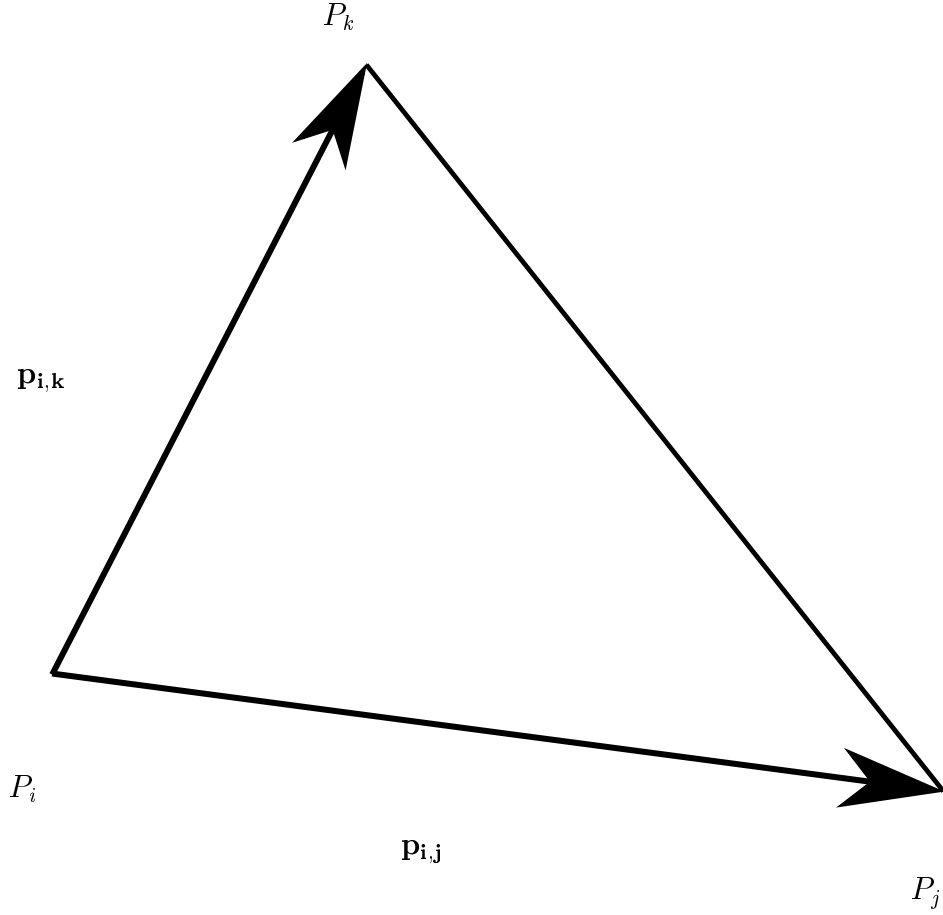


Fig. – 2.2 The bilateration problem.

2.2.2 Bilateration-based system of equations

First, according to the notation of Fig. 2.1, let us compute $\mathbf{p}_{1,3}$ from θ and the location of the revolute joint centers P_1 and P_2 . That is,

$$\mathbf{p}_{1,3} = \mathbf{Z}_{1,2,3} \mathbf{p}_{1,2} \quad (2.3)$$

with $s_{1,3} = s_{1,2} + s_{2,3} - 2d_{1,2}d_{2,3} \cos \theta$. Now, following a simple geometric constructive process from $\mathbf{p}_{1,3}$, we get

$$\mathbf{p}_{1,4} = \mathbf{Z}_{1,3,4} \mathbf{p}_{1,3}, \quad (2.4)$$

$$\mathbf{p}_{1,5} = \mathbf{Z}_{1,4,5} \mathbf{p}_{1,4} = \mathbf{Z}_{1,4,5} \mathbf{Z}_{1,3,4} \mathbf{p}_{1,3}, \text{ and} \quad (2.5)$$

$$\mathbf{p}_{1,6} = \mathbf{Z}_{1,3,6} \mathbf{p}_{1,3}. \quad (2.6)$$

Thus,

$$\mathbf{p}_{5,6} = -\mathbf{p}_{1,5} + \mathbf{p}_{1,6} = (-\mathbf{Z}_{1,4,5}\mathbf{Z}_{1,3,4} + \mathbf{Z}_{1,3,6})\mathbf{p}_{1,3}. \quad (2.7)$$

Then,

$$s_{5,6} = \det(-\mathbf{Z}_{1,4,5}\mathbf{Z}_{1,3,4} + \mathbf{Z}_{1,3,6})s_{1,3}. \quad (2.8)$$

Finally, from $\mathbf{p}_{5,6}$, we get

$$\mathbf{p}_{6,7} = -\mathbf{Z}_{6,5,7}\mathbf{p}_{5,6}, \quad (2.9)$$

$$\begin{aligned} \mathbf{p}_{6,8} &= \mathbf{Z}_{6,7,8}\mathbf{p}_{6,7} \\ &= -\mathbf{Z}_{6,7,8}\mathbf{Z}_{6,5,7}(-\mathbf{Z}_{1,4,5}\mathbf{Z}_{1,3,4} + \mathbf{Z}_{1,3,6})\mathbf{p}_{1,3}. \end{aligned} \quad (2.10)$$

Then,

$$\begin{aligned} \mathbf{p}_{1,8} &= \mathbf{p}_{1,6} + \mathbf{p}_{6,8} \\ &= \left(\mathbf{Z}_{1,3,6} - \mathbf{Z}_{6,7,8}\mathbf{Z}_{6,5,7}(-\mathbf{Z}_{1,4,5}\mathbf{Z}_{1,3,4} \right. \\ &\quad \left. + \mathbf{Z}_{1,3,6}) \right) \mathbf{Z}_{1,2,3}\mathbf{p}_{1,2}. \end{aligned} \quad (2.11)$$

Equation (2.11) defines the location of point P_8 , the foot of a Jansen leg. This equation depends on the set of link dimensions (S), the angle of the input link (θ), the orientation sign of the oriented areas $A_{1,2,3}$, $A_{1,3,4}$, $A_{1,3,6}$, and $A_{6,5,7}$, and the location of P_1 and P_2 , the centers of the grounded revolute joints. For a given set of values for all these variables, a specific configuration of a Jansen leg is determined, that is, the point P_8 is uniquely defined. We represent a configuration of a Jansen leg as $(S, \theta, \eta, P_1, P_2)$ where $\eta = 0, \dots, 15$ specifies the combination of signs for the areas $A_{1,2,3}$, $A_{1,3,4}$, $A_{1,3,6}$, and $A_{6,5,7}$. Thus, for example, $\eta = 10 = (1010)_2 \equiv + - + -$ implies that $A_{1,2,3} > 0$, $A_{1,3,4} < 0$, $A_{1,3,6} > 0$, and $A_{6,5,7} < 0$.

The ability of bilateration matrices to represent the solution of complex problems in a very compact form can be appreciated when comparing the solution for the position analysis of a Jansen leg presented in [73] with the bilateration-based result of equation (2.11).

2.2.3 Equations of velocity and acceleration

The velocity and acceleration of the bilateration problem can be readily obtained from the differential and second order differential respect to time of equation (2.1), respectively. That is,

$$\dot{\mathbf{p}}_{i,k} = \dot{\mathbf{Z}}_{i,j,k} \mathbf{p}_{i,j} + \mathbf{Z}_{i,j,k} \dot{\mathbf{p}}_{i,j}, \quad (2.12)$$

$$\ddot{\mathbf{p}}_{i,k} = \ddot{\mathbf{Z}}_{i,j,k} \mathbf{p}_{i,j} + 2\dot{\mathbf{Z}}_{i,j,k} \dot{\mathbf{p}}_{i,j} + \mathbf{Z}_{i,j,k} \ddot{\mathbf{p}}_{i,j}, \quad (2.13)$$

The specific expressions for $\dot{\mathbf{Z}}_{i,j,k}$ and $\ddot{\mathbf{Z}}_{i,j,k}$ depend on the variable sides of $\Delta P_i P_j P_k$. For example, in the case $\|\mathbf{p}_{i,k}\|$ and $\|\mathbf{p}_{j,k}\|$ are both fixed lengths, $\dot{\mathbf{Z}}_{i,j,k}$ reduces to

$$\dot{\mathbf{Z}}_{i,j,k} = \frac{1}{2s_{i,j}^2} \begin{bmatrix} \dot{s}_{i,j}(s_{i,k} - s_{i,j}) & 4(\dot{s}_{i,j}A - s_{i,j}\dot{A}) \\ 4(\dot{s}_{i,j}A - s_{i,j}\dot{A}) & \dot{s}_{i,j}(s_{j,k} - s_{i,k}) \end{bmatrix},$$

$$\dot{A}_{i,j,k} = \pm \frac{\dot{s}_{i,j}(s_{i,k} + s_{j,k} - s_{i,j})}{4\sqrt{(s_{i,j} + s_{i,k} + s_{j,k})^2 - 2(s_{i,j}^2 + s_{i,k}^2 + s_{j,k}^2)}}.$$

The bilateration-based equations for the velocity and acceleration of the foot of a Jansen leg can be similarly computed. Then, by properly differentiating equation (2.11), we have

$$\begin{aligned} \dot{\mathbf{p}}_{1,8} = & \left[\left(\mathbf{Z}_{6,7,8} \mathbf{Z}_{6,5,7} (\mathbf{Z}_{1,4,5} \mathbf{Z}_{1,3,4} - \mathbf{Z}_{1,3,6}) + \mathbf{Z}_{1,3,6} \right) \dot{\mathbf{Z}}_{1,2,3} \right. \\ & + \left(\mathbf{Z}_{1,3,6} + \mathbf{Z}_{6,7,8} \left(\mathbf{Z}_{6,5,7} (\mathbf{Z}_{1,4,5} \dot{\mathbf{Z}}_{1,3,4} - \dot{\mathbf{Z}}_{1,3,6}) \right. \right. \\ & \left. \left. + \dot{\mathbf{Z}}_{6,5,7} (\mathbf{Z}_{1,4,5} \mathbf{Z}_{1,3,4} - \mathbf{Z}_{1,3,6}) \right) \right) \mathbf{Z}_{1,2,3} \Big] \mathbf{p}_{1,2}, \end{aligned} \quad (2.14)$$

$$\begin{aligned} \ddot{\mathbf{p}}_{1,8} = & \left[(\mathbf{Z}_{1,3,6} \ddot{\mathbf{Z}}_{1,2,3} + 2\dot{\mathbf{Z}}_{1,3,6} \dot{\mathbf{Z}}_{1,2,3} + \ddot{\mathbf{Z}}_{1,3,6} \mathbf{Z}_{1,2,3}) \right. \\ & + \mathbf{Z}_{6,7,8} \left((\mathbf{Z}_{1,4,5} \mathbf{Z}_{1,3,4} - \mathbf{Z}_{1,3,6}) (\mathbf{Z}_{6,5,7} \ddot{\mathbf{Z}}_{1,2,3} \right. \\ & + 2\dot{\mathbf{Z}}_{6,5,7} \dot{\mathbf{Z}}_{1,2,3} + \ddot{\mathbf{Z}}_{6,5,7} \mathbf{Z}_{1,2,3}) + 2(\mathbf{Z}_{1,4,5} \dot{\mathbf{Z}}_{1,3,4} - \dot{\mathbf{Z}}_{1,3,6}) \\ & \left. (\mathbf{Z}_{6,5,7} \dot{\mathbf{Z}}_{1,2,3} + \dot{\mathbf{Z}}_{6,5,7} \mathbf{Z}_{1,2,3}) + (\mathbf{Z}_{1,4,5} \ddot{\mathbf{Z}}_{1,3,4} - \ddot{\mathbf{Z}}_{1,3,6}) \right. \\ & \left. \left. \mathbf{Z}_{6,5,7} \mathbf{Z}_{1,2,3} \right) \right] \mathbf{p}_{1,2}. \end{aligned} \quad (2.15)$$

2.3 Beyond the standard Theo Jansen linkage: New gait patterns

Our main aim is to design a novel reconfigurable Theo Jansen linkage that produces a wide variety of gait cycles in order to open new possibilities for innovative applications while maintaining its mechanical simplicity. To this end, those new gait patterns must be based on the topology of a Jansen leg and satisfy at least one of the following goals:

- i) mimicry of different animal species,
- ii) significant improvements of the locomotion efficiency in non-even surfaces, a range of materials, and external perturbations such as strong winds, and
- iii) transform the motion into behaviors beyond locomotion — *e.g.*, manipulation skills.

2.3.1 Tracing the coupler curve of a Jansen leg

Figure 2.3(top) presents all possible locations of point P_8 , computed from equation (2.11), for sampled values of θ at increments of $\frac{1}{100}$ for the case in which $s_{1,2} = 1073.55$, $s_{1,4} = 553.61$, $s_{1,5} = 631.72$, $s_{1,6} = 552.63$, $s_{2,3} = 117.38$, $s_{3,4} = 1216.96$, $s_{3,6} = 1468.58$, $s_{4,5} = 1045.75$, $s_{5,7} = 572.84$, $s_{6,7} = 642.22$, $s_{6,8} = 1292.26$, and $s_{7,8} = 1900.87$, with $P_1 = (0, 0)^T$ and $P_2 = (32.436, 4.632)^T$. In this procedure, for each value of θ , sixteen possible locations for the point P_8 are calculated, one per each combination of signs for the oriented areas $A_{1,2,3}$, $A_{1,3,4}$, $A_{1,3,6}$, and $A_{6,5,7}$. This set of link dimensions corresponds to our standard values of a Jansen leg. From Fig. 2.3(top), a result that contains no information on the connectivity of each sample to its neighbors, we observe that point P_8 shapes to different trajectories. In fact, since a Jansen leg corresponds to a one degree-of-freedom pin-jointed planar linkage, any arbitrary point on it generates a plane curve, called coupler curve, when the mechanism moves.

A novel approach to trace coupler curves, that takes advantage from the geometric information of bilateration-based equations, has been recently discussed in [72]. By tracing we mean that the connectivity between samples is known. Following such method, for the particular case of a Jansen leg, the curve generated from a known initial feasible

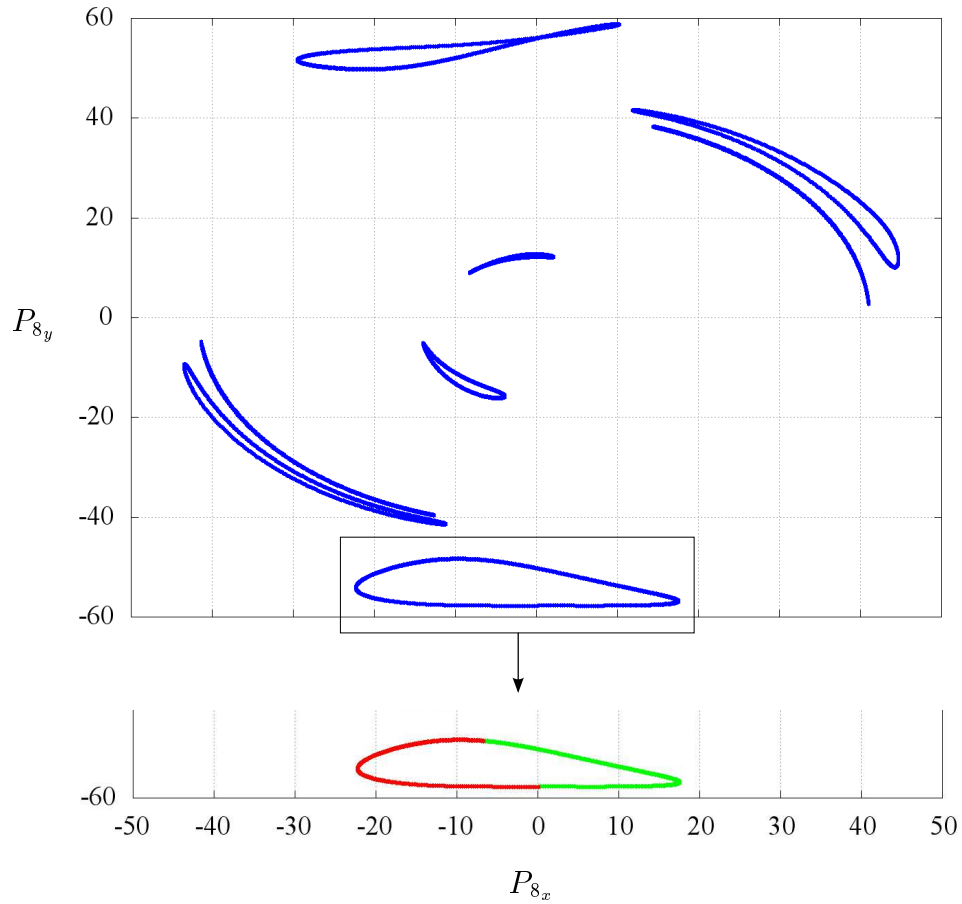


Fig. – 2.3 Top: Possible locations of point P_8 , the foot, in all assembly modes of a standard Jansen leg. The lowest sampled curve corresponds to the trajectory used in walking platforms. **Bottom:** Traced foot trajectory of a standard Jansen leg. The green path corresponds to the assembly mode family given by $A_{1,2,3} > 0$, $A_{1,3,4} > 0$, $A_{1,3,6} < 0$, and $A_{6,5,7} < 0$. In the red path, $A_{1,2,3} < 0$, $A_{1,3,4} > 0$, $A_{1,3,6} < 0$, and $A_{6,5,7} < 0$.

configuration $(S, \theta, \eta, P_1, P_2)$ by point P_8 —the foot trajectory— can be traced following these steps:

1. Compute P_8 using equation (2.11).
2. Evaluate the oriented areas $A_{1,2,3}$, $A_{1,3,4}$, $A_{1,3,6}$, and $A_{5,6,7}$ with the current value of θ . If any of them is equal to zero, the current configuration —*i.e.*, the current tuple $(S, \theta, \eta, P_1, P_2)$ — belongs to more than one family of assembly modes (combinations of signs of the oriented areas $A_{1,2,3}$, $A_{1,3,4}$, $A_{1,3,6}$, and $A_{5,6,7}$) and the leg movement may evolve along different paths. Identify all these families, that is, determine all feasible values that η can assume.
3. Increase θ at a specified rate. When θ reaches the limit imposed by the triangular inequalities associated to $\triangle P_1P_2P_3$, $\triangle P_1P_3P_4$, and $\triangle P_1P_3P_6$, start to decrease the variable.
4. Repeat steps 1 to 3 for each tuple $(S, \theta, \eta, P_1, P_2)$ until the whole range of θ has been evaluated.

In a standard Jansen leg, the foot trajectory used in walking platforms —the lowest sampled curve in Fig. 2.3(top)— can be easily traced following the above procedure from any θ between 0 and π with $A_{1,2,3} > 0$, $A_{1,3,4} > 0$, $A_{1,3,6} < 0$, and $A_{5,6,7} < 0$. The corresponding result is depicted in Fig. 2.3(bottom). It is interesting to note that the standard foot trajectory of a Jansen leg resembles to the plantigrade locomotion of some terrestrial animals. In fact, this trajectory is quite similar to those of the ankles of rats during single step cycles [74].

2.3.2 Finding the new gait patterns

According to Kuo et al. [75], a linkage can be considered as reconfigurable if during its operation at least one of the following features varies: a) the effective number of links and/or joints, b) the kinematic type —*i.e.*, the contact constraint— of some joints, c) the adjacency and incidence of links and joints, and d) the relative arrangement between joints, or more generally, the relative geometrical relation between joints and links. An interesting consideration for designing reconfigurable mechanisms is that by simply re-allocating the joint positions of pin-jointed planar linkages, all types of reconfiguration

characteristics, excepting the change of contact constraints in kinematic pairs, may be obtained [76].

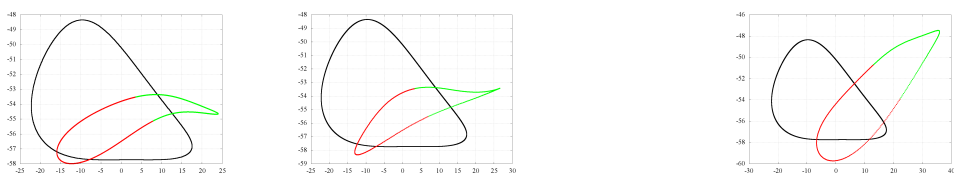
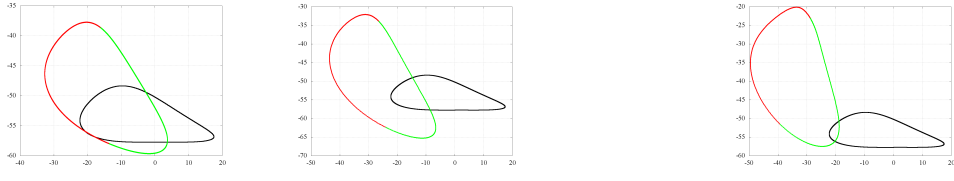
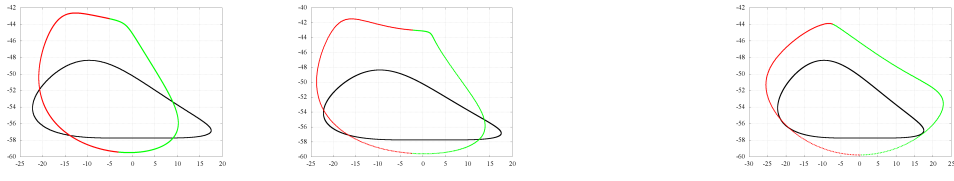
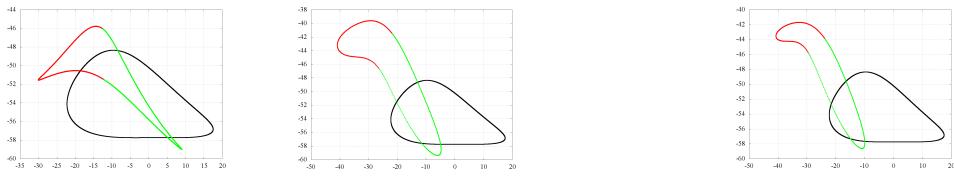
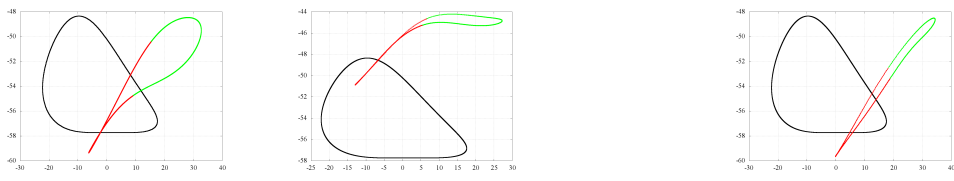
In the case of one degree-of-freedom pin-jointed planar linkages, it is well-known that a change in the link dimensions, that is, a modification in the relative distance between connected joints, a reallocation of joint positions, generates new and different coupler curves. With this basic principle in mind, our approach to obtain novel gait patterns of a Jansen leg is to identify whether by performing small variations in the lengths of the links, interesting foot trajectories can be obtained. To this end, a simple exploratory design study is suggested: vary the standard dimensions of the links in $\pm 20\%$, first link by link, later in couples, and finally in trios, and register the resulting coupler curves – computed using the discussed procedure– to detect useful gait cycles for future innovative applications in robotics. Following the proposed scheme, we present here five gait patterns, that extend the capabilities of the original Jansen leg, generated through minimal changes of link dimensions. Next, each of them is described.

Digitigrade locomotion (Cat walking)

The standard foot trajectory of a Jansen leg corresponds to a kind of plantigrade locomotion. A plantigrade is an animal that stands or walks with its podials, such as humans regularly do—an experimental analysis and characterization of the human straight walking can be found in [77]. In contrast, digitigrades walk on their digits or toes. Example of these kind of animals include dogs, cats, many other mammals, and most birds. Since in each step of digitigrades less foot is touching the surface, these animals present less friction and waste of energy than plantigrades. In consequence, digitigrades tend to be very fast runners [78]. This fact makes digitigrade locomotion of great interest for the development of walking platforms.

Table 2.1 depicts the foot trajectory of a Jansen leg when the length of the binary link connecting the revolute joint centers P_5 and P_7 is increased by 20% respect to its standard value -First row, column “single link”. The shape of this curve is quite similar to the gait cycle of a cat [79, Fig. 2]. This result is relevant because it shows that by modifying the link dimensions of a standard Jansen leg, that is, by reconfiguring a one degree-of-freedom mechanism, we can switch from a plantigrade locomotion to a digitigrade locomotion. Columns “couple of links” and “trio of links” in the first row of Table 2.1 present other

Table – 2.1 Identified foot trajectory patterns of interest for nested reconfiguration applications

Pattern	Single link	Couple of links	Trio of links
Digitigrade locomotion <i>Cat walking</i>	$d_{5,7} : +20\% \star$	$d_{1,2} : +10\%, d_{7,8} : +20\%$ $d_{3,4} : -12\%, d_{7,8} : +20\% \star$ $d_{5,7} : +10\%, \Delta P_1 P_4 P_5 : -20\%$ $d_{3,4} : +12\%, \Delta P_6 P_7 P_8 : +20\%$	$d_{1,2} : -8\%, d_{5,7} : +20\%, d_{3,6} : -20\% \star$ $d_{3,4} : -12\%, d_{7,8} : +20\%, d_{5,7} : +20\%$ $d_{3,4} : -12\%, d_{7,8} : +20\%, \Delta P_1 P_4 P_5 : -10\%$
			
Obstacle avoidance	$d_{7,8} : -20\% \star$	$d_{6,8} : +20\%, d_{7,8} : -20\% \star$ $d_{3,4} : -20\%, d_{3,6} : -20\%$	$d_{6,8} : +20\%, d_{7,8} : -20\%, d_{1,2} : +20\%$ $d_{6,8} : +20\%, d_{7,8} : -20\%, d_{3,4} : -20\% \star$
			
Jam avoidance <i>Walking on mud</i>	$d_{1,2} : +20\% \star$	$d_{1,2} : +20\%, d_{2,3} : +20\% \star$	$d_{1,2} : -20\%, d_{3,4} : -20\%, d_{3,6} : -20\% \star$
			
Step climbing	$d_{3,6} : +16\% \star$	$d_{2,3} : -10\%, d_{3,6} : +20\%$ $d_{3,6} : +16\%, d_{7,8} : -20\% \star$ $d_{3,4} : +20\%, d_{7,8} : +20\%$	$d_{1,2} : +20\%, d_{2,3} : +20\%, d_{3,6} : +20\%$ $d_{2,3} : -14\%, d_{3,6} : +20\%, d_{7,8} : -20\% \star$ $d_{3,4} : +20\%, d_{5,7} : +20\%, d_{7,8} : +20\%$
			
Drilling motion	$d_{7,8} : +20\% \star$	$d_{1,2} : -8\%, d_{5,7} : +20\%$ $d_{2,3} : +16\%, d_{6,8} : -20\% \star$ $d_{6,8} : -20\%, d_{7,8} : +2\%$	$d_{1,2} : +10\%, d_{3,4} : +20\%, d_{7,8} : +20\%$ $d_{2,3} : -20\%, d_{6,8} : -20\%, d_{7,8} : +4\%$ $d_{1,2} : +10\%, d_{7,8} : +20\%, \Delta P_1 P_4 P_5 : -20\% \star$
			

modifications in the link dimensions that further yield digitigrade behaviors. The foot trajectories of the combinations with the \star symbols in the columns are depicted. In each of these figures, the gait of the standard Jansen leg is presented for reference as a black curve. These conventions apply in all next cases.

Obstacle avoidance

The height of the foot trajectory of a standard Jansen leg is 9.38 units (Fig. 2.3), that is a 16.26% of the total height of the leg, a value computed from the grounded revolute joint center $P_1 = (0, 0)^T$ to the lowest point of the foot trajectory. Therefore, a walking platform based on standard Jansen legs cannot in principle overpass obstacles higher than this limit (> 9.38 units). This is an important drawback because although a Jansen-based system is highly efficient, its operability in rough terrain is reduced.

Second row, column “single link”, of Table 2.1 shows the foot trajectory of a Jansen leg when the side length associated to points P_7 and P_8 of the coupler link $\triangle P_6 P_7 P_8$ is decreased by 20% respect to its standard value. In this case, the height of the foot trajectory is 21.91 units, that is a 36.74% of the total height of the leg. This new height is more than twice the foot trajectory of a standard Jansen leg. This reconfigurability characteristic could be of interest for applications in uneven terrains —think, for instance, in a team of walking platforms for space exploration missions, that is, exploration of asteroids, comets, planets, and so on. Similar obstacle avoidance patterns can be obtained by simultaneously changing different link lengths of a Jansen leg. These results are presented in the second row, columns “couple of links” and “trio of links”, of Table 2.1.

Jam avoidance (Walking on mud)

In soft terrains, walkers can easily get stuck because of the soil conditions. To overcome such situations, a change in the walker’s gait cycle has to be introduced, a versatility that a walking platform based on standard Jansen legs does not offer in its current form. For example, in a transition from a dry soil to a semi-wet mud terrain, the typical foot trajectory of a Jansen leg seems inadequate because of the rigidity variation of the soil in the two scenarios. A gait with the potential to solve this issue is depicted in the third row, column “single link”, of Table 2.1. Such curve is obtained by increasing 20% the distance between the grounded revolute joint centers P_1 and P_2 . Beyond its height, this type of trajectory is of interest because facing the soil with an arc shape, while

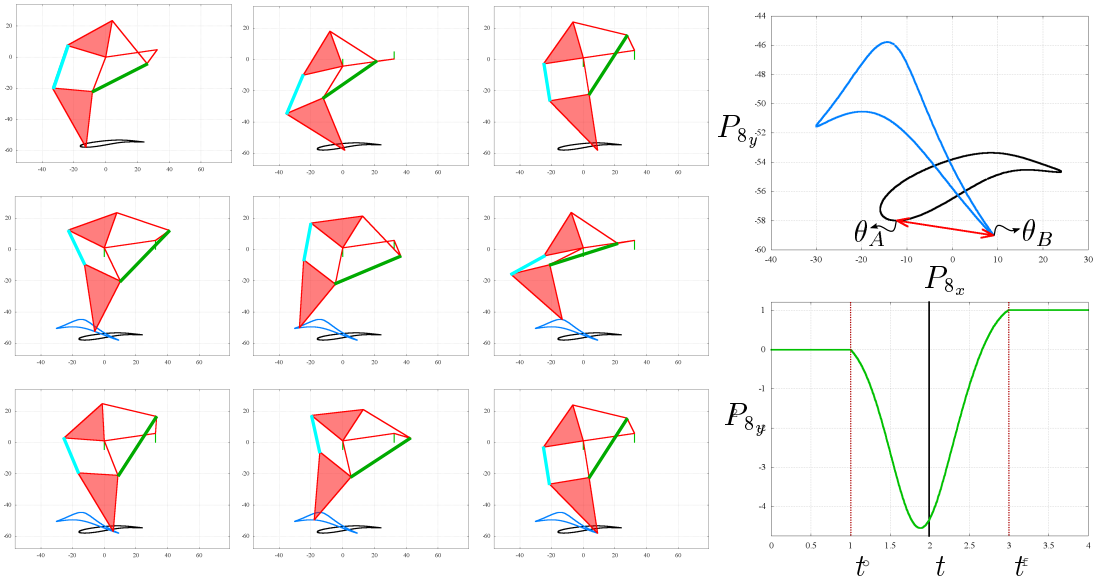


Fig. – 2.4 Transformation from digitigrade locomotion ($d_{5,7} : +20\%$) to step climbing ($d_{3,6} : +16\%$). **Left:** Some steps of a simulation of the leg transformation, the binary links of variable dimension and the vertical movement of the grounded revolute joint centers are highlighted in cyan and light green. The corresponding foot trajectories are also depicted –digitigrade locomotion in black and step climbing in blue. **Right-top:** The lowest values of P_{8y} for each of the foot trajectories in the transformation are connected by an arrow. These values are used to determine the initial and final input angles, θ_A and θ_B respectively, in the transformation process. **Right-below:** The evolution of P_{1y} from $t = t_o$ to $t = t_f$.

maintaining a step length close to the original one, allows to extract material and look for a suitable support point at the same time. As in the other reconfigurability characteristics previously discussed, similar jam avoidance patterns can be obtained by simultaneously changing different link lengths of a Jansen leg. The corresponding combinations of link dimensions are presented in the third row, columns “couple of links” and “trio of links”, of Table 2.1.

Step climbing

Fourth row of Table 2.1 presents the modifications in the link dimensions of a standard Jansen leg that yield foot trajectories for climbing steps. This curve results from increasing 16% the distance between the grounded revolute joint centers P_3 and P_6 . These gamma-like patterns are more appropriate for climbing steps than the normal foot trajectory due to the significantly shorter contact line with the floor —think, for example, the length of the steps.

Drilling motion

In kinematics of mechanisms, reciprocating motion is in general defined as a recurrent up-and-down or back-and-forth movement. It is normally associated to a repetitive straight line motion resulting from or giving rise to a full rotation. When considering complex one degree-of-freedom planar linkages —*i.e.*, mechanisms with coupler curves of order much higher than six, the degree of a four-bar linkage coupler curve, such standard concept should be extended because overlapping motions different to a straight line can be obtained in specific ranges of the input joint. An example of this kind of reciprocating motion in a double butterfly linkage, a mechanism whose coupler curves can reach order 48, is presented in [80]. Observe that this behavior also occurs in a standard Jansen leg as it can be verified in the sampled curves presented in Fig. 2.3(top).

Fifth row of Table 2.1 presents the modifications in the link dimensions of a standard Jansen leg that yield foot trajectories with reciprocating characteristics. These curves, product of increasing 20% the distance between the joint center P_7 and the foot point P_8 for the case of single-link modification, are of interest because their needle-like shapes can be used for drilling activities. With this resulting reconfigurability characteristic we go one step further because it shows that by varying the link dimensions of a standard Jansen leg we can, in addition to modify the gait patterns of the walking platform, change the behavior of the system. In this case, from a walker to a driller.

2.4 Characterization of leg transformation

We have shown so far that by changing the link dimensions of a standard Jansen leg, a variety of gait patterns of interest for innovative applications in robotics can be identified, *i.e.*, digitigrade locomotion, obstacle avoidance, jam avoidance, step climbing, and drilling motion. An important design challenge is how to perform a proper transformation between gait patterns. By proper we mean, for example, that undesired floor contacts must be avoided during the transformation process. Note that the answer to this question has implications in the control and design of the proposed Jansen leg with variable link dimensions.

Following the above discussion, we have devised a simple procedure for transforming

a reconfigurable Jansen leg from a pattern A to a pattern B , where both A and B are different and belong to the set of patterns {plantigrade locomotion, digitigrade locomotion, obstacle avoidance, jam avoidance, step climbing, and drilling motion} as described in section 2.3. As a proof of concept, we consider the transformation from digitigrade locomotion ($d_{5,7} : +20\%$) to step climbing ($d_{3,6} : +16\%$). The proposed method is as follows:

1. For pattern A , from the current location of the grounded revolute joint centers P_1 and P_2 , determine the lowest value of $P_{3,y}$ and the corresponding input angle θ , say θ_A , using equation (2.11) with increasing of θ at a specified rate. For our transformation example from digitigrade locomotion to step climbing, with $P_1 = (0, 0)^T$, $P_2 = (32.436, 4.632)^T$, and increments of $\frac{1}{100}$ for θ , we get $\theta_A = 5.48$ rad [Fig. 2.4(right-top)].
2. Repeat step 1 for pattern B . In our example, $\theta_B = 1.27$ rad [Fig. 2.4(right-top)].
3. Define the transformation time values. The transformation starts at time $t = t_o$ and finalizes at time $t = t_f$. Transformation time $\Delta t = t_f - t_o$. For the case study, $\Delta t = 2$ with $t_o = 1$ and $t_f = 3$ [Fig. 2.4(right-bottom)].
4. From patterns A and B , determine the link dimensions that have to be changed from a l_o value at time $t = t_o$ (pattern A) to a l_f value at time $t = t_f$ (pattern B). That is, in the case of our example:

Link dimension	l_o	l_f
$d_{5,7}$	28.7208 (+20%)	23.9340 (0%)
$d_{3,6}$	38.3220 (0%)	44.4535 (+16%)

5. Start the transformation, $t = t_o$. Set the input angle $\theta = \theta_A$ and determine the current location of the foot, say P_{8c} , from the values compute in step 1.
6. For each of the link dimensions determined in step 4, compute $l_c = \frac{l_f - l_o}{\Delta t}(t - t_o) + l_o$, where l_c is the current length of the corresponding variable link. Now, compute

$\theta_c = \frac{\theta_B - \theta_A}{\Delta t}(t - t_o) + \theta_A$, where θ_c is the current value of the input angle.

7. From the fixed link dimensions, the corresponding l_c values of the variable links, the input angle θ_c , and the current locations of the grounded revolute joint centers P_1 and P_2 , compute the new foot location, say P_{8n} , using equation (2.11).
8. Compute the offset $\Delta y = P_{8n_y} - P_{8c_y}$ and set $P_{8c} = P_{8n}$.
9. Update the vertical position of the grounded revolute joint centers P_1 and P_2 by subtracting Δy from both ordinates. For the case study, the evolution of P_{1y} from $t = t_o$ to $t = t_f$ is depicted in Fig. 2.4(right-bottom).
10. Increase time t at a specified rate δt , that is, $t = t + \delta t$. In our example, $\delta t = \frac{1}{100}$.
11. Repeat steps 6 to 9 until $t = t_f$.

This procedure is summarized in the flowchart presented in Fig. 2.5. Fig. 2.4(left) shows some steps of a simulation of the leg transformation from digitigrade locomotion ($d_{5,7} : +20\%$) to step climbing ($d_{3,6} : +16\%$). The binary links of variable dimension and the vertical movement of the grounded revolute joint centers are highlighted in cyan and light green.

2.5 Implementation of a reconfigurable Jansen leg

Figure 2.6(center) presents the complete CAD design of a fully-functional reconfigurable Jansen leg with four actuators suitable for the transformation procedure discussed in section 2.4. In this design we consider transformations of patterns by changing the lengths of single links —*i.e.*, link combinations presented in column “single link” of Table 2.1. Note that for such transformations only four length variables are needed, namely, $d_{1,2}$, $d_{3,6}$, $d_{5,7}$, and $d_{7,8}$. In this design, the extendable links, that can be modeled as a revolute-prismatic-revolute kinematic chain with an actuated slider joint, correspond to linear actuators utilizing ball screw with two hinge holes at its ends. The base link is designed to allow the up and down movement of the reconfigurable Jansen leg as required by the transformation procedure. Next, such conceptions are detailed.

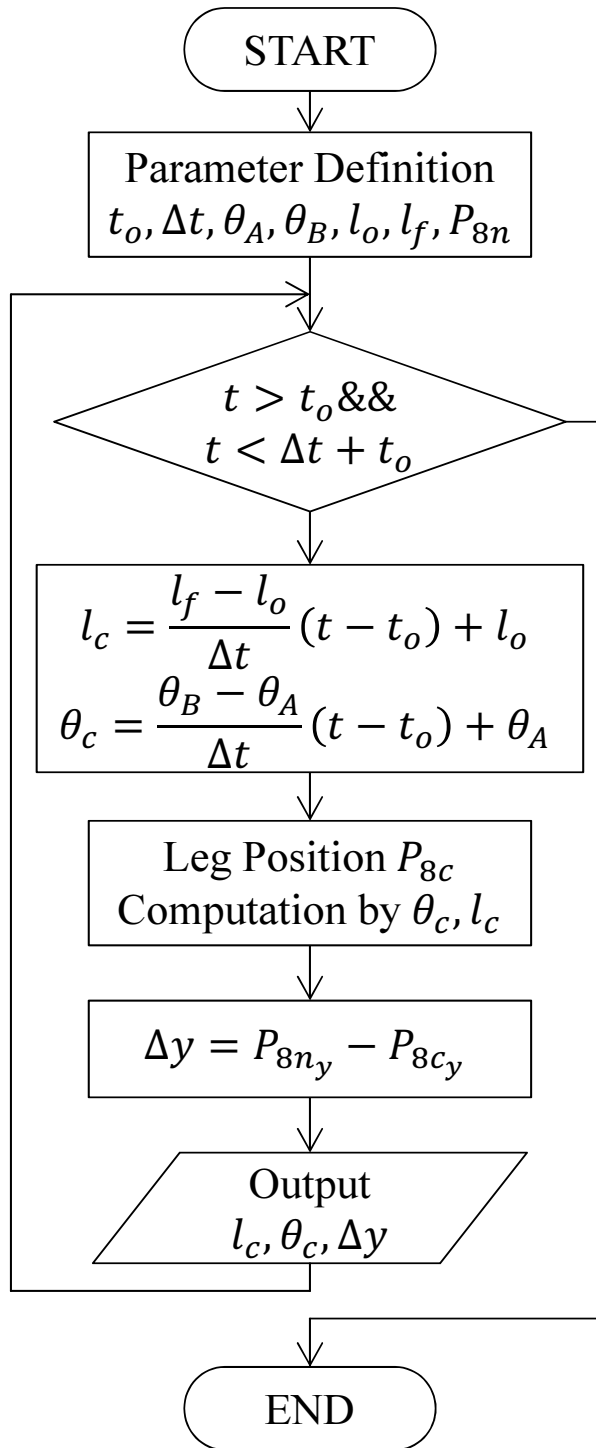


Fig. – 2.5 Flowchart of the proposed method for leg transformation (see text for details).

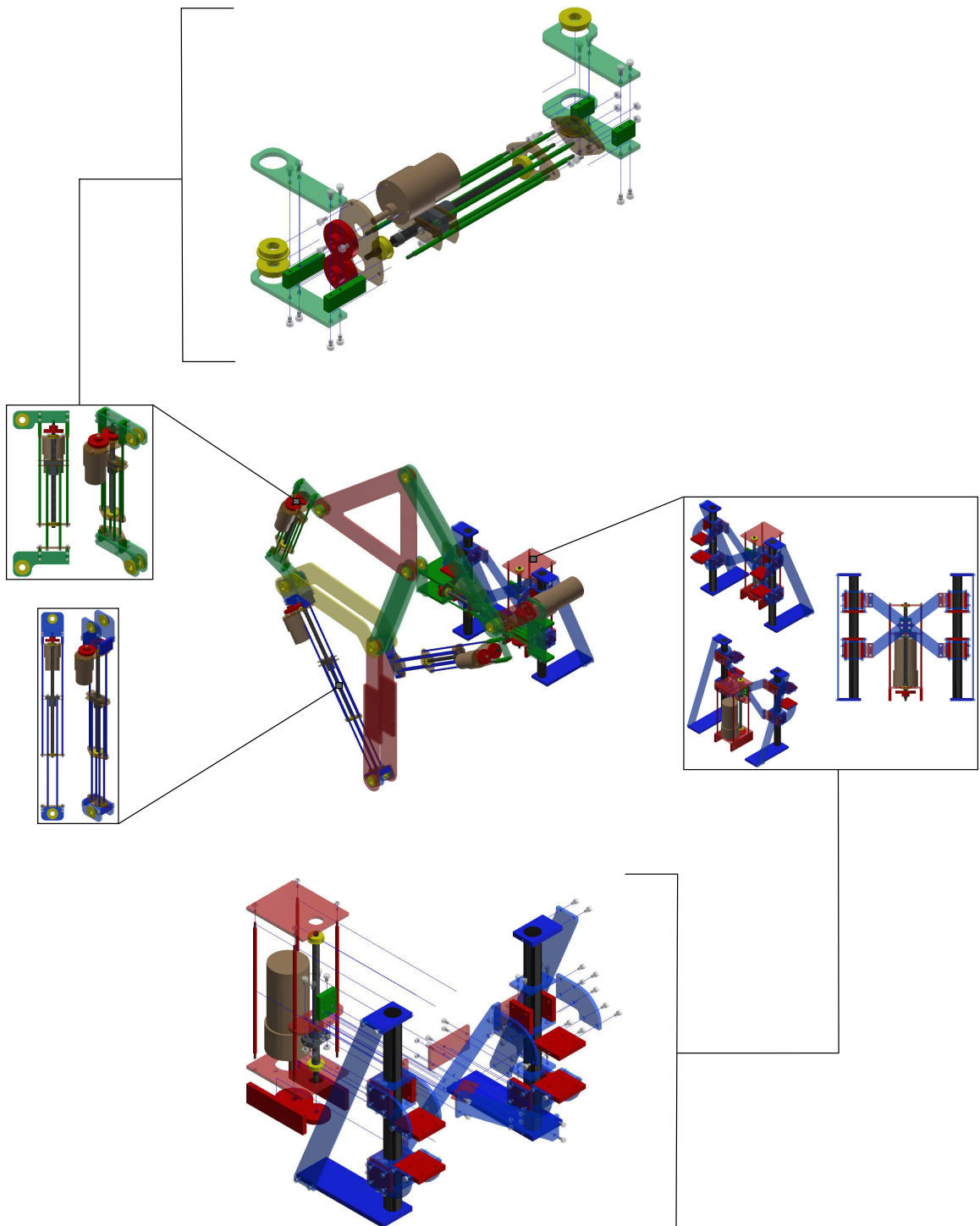


Fig. – 2.6 A fully-functional reconfigurable Jansen leg with four linear actuators suitable for the transformation procedure presented in section 2.4 (link combinations presented in column “single link” of Table 2.1) (**center**). Zoomed areas present the base system (**center-right**) and links of variable dimension —extendable links (**center-left**). Details of these designs can be observed in the corresponding exploded views —base system (**bottom**) and extendable links (**top**).

2.5.1 Extendable links

From Table 2.1, it is known that the binary links associated to the length variables $d_{1,2}$, $d_{3,6}$, $d_{5,7}$ and $d_{7,8}$ have to be changed from standard size (0%) to -20%, +16%, and +20% for obtaining the multiple gait patterns: plantigrade locomotion, digitigrade locomotion, obstacle avoidance, jam avoidance, step climbing, and drilling motion. The linear actuator for these extendable links can be designed to uniquely satisfy these specific requirements —*i.e.*, a linear actuator with a discrete number of positions, but, thinking in future works where other modifications may be necessary, a solution with a continuous set of positions is preferred. Moreover, the proposed design should be able to change the link dimension without run off the edge where the two revolute joint centers are located (the hinge holes) because it might generate undesirable contacts between other links in the linkage as it could happen if, for example, the module for reconfiguration by reallocation of joint positions in pin-jointed planar linkages suggested in [76] is used.

Details of the extendable links designed to satisfy the described conditions can be observed in the exploded view presented in Fig. 2.6(top). The proposed design is based on a ball screw with a motor properly installed in parallel utilizing gears. Since ball screws tend to back drive because of their low friction, for simplicity, we opted to use motors of high torque and low speed instead of implementing a brake in the system in order to hold the link dimensions. A prototype of this design using a DC motor (SPG30E-300K, rated torque: 1176 N.mm, rated speed: 12 RPM) and aluminum is shown in Fig. 2.7(left). It can be verified through simulation that the highest back-drive torques —*i.e* torque required to support a load in position in a screw— during locomotion are lower than 15.92 N.mm (\ll 1176 N.mm). As an alternative, motors with a low/high relationship between torque and speed can be used to improve the efficiency of the system, but in this case the extendable link design should include a non-backdrivable mechanism for avoiding undesired changes in the link dimensions during normal operation.

2.5.2 Base system

In order to realize the transformation process without floor contacts as discussed in section 2.4, the reconfigurable Jansen leg has to be moved up and down. The easiest way to solve this is to install a linear actuator in the base link, taking into account that

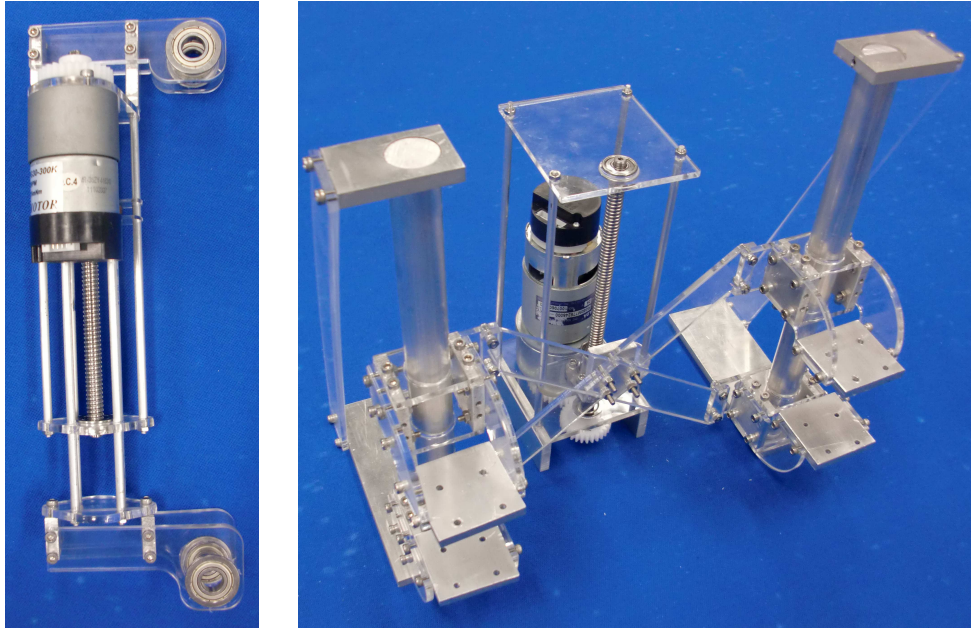


Fig. – 2.7 Prototypes of the base system (**right**) and extendable links (**left**).

such base system must support the moment of the whole mechanism. Observe that if the moment is applied directly to the linear actuator, its motion could be affected and, in the worst case, the system could break. To avoid this, two straight guides are designed to support the base link and its up-and-down movement. The base link, and in consequence the reconfigurable Jansen leg, are fixed to the guides by four points, two in each guide, which are connected to the linear actuator.

Details of the base system design can be observed in the exploded view presented in Fig. 2.6(bottom). A prototype of this design is shown in Fig. 2.7, in which a DC motor (RG50M775245000-120K, rated torque: 4.9 N.m, rated speed: 30 RPM) was installed for driving the reconfigurable linkage. Since it has been shown that a torque of 1 N.m is necessary to drive the Jansen leg at a constant speed [81]; the selected motor has a safety factor of 4.9, a value high enough to resist variations in the torque requirement resulting from, for instance, errors in the parameters.

The base system and extendable links are the principal components of the proposed design of a reconfigurable Jansen leg. Figure 1.4 presents a working prototype of this mechanism. This implementation uses acrylic for the links of fixed dimension and has been carried out in the SUTD Fabrication Lab using a minimum amount of off-the-shelf parts. In next section some experimental results obtained with this prototype are discussed.

2.6 Experimental results

Table – 2.2 Numerical analysis of experiment results

Pattern		Simulation [cm]	Experiment [cm]	Error [cm]	Percent error [%]	Standard deviation [cm]
Plantigrade locomotion	Width	39.82	33.42	6.40	16.07	0.47
	Height	9.39	7.59	1.79	19.12	
Digitigrade locomotion	Width	39.97	33.40	6.57	16.45	0.63
	Height	4.64	3.66	0.98	21.15	
Obstacle avoidance	Width	36.48	30.01	6.47	17.74	0.67
	Height	21.92	18.59	3.32	15.16	
Step climbing	Width	39.17	32.46	6.71	17.17	0.41
	Height	13.23	7.94	5.29	40.01	
Drilling motion	Width	39.05	33.08	5.97	15.27	0.52
	Height	10.90	9.00	1.90	17.41	

Effectiveness of the design and prototype of the reconfigurable Jansen leg presented in section 2.5, for generating the multiple gait patterns —section 2.3— as well as the proposed transformation process —section 2.4, was verified through experimentation. In the experiments the linear actuators of the reconfigurable Jansen leg were driven at constant speed by PID controllers (gains: P=50, I=0.008, and D=0.01), ideal trajectories were generated using the procedure of Fig. 2.5. The resulting leg trajectories were obtained using image processing tools. For measuring the rotation angle of each motor, rotary encoders, utilizing hole sensors, were installed and “Arduino MEGA 2560” was used as control CPU. The obtained experimental results are discussed next.

2.6.1 Generation of gait patterns

The first experiment consisted in comparing the simulated and experimental leg trajectories for the different gait patterns. To this end, the link dimensions of the reconfigurable Jansen leg were set according to the link combinations presented in column “single link” of Table 2.1 for then actuating the input joint (motor) for ten cycles. The results of this process are shown in Fig. 2.8 for the gait patterns plantigrade locomotion (standard trajectory of a Jansen leg), digitigrade locomotion, obstacle avoidance, step climbing, and drilling motion. After experimentation, it was discovered that the jam avoidance pattern cannot be generated with the current prototype because when the angle between the input

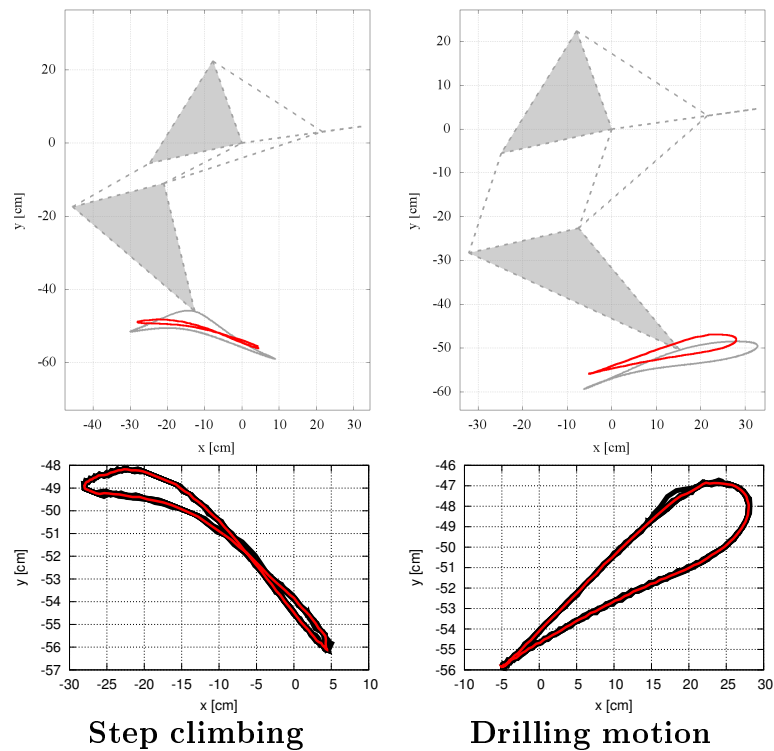
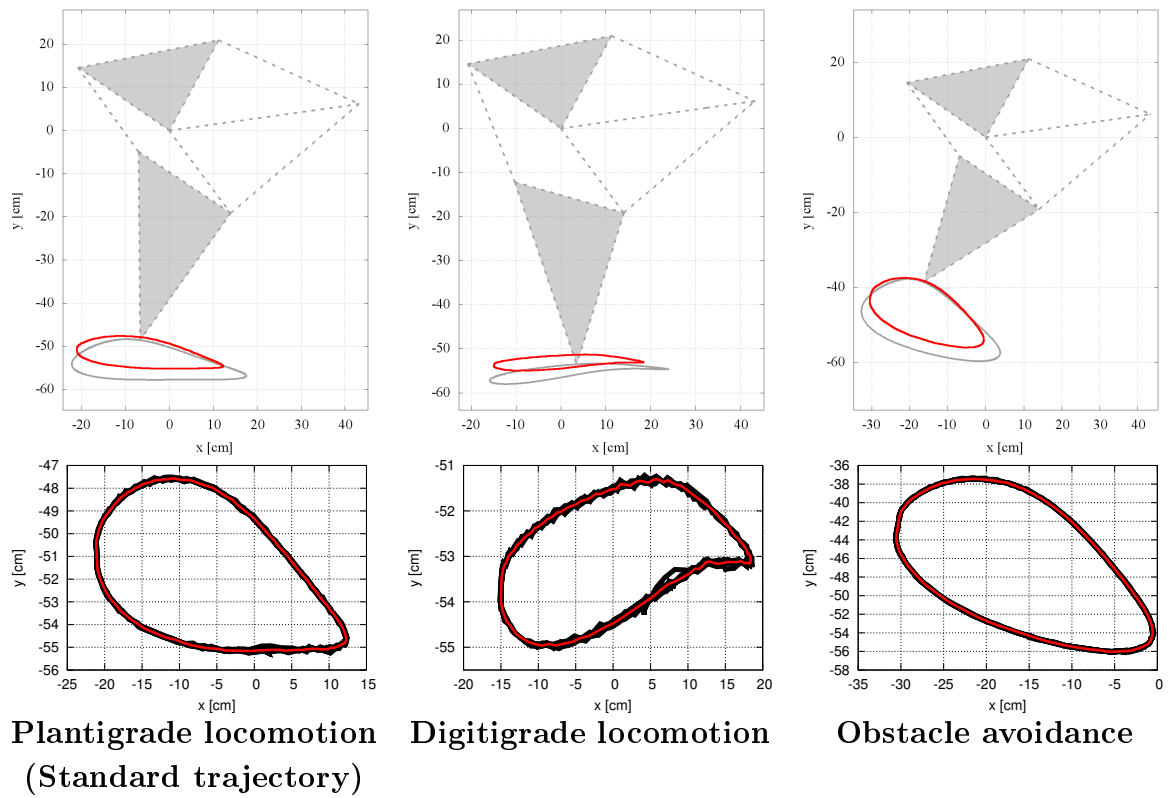


Fig. – 2.8 Comparison between the simulated leg trajectory (in gray) and the average experimental trajectory (in red) obtained after ten cycles of the input joint (curves depicted in black) for the gait patterns plantigrade locomotion (standard trajectory of a Jansen leg), digitigrade locomotion, obstacle avoidance, step climbing, and drilling motion.

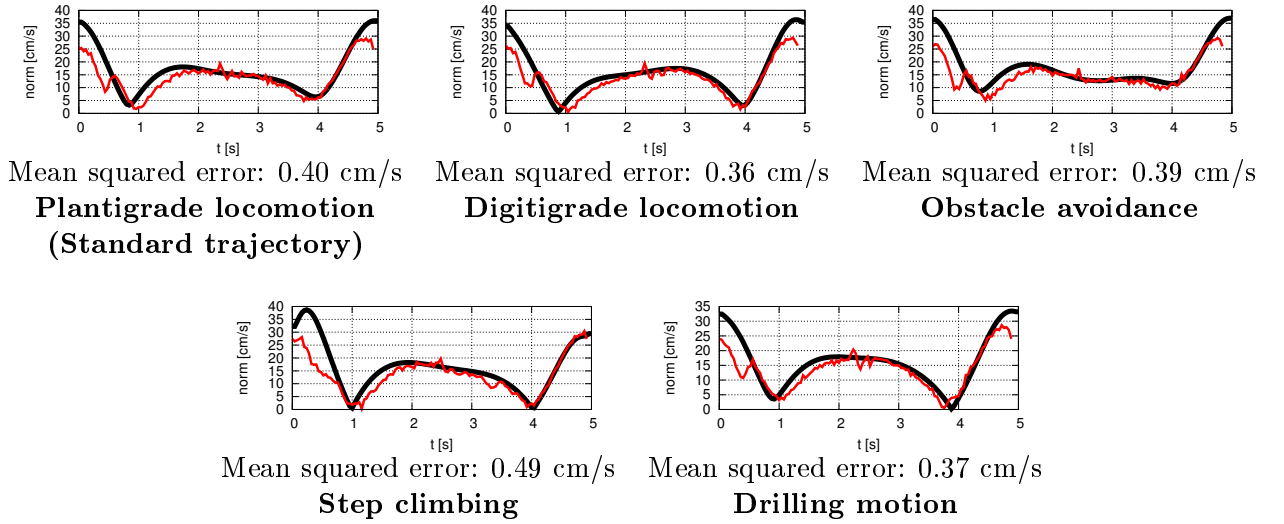


Fig. – 2.9 Comparison between the simulated speed at the foot point (in black) —*i.e.*, magnitude (Euclidean norm) of equation (2.14)— and the average experimental speed (in red) computed from the average experimental trajectory (Fig. 2.8) for the gait patterns plantigrade locomotion (standard trajectory of a Jansen leg), digitigrade locomotion, obstacle avoidance, step climbing, and drilling motion.

link (corresponding to the line segment $\overline{P_2P_3}$ in Fig. 2.1) and the base link (line segment $\overline{P_1P_2}$) is 3.1 rad, the distance between the revolute joint centers P_1 and P_7 is 2.07 cm, a value that exceeds the minimum able to be reproduced with the current implementation (6.32 cm). Future developments of the reconfigurable Jansen leg will resolve this limitation by thinning the structure surrounding the link pin holes.

Table 2.2 shows the error and percent error of comparing the width and height of the average experimental trajectory with those of the simulated trajectory, for each of the gait patterns presented in Fig. 2.8. A percent error of less than 22 % is obtained for all cases but the step climbing pattern. The origin of such errors is principally due to the non-conformity of link lengths and the presence of joint clearances in the prototype. Both error sources are almost inherent to the fabrication of mechanical designs and are the typical elements that affect the performance of linkages and mechanisms [82]. The big error in the step climbing pattern, 40.01 % in height, is given by the greater moment generated by the mechanism. It can be easily shown by simulation that the farthest center of mass point, respect to the base link, is achieved in such pattern, as a consequence, the joint clearance (backlash effect) affects more this pattern than the others. Table 2.2

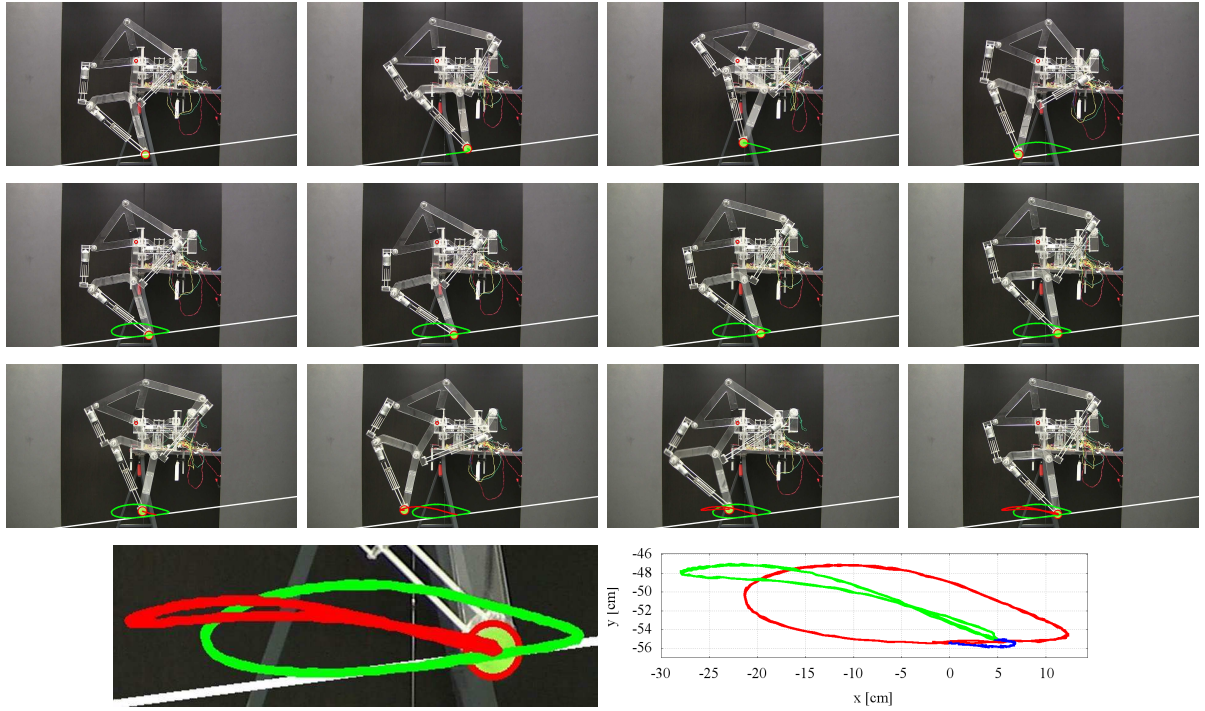


Fig. – 2.10 Experimental transformation process from plantigrade locomotion to step climbing ($d_{5,7} : +20\%$). **Top:** Snapshots of the experiment. A green marker, circled by a red line, located in the foot point is tracked. The green and red trajectories represent the plantigrade locomotion pattern and the step climbing pattern, respectively. The white line represents an estimated ground, it is computed because the prototype is tilted due to an inclination in the base system. The small red circle represents the origin of the reference frame. **Bottom-left:** Zoomed view of the tracked trajectories. **Bottom-right:** Rotated experimental leg trajectories in which the ground line is parallel to the x-axis of the reference frame. The resulting curve during the transformation process is shown in blue.

also presents the standard deviation of the experimental leg trajectories for each of the evaluated patterns; in all cases these values are small, showing the good repeatability of the developed prototype.

The above experimental validation is completed by the results presented in Fig. 2.9, in which a comparison between the simulated speed at the foot point, magnitude of the velocity vector of equation (2.14), and the average experimental speed, computed from the average experimental trajectory —Fig. 2.8, is presented for the gait patterns plantigrade locomotion, digitigrade locomotion, obstacle avoidance, step climbing, and drilling motion. For all these cases, the obtained results and corresponding mean squared

errors prove the adequate generation of gait patterns of the reconfigurable Jansen leg prototype.

2.6.2 Leg transformation

The second experiment consisted in verifying the transformation process presented in section 2.4. To this end, the transformation from plantigrade locomotion to step climbing was tested. In this experiment, the start time of transformation was set to $t_o = 3.0$ s with a transformation time of $\Delta t = 180$ s. Figure 2.10 shows some snapshots of the experiment, highlighting the corresponding leg trajectories during the process. The results verify that the transformation is carried out without undesired floor contacts.

2.7 Conclusions

An original design approach has been presented in this chapter to achieve adaptive gait patterns in legged robots for which Theo Jansen linkage forms the core. This one degree-of-freedom linkage, that is very efficient and widely adopted in walking platforms, has been modified to produce a wide variety of gait cycles using the reconfiguration principle of variable allocation of joint positions. We have discussed novel approaches to address the position analysis problem and to characterize leg transformation in this reconfigurable design. Five gait patterns of interest have been identified, analyzed and discussed in relation to potential future applications. These exemplary gait variations considerably extend the capabilities of the original design not only to produce novel gait patterns but also to realize behaviors beyond locomotion. A fully-functional design has been presented, which enables all single-link transformations, and experimental results with a working prototype have been reported.

A four-legged robot is currently being assembled with reconfigurable Jansen legs based on the design herein presented. The objective with this robot is to test different reconfiguration scenarios and control strategies for limb specialization and graceful degradation. Our long-term aim is to develop systematic methods to design reconfigurable robots capable of transforming in response to needs associated with environment, task, or failures.

3 . Speed Control of Jansen Linkage Mechanism for Exquisite Tasks

The reconfigurable Jansen linkage mechanism has the gait pattern for the plane as well as variety of gait patterns through changing its link length, and is capable of achieving required tasks in response to various environments. We have explored the effective gait patterns for some tasks by utilizing the forward kinematics of the Jansen linkage mechanism, and demonstrated its repeatability and possibility via the experiments with the real prototype. This chapter reports a toe speed control to achieve more complex tasks with the Jansen linkage mechanism. In order to achieve more complex tasks, delicate control of the toe is required. Since the Jansen linkage mechanism is one of the closed loop linkage mechanism, the trajectory of the toe is defined uniquely depending on combination of the link length. Hence, by controlling the toe speed, the locomotion of the toe can be controlled arbitrarily in response to intended purposes of its gait pattern. In this chapter, as representative example of the speed control, the angle trajectory capable of realizing the constant speed control of the toe is derived, and it is verified that the constant speed control of the toe can be realized by utilizing the derived angle trajectory through numerical simulation.

3.1 Trajectory Design for Constant Speed Control of Toes

This section designs the trajectory for the constant speed control of the toe based on the forward kinematics of the Jansen linkage mechanism. From (2.11), by solving Bilateralization

problem, the forward kinematics of the Jansen linkage mechanism can be obtain as follows:

$$\begin{aligned}\mathbf{p}_{1,8} &= \left(\mathbf{Z}_{1,3,6} - \mathbf{Z}_{6,7,8} \mathbf{Z}_{6,5,7} (-\mathbf{Z}_{1,4,5} \mathbf{Z}_{1,3,4} + \mathbf{Z}_{1,3,6}) \right) \mathbf{Z}_{1,2,3} \mathbf{p}_{1,2}, \\ &= \mathbf{Z}_{1,2,8}(\theta) \mathbf{p}_{1,2},\end{aligned}\quad (3.1)$$

where, θ represents the angle between the base link and the driving link from Fig. 2.1. And, by differentiating (3.1), the toe speed can be obtained as follows:

$$\dot{\mathbf{p}}_{1,8} = \dot{\mathbf{Z}}_{1,2,8}(\theta) \mathbf{p}_{1,2} + \mathbf{Z}_{1,2,8}(\theta) \dot{\mathbf{p}}_{1,2}.$$

Since $\dot{\mathbf{p}}_{1,2} = 0$ and $\dot{\mathbf{Z}}_{1,2,8}(\theta) = \frac{\partial}{\partial \theta} \mathbf{Z}_{1,2,8}(\theta) \dot{\theta}$,

$$\dot{\mathbf{p}}_{1,8} = \frac{\partial}{\partial \theta} \mathbf{Z}_{1,2,8}(\theta) \mathbf{p}_{1,2} \dot{\theta}. \quad (3.2)$$

Hence,

$$\left\| \dot{\mathbf{p}}_{1,8} \right\| = \left\| \frac{\partial}{\partial \theta} \mathbf{Z}_{1,2,8}(\theta) \mathbf{p}_{1,2} \right\| \left| \dot{\theta} \right|. \quad (3.3)$$

From (3.3), let a target speed of the toe is $\|\dot{\mathbf{r}}\|$ on a angle θ of the driving link, a target angular velocity of the driving link can be formulated as follows:

$$\dot{\theta} = \frac{\|\dot{\mathbf{r}}\|}{\left\| \frac{\partial}{\partial \theta} \mathbf{Z}_{1,2,8}(\theta) \mathbf{p}_{1,2} \right\|}. \quad (3.4)$$

Finally, by integrating (3.4), we obtain the target driving link angle as follows:

$$\theta = \int \frac{\|\dot{\mathbf{r}}\|}{\left\| \frac{\partial}{\partial \theta} \mathbf{Z}_{1,2,8}(\theta) \mathbf{p}_{1,2} \right\|} dt. \quad (3.5)$$

3.2 Numerical Simulation

This section verify that the constant speed of the toe can be realized by referencing (3.5) through numerical simulation. In the simulation, the target driving link angle from (3.5) is substituted into equation (3.1). Also, the target speed of the toe is set as $\|\dot{\mathbf{r}}\| = 4$ cm/s. Figs. 3.1-3.4 shows the simulation results, where the red line represents the results of the proposed method and the green line represents the results of in the case of controlling the driving link with constant angular velocity, respectively.

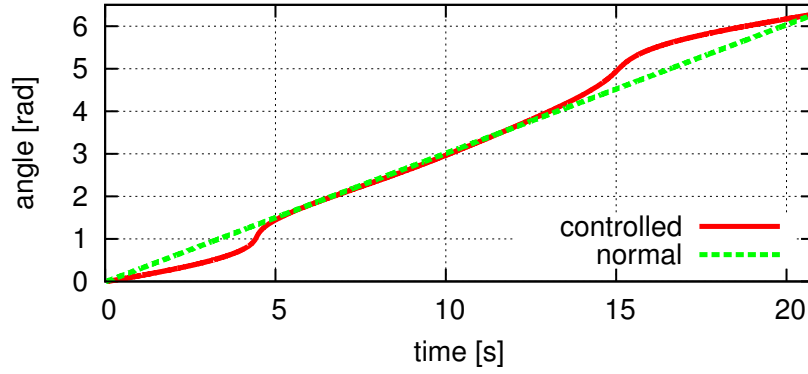


Fig. – 3.1 The time variation of the angle of the driving link.

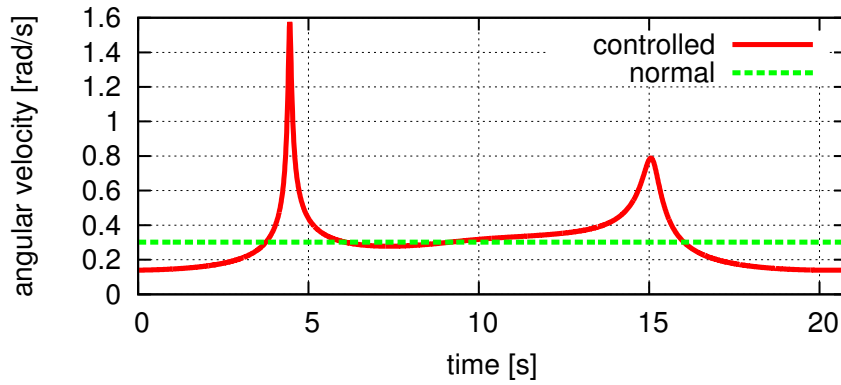


Fig. – 3.2 The time variation of the angular velocity of the driving link.

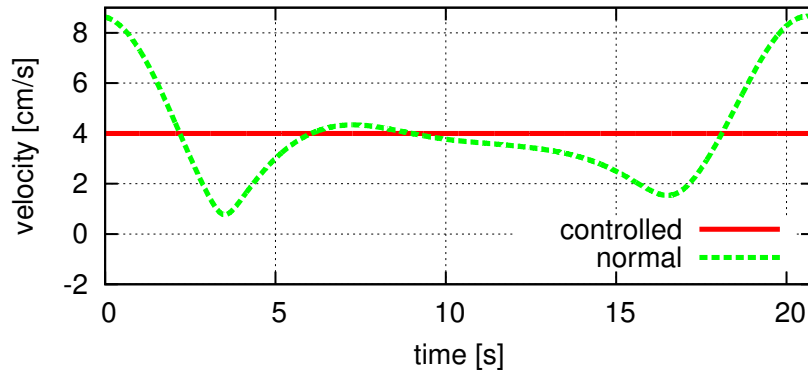


Fig. – 3.3 The time variation of the norm of the velocity vector of the toe.

From Fig. 3.3 and Fig. 3.4, it is confirmed that the norm of the velocity vector of the toe maintains the target velocity (4 cm/s) by utilizing the proposed method. Hence, the speed control of the toe can be realized by utilizing both the target angle shown in Fig. 3.1 and the target angular velocity shown in Fig. 3.2.

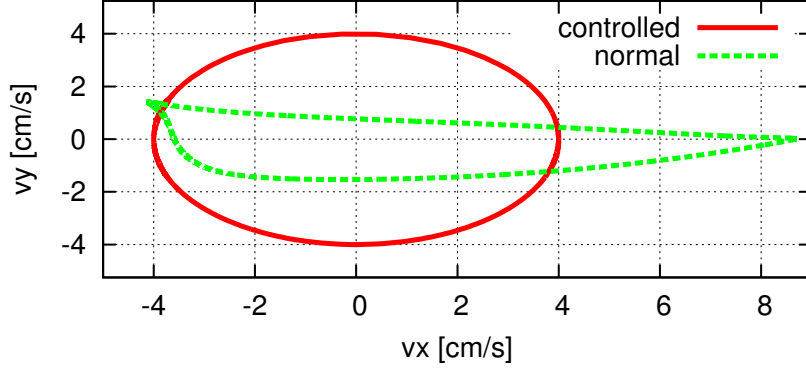


Fig. – 3.4 The trajectory of the norm of the velocity vector of the toe.

3.3 Application of Proposed Method

We have so far showed that the constant speed control of the toe can be realized by proposed method. This section applies the proposed method, and the angle trajectory capable of the speed control of the toe in horizontal direction is derived. For example, a multi-legged robot requires to control the relationship between COG and the toe position appropriately to maintain stability. However, it is difficult for a multi-legged robot with the Jansen linkage mechanisms to control considering the stability due to its complexity. Since the feed speeds of the toes can be controlled by this application method, the control considering the stability can be realized.

Let the target velocity of the toe in the horizontal direction is r_x . Then, we obtain unknown target velocity in the vertical direction r_y because the velocity of a closed linkage mechanism is determined uniquely. Moreover, since it is difficult to obtain r_y without solving the forward kinematics, r_y should be handled as unknown parameter. Thus, since it is difficult to obtain the norm of the target velocity in this situation, (3.5) cannot be solved. In the application method, (3.2) is focused. In equation, we define

$$\frac{\partial}{\partial \theta} \mathbf{Z}_{1,2,8}(\theta) \mathbf{p}_{1,2} := \begin{bmatrix} p_x \\ p_y \end{bmatrix},$$

and obtain as follows:

$$\begin{bmatrix} r_x \\ r_y \end{bmatrix} = \begin{bmatrix} p_x \\ p_y \end{bmatrix} \dot{\theta}. \quad (3.6)$$

From (3.6), since

$$r_x = p_x \dot{\theta},$$

the target driving link angle can be obtained as follows:

$$\theta = \int \frac{r_x}{p_x} dt. \quad (3.7)$$

By utilizing (3.7), in the case of the multi-legged robot as an example, since the velocity of the all supporting legs can be controlled arbitrarily, the walking control considering the stability of the robot can be realized.

3.4 Conclusion

This chapter has reported the toe speed control to achieve more complex tasks with the Jansen linkage mechanism. It has been proven that the norm of the toe speed bears a proportionate relationship to the angular velocity of the driving link. And, the angle trajectory of the driving link capable of the constant speed control of the toe of the Jansen linkage mechanism is generated by utilizing the relationship. In addition, it has been verified that the constant speed control of the toe can be realized by utilizing the derived angle trajectory through numerical simulation.

The angle trajectory capable of the speed control of the toe in horizontal direction has been derived as an application of the proposed method. By utilizing the application method, in the case of the multi-legged robot as an example, since the velocity of the all supporting legs can be controlled arbitrarily, the walking control considering the stability of the robot can be realized.

4 . An Approach to Gait Synchronization and Transition for Reconfigurable Walking Platforms

Legged robots based on one degree-of-freedom reconfigurable planar leg mechanisms, that are capable of generating multiple useful gaits, are highly desired due to the possibility of handling environments and tasks of high complexity while maintaining simple control schemes. An essential consideration in these reconfigurable legged robots is to attain stability in motion, at rest as well as while transforming from one configuration to another with the minimum number of legs as long as the full range of their walking patterns, resulting from the different gait cycles of their legs, is achieved. To this end, in this chapter, we present a method for the generation of input joint trajectories to properly synchronize the movement of quadruped robots with reconfigurable legs. The approach is exemplified in a four-legged robot with reconfigurable Jansen legs capable of generating up to six useful different gait cycles. The proposed technique is validated through simulated results that show the platform 's stability across its six feasible walking patterns and during gait transition phases, thus considerably extending the capabilities of the non-reconfigurable design.

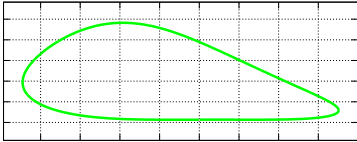
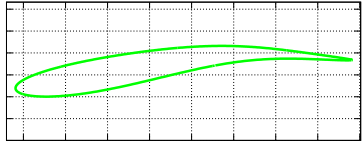
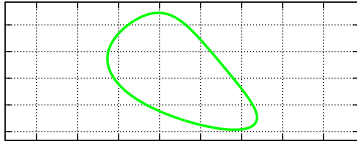
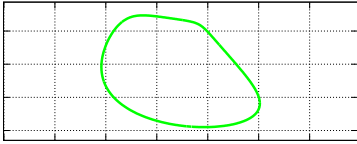
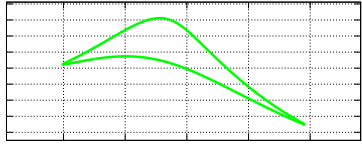
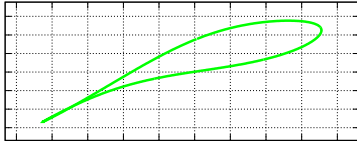
4.1 Specification of the Reconfigurable Jansen Platform

In this section, specifications of a developed reconfigurable Jansen legged robot are discussed. This reconfigurable walking platform is used herein as case study for the generation of input joint trajectories to synchronize multiple reconfigurable one-degree-

of-freedom legs for realizing stable walking gaits.

In a previous study, we reported a reconfigurable approach to robotic legged locomotion that produces a wide variety of gait curves, opening new possibilities for innovative applications [18]. Such robot can vary its hardware morphology by parametric changes of its link lengths. In particular, this reconfigurable linkage switches from a pin-jointed Grübler kinematic chain to a five degree-of-freedom mechanism with slider joints during the reconfiguration process. The identified novel gait patterns are shown in Table 4.1.

Table – 4.1 The identified novel gait patterns

Default curve	Digitigrade locomotion	Obstacle avoidance
		
<p>It is interesting to note that the standard foot trajectory of a Jansen leg resembles to the plantigrade locomotion of some terrestrial animals. In fact, this trajectory is quite similar to those of the ankles of rats [74].</p>	<p>The shape of this curve is quite similar to the gait cycle of a cat [79, Fig. 2]. Digitigrades tend to be very fast runners [78].</p>	<p>In this case, the height of the foot trajectory is a 36.74% of the total height of the leg.</p>
Jam avoidance	Step climbing	Drilling motion
		
<p>This type of trajectory is of interest because facing the soil with an arc shape, allows to look for a suitable support point at the same time.</p>	<p>This gamma-like pattern is appropriate for climbing steps.</p>	<p>This curve is of interest because its needle-like shape can be used for drilling activities.</p>

An essential consideration in most legged platforms that determines the required number of legs is the ability to attain stability both in motion and rest. Previous works related to legged platforms based on standard non-reconfigurable Jansen legs have overcome the

stability issues by utilizing more than four legs –*e.g.* [38]. However, increasing the number of legs gives rise to a range of other problems including greater cost and size, a more complex electro-mechanical control system, and maintenance issues. This problem becomes even more evident in the case of reconfigurable design approaches that realize different gaits via, for instance, changing dimensions of a set of links in the legs. Then, any increase in the number of legs directly contribute to the complexity of the entire system.

Given the discussed factors, the development of reconfigurable walking platforms with a minimum number of legs is a must. However, reconfigurable designs with less than four legs should be avoided in order to maintain simplicity and evade the related considerations of Zero Moment Point (ZMP) approaches for achieving static and/or dynamic stability [83–85]. In addition, in Jansen platforms, previous studies have shown the need to account for toe slipping while realizing walking patterns due to difference in speeds at which each leg moves [81]. Therefore, a ZMP-centered solution seems inappropriate. In consequence, a four-legged reconfigurable Jansen platform is considered for the analysis discussed in this work.

A novel mechanical approach for achieving dynamic walking stability in a standard four-legged Jansen platform has been previously proposed and validated [86]. In this approach, a special gear system is designed to enable 3 point leg contact with the ground surface at any time during the walking process, thus achieving stability. However, adopting the mechanical approach in a reconfigurable Jansen platform would require an additional gear module for each new gait produced or every configuration of the robot. An alternative control theoretic approach is here adopted to overcome the need for additional gear modules and associated mechanical complexities to achieve walking stability.

Figure 1.5 shows the CAD design of a four-legged reconfigurable Jansen platform. For details of the reconfigurable Jansen leg and its different gait cycles, the interested reader is addressed to [18]. In this robot, which possesses reconfigurable capabilities that result from the six gait patterns presented in Table 4.1, each leg is controlled independently by a rotary actuator. In next section, the formulation for the trajectory generation of input joints is presented.

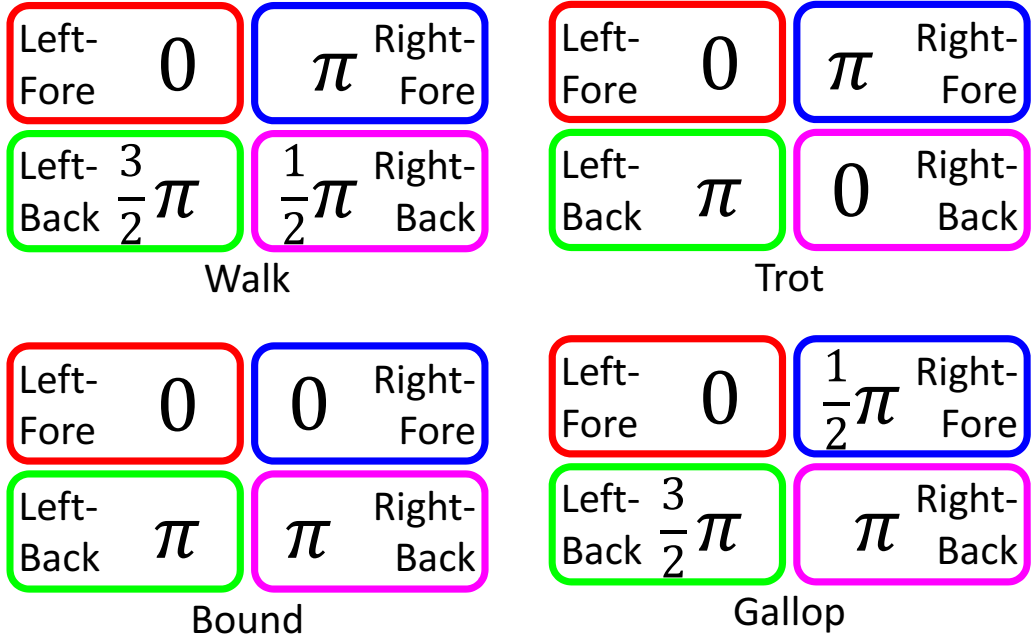


Fig. – 4.1 Walking patterns in quadruped robots

4.2 Design of The Trajectory Generator

A fifth degree polynomial interpolation generates a smooth trajectory from a starting point of a gait to an ending point as the speed and the acceleration are represented as fourth and third degrees respectively. Since, all trajectory parameters (position, speed and acceleration) in this approach are represented as a continuous function, load forces to the actuators can be decreased. Given these advantages, we use this technique for our generation of trajectories, an approach that has been successfully used previously in the community [87] [88] [89].

The trajectories of position $r(t)$, speed $\dot{r}(t)$ and acceleration $\ddot{r}(t)$ in terms of time t are defined as follows

$$r(t) = a_5 t^5 + a_4 t^4 + a_3 t^3 + a_2 t^2 + a_1 t + a_0, \quad (4.1)$$

$$\dot{r}(t) = 5a_5 t^4 + 4a_4 t^3 + 3a_3 t^2 + 2a_2 t + a_1, \quad (4.2)$$

$$\ddot{r}(t) = 20a_5 t^3 + 12a_4 t^2 + 6a_3 t + 2a_2, \quad (4.3)$$

where $a_i (i = 0, \dots, 5)$ represents coefficients and these are derived from initial states and final states of a given gait. The initial and the final states are defined as x_s and x_f

respectively, and it is assumed that the states are transformed in time $0 \sim T$ (constant) [s]. Using equations (4.1)-(4.3), the initial states at the starting time, a_0 , a_1 and a_2 are derived as follows

$$r(0) = a_0 = x_s, \quad (4.4)$$

$$\dot{r}(0) = a_1 = \dot{x}_s, \quad (4.5)$$

$$\ddot{r}(0) = 2a_2 = \ddot{x}_s. \quad (4.6)$$

Also, from the relation of the final states at the ending time, we have

$$r(T) = a_5 T^5 + a_4 T^4 + a_3 T^3 + a_2 T^2 + a_1 T + a_0 = x_f, \quad (4.7)$$

$$\dot{r}(T) = 5a_5 T^4 + 4a_4 T^3 + 3a_3 T^2 + 2a_2 T + a_1 = \dot{x}_f, \quad (4.8)$$

$$\ddot{r}(T) = 20a_5 T^3 + 12a_4 T^2 + 6a_3 T + 2a_2 = \ddot{x}_f. \quad (4.9)$$

By representing equations (4.7)-(4.9) as a matrix form, a_3 , a_4 and a_5 are derived as follows

$$\begin{bmatrix} a_5 \\ a_4 \\ a_3 \end{bmatrix} = A^{-1} \begin{bmatrix} x_f - x_s - \dot{x}_s T - \frac{\ddot{x}_s}{2} T^2 \\ \dot{x}_f - \dot{x}_s - \ddot{x}_s T \\ \ddot{x}_f - \ddot{x}_s \end{bmatrix}, \quad (4.10)$$

where

$$A = \begin{bmatrix} T^5 & T^4 & T^3 \\ 5T^4 & 4T^3 & 3T^2 \\ 20T^3 & 12T^2 & 6T \end{bmatrix}.$$

Our strategy for synchronization is designed based on the trajectory generator presented in this section. As the fifth degree polynomial interpolation can be calculated uniquely depending upon the initial conditions x_s , the final conditions x_f and the transformation time T , the synchronization strategy is therefore designed by defining these states.

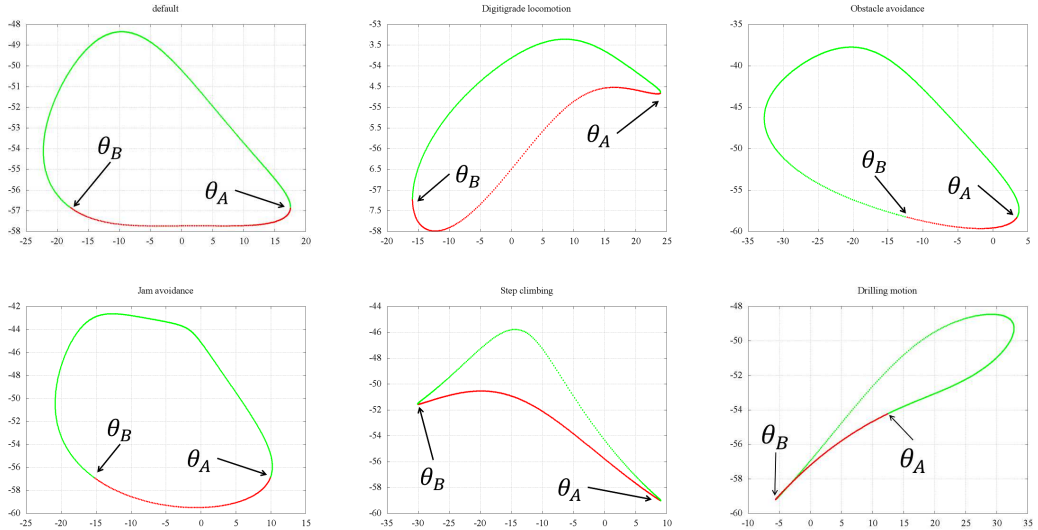


Fig. – 4.2 The switching angles of support leg and idling leg. The red and green curves represent the sections of the support leg and idling leg, respectively.

Table – 4.2 The switching angles of support leg and idling leg

	Default curve	Digitigrade locomotion	Obstacle avoidance	Jam avoidance	Step climbing	Drilling motion
θ_A [rad]	1.05	1.09	0.91	0.88	1.24	3.00
θ_B [rad]	5.55	4.97	$0.04+2\pi$	5.70	$5.05-2\pi$	$4.89-2\pi$

4.3 Synchronization

A leg synchronization strategy for realizing a set of stable walking gaits in reconfigurable quadruped Jansen platform is proposed. Several locomotion patterns are available from the literature for the case of a general quadruped robot as shown in Fig. 4.1 (adapted from [90]). Particularly, in this work, we focus on the synchronization strategy for the “walk” pattern. The other three patterns, that involve situations wherein only two legs contact the ground surface, are left for future work.

From Fig. 4.1, it can be observed that in walk there is a switch of the idling leg with phase of 90 degrees, and the switching sequence of the idling leg is “Left-Fore” \rightarrow “Right-Back” \rightarrow “Right-Fore” \rightarrow “Left-Back” \rightarrow “Left-Fore” \rightarrow , and so on. It could be concluded as well that the state sequences for the walk pattern has a constant phase, if the idling leg is assumed as a state. We use the trajectory generator introduced in section 4.2 to produce

Table – 4.3 Initial states of each leg for the synchronization (n : count of loop of PHASE, $\eta = (\theta_A - \theta_B + 2\pi)/3$)

	PHASE 1 [rad]	PHASE 2 [rad]	PHASE 3 [rad]	PHASE 4 [rad]	Speed [rad/s]
Left Fore	$\theta_A + 2\pi n$	$\theta_B + 2\pi n$	$\theta_B + \eta + 2\pi n$	$\theta_A - \eta + 2\pi(n + 1)$	η/T
Left Back	$\theta_A - 2\pi(n - 1)$	$\theta_A - \eta - 2\pi(n - 1)$	$\theta_B + \eta - 2\pi n$	$\theta_B - 2\pi n$	$-\eta/T$
Right Fore	$\theta_B + \eta + 2\pi(n - 1)$	$\theta_A - \eta + 2\pi n$	$\theta_A + 2\pi n$	$\theta_B + 2\pi n$	η/T
Right Back	$\theta_B + \eta - 2\pi n$	$\theta_B - 2\pi n$	$\theta_A - 2\pi n$	$\theta_A - \eta - 2\pi n$	$-\eta/T$

trajectories to move from one state to next one. Note that, since the walking platform under study is based on a one degree-of-freedom reconfigurable linkage, there is no need of a stabilization controller for the resulting trajectories.

Since the height of a leg in a platform that is based on a Jansen linkage depends only on the angle of the driving link, the angle of the input joint, say θ , the support leg and the idling leg can be switched depending on the value of such angle. In addition, the state transition can also be controlled by the angle of the driving link. For the purpose of defining the order of the states through naming convention, we define the states of the idling leg “Left-Fore”, “Right-Back”, “Right-Fore” and “Left-Back” as “PHASE 1”, “PHASE 2”, “PHASE 3”, and “PHASE 4”, respectively. The switch angles of the support and idling legs for gaits presented in Table 4.1 are presented in Figure 4.2 and Table 4.2.

In Figure 4.2, θ_A and θ_B are defined by the nature of each individual gait pattern. For the “default curve”, θ_A is defined by angle of curvature at the rightmost point of the gait pattern, and θ_B is defined by the angle of curvature at the equivalent point at same height on the vertical axis as θ_A . For the “Digitigrade locomotion” and “Step climbing”, θ_A is defined by the angle of curvature at the rightmost point of the gait pattern, and θ_B is defined by the angle of curvature at the leftmost point. For the “Obstacle avoidance” and “Jam avoidance”, θ_A and θ_B are defined by the angle of curvature at two points of the gait pattern that intersects an arbitrary threshold set on the vertical height axis whose value is chosen to be lower than the height of the rightmost point of the gait.

In the case of “Drilling motion”, θ_B is defined by the angle of curvature at the lowest vertical height point of the gait pattern and θ_A is defined by the angle of curvature of an arbitrary point on the right-center of the gait pattern. Such atypical angular values are utilized for the “Drilling motion” because the pattern represents a tooling task that

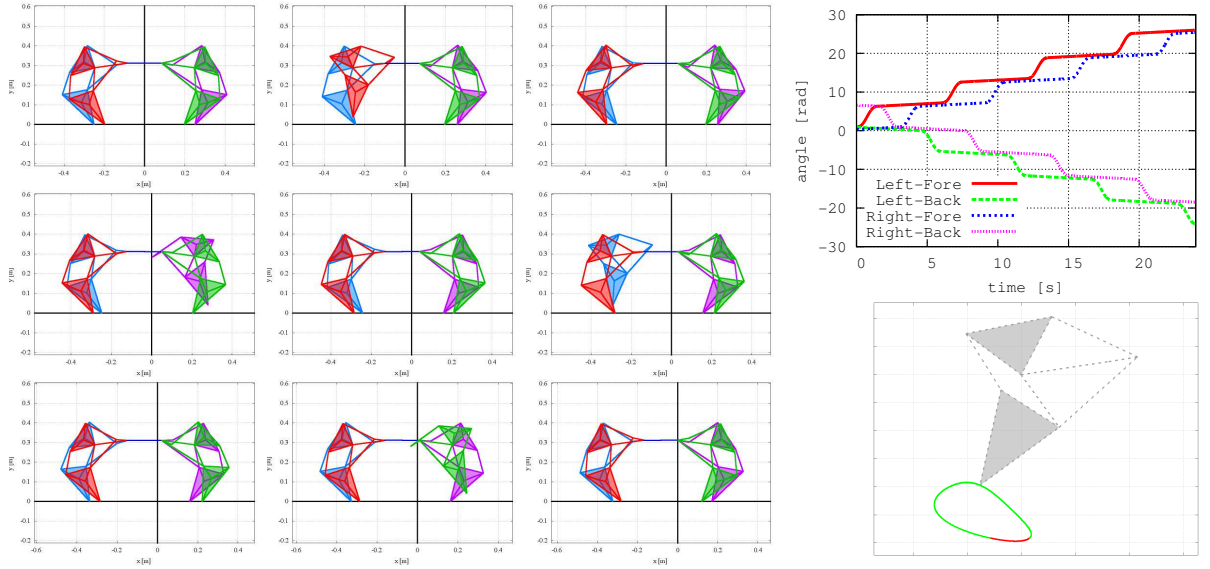


Fig. – 4.3 The simulation result of the synchronization for the stable walking (**left**). **Red leg** : Left-Fore leg. **Green leg** : Left-Back. **Blue leg** : Right-Fore. **Purple leg** : Right-Back. The generated trajectories for the driving link (**right-top**). The gait pattern of “Obstacle avoidance” (**right-bottom**).

is very different from walking, as it is the case in the other gait cycles. The initial states of each PHASE are presented in Table 4.3 and the final states of each PHASE are the initial states of next PHASE. By utilizing these initial and final states and the trajectory generator designed in section 4.2, the stable walking for the obstacle avoidance gait can be realized as shown in Figure 4.3.

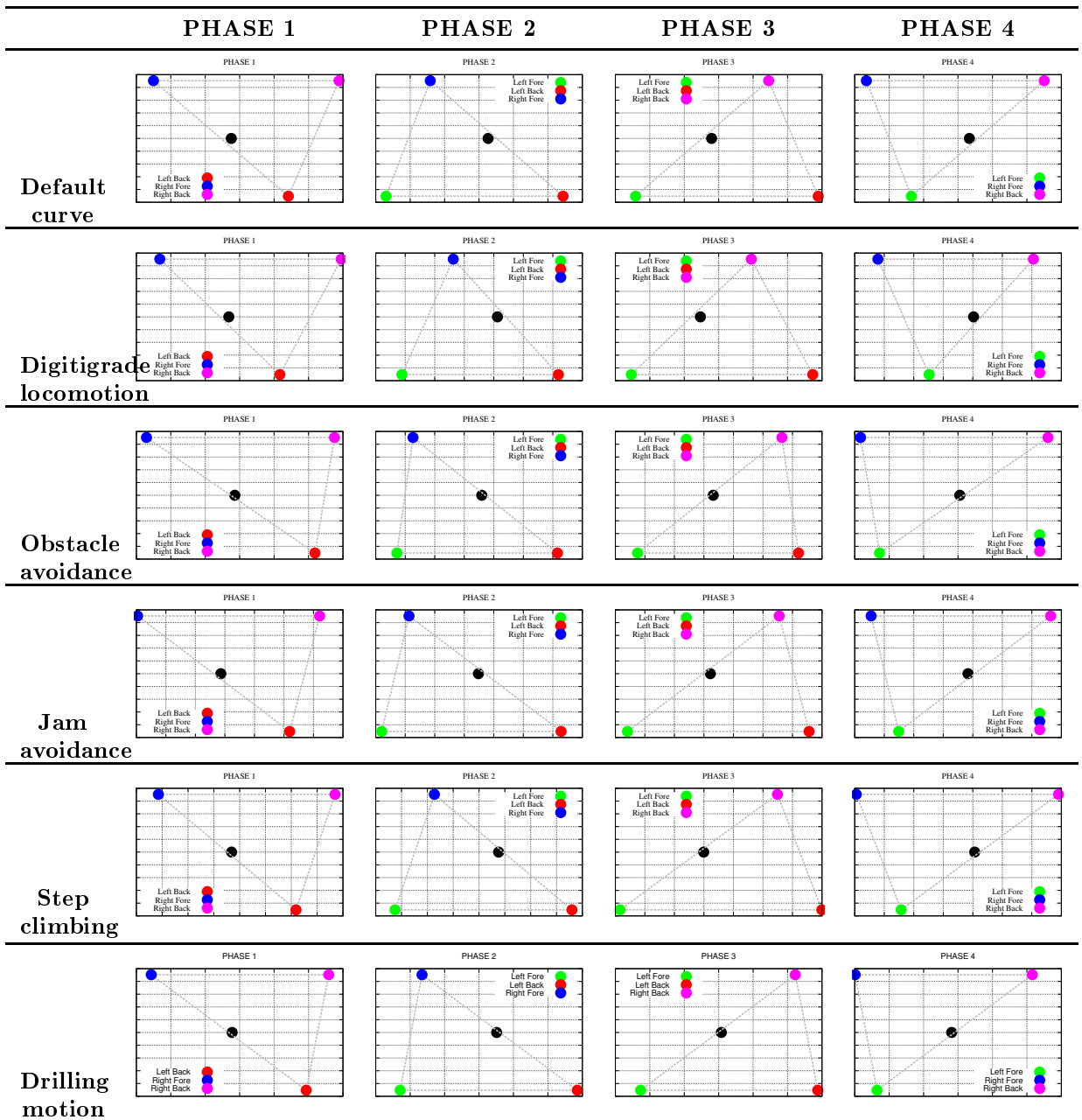
The proposed trajectory generator is useful in realizing a set of stable walking gaits achieved through synchronization of leg movements.

4.4 Static Stability Analysis of the Realized Gaits

This section presents the results of the static stability analysis for the intermediary phases of the walking gaits considered in this study. Relation between the support legs and center of gravity (COG) of the robot are presented in Table 4.4 where black points represents the COG of the robot, and red points, blue points, green points and purple points represents the contact point of the support legs, and the gray line represents the static stability zone.

These static stability results show the proposed approach generates walking gaits whose

Table – 4.4 Results of the static stability analysis of the synchronization



constituent phases possess static stability —observed by the existence of center of gravity within the static stability zone. However, low stability margins are witnessed in Table 4.4 when computed by known evaluation methods [91–93]. This results from the fact that the idling leg moves on a specific plane, and movements outside it cannot be physically achieved or controlled. Several solutions can be identified in order to improve such margins while maintaining the simplicity of control, for example, adding a horizontal moving weight in the body that moves away from the idling leg. In any case, this is an aspect

that deserves further research.

4.5 Characterization of Gait Transition

We have so far discussed leg synchronization problem associated with gait generation and stability analysis for a set of synthesized walking gaits in a reconfigurable Jansen platform. Another key challenge in such shaping shifting robots is to realize a stable gait transition. Two approaches have been put forward in the literature, [94] proposes a strategy that involves gait transition at rest (Static gait transition) and [95] studies gait transition while in motion (Dynamic gait transition). The static gait transition has obvious advantages allowing switching of gaits within a restricted space as well as increased stability due to the robot platform being at rest. On the other hand, the dynamic gait transition allows for a seamless switching of gaits as the process happens in motion without any disruption. In this chapter, we presents our experiments utilising both the static and dynamic approaches to gait transition. Both the approaches are compatible with the proposed trajectory generator where the transition of gaits is achieved by substituting the initial and final states together with the link dimension and angle of the driving link into the trajectory generator as discussed in Section 4. These set of associated variables are then defined namely, θ represents the angle of the driving link, l represents the length of the variable link (for example, it is $\overline{P_1P_2}$ and $\overline{P_7P_8}$ in the case of transitioning from “Obstacle avoidance” into “Jam avoidance”, see details in [18]), and y represents the height of whole leg. In addition, a prime added $'$ to these variables represents the state after transition.

4.5.1 Gait Transition I -*Static gait transition-*

In this method, the robot changes gait while at rest involving transitioning of all legs at the same time while in contact with the ground. Such an approach where the initial state of gait transition corresponds to the resting PHASE is set to ensure increased stability. In general, a gait transition in this case would start with bringing the robot platform to rest at the initial state of either one of the PHASE, realize gait transition and restart motion upon completion of the structural changes needed for the gait transition.

In the case of transitioning from PHASE $i(i = 1, \dots, 4)$ of pattern A to another pattern B ; θ, l on the PHASE $i(i = 1, \dots, 4)$ are defined as the angle of the driving link and length of the variable link at the initial state and θ', l' are defined as the values at the final state. These values are then fed to the proposed trajectory generators to achieve

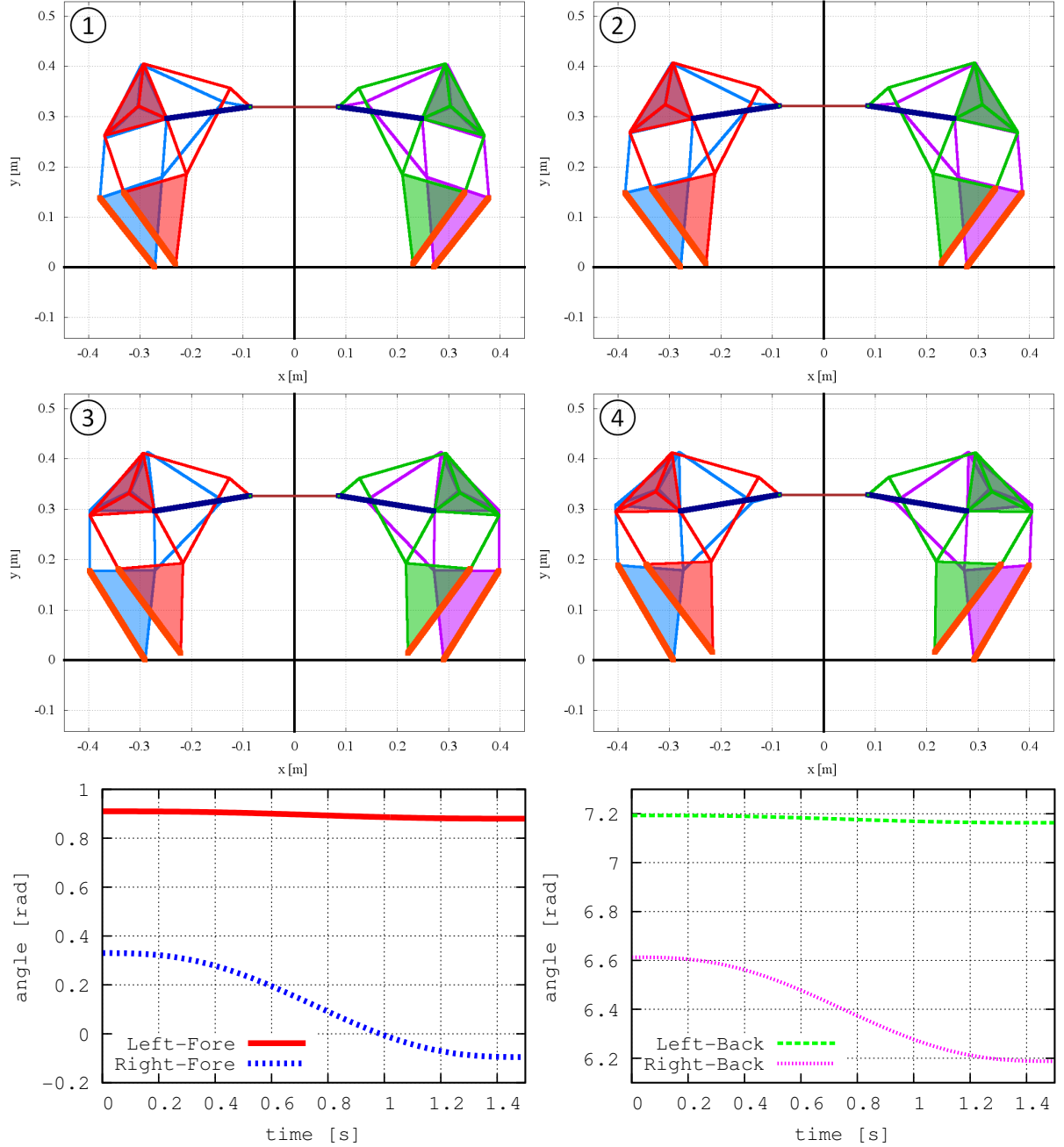


Fig. – 4.4 The transformation from “Obstacle avoidance” to “Jam avoidance” by Static Transformation. **Top:** Some steps of the transformation. The binary links of variable dimension are highlighted in orange-red and dark-blue. **Bottom:** The generated trajectories for the driving link.

synchronisation of legs for stable gait transition. Since it is assumed that the robot is at rest at the initial and final states, their velocity components are defined as $\dot{\theta} = 0$, $\dot{\theta}' = 0$, $\dot{\mathbf{l}} = 0$, $\dot{\mathbf{l}}' = 0$. Figure 4.4 presents the gait transition from “Obstacle avoidance” into “Jam avoidance” at rest as an example. The binary links of variable dimension are highlighted in orange-red and dark-blue in the presented figure.

4.5.2 Gait Transition II -*Dynamic gait transition-*

In this method, the gait transition occurs while in motion and specifically during walking in this case. The proposed trajectory generator as discussed in the previous sections is utilised to achieve synchronisation of the legs needs for stable gait transition. Gait transition in this case may involve legs in different configurations leading to large height difference between the supporting legs irrespective of having a same height of θ_A and θ_B set during the synchronisation phase. Other negative implications could involve supporting legs not coming in contact with the ground or idling leg coming in contact with the ground. To avoid these pitfalls, the height of the leg after transition is set to the same height of θ_A that exists before gait transition. In our previous study [18], the height of each leg in specific configuration was dependent directly on the angle of the driving link and the link dimensions while the gait transition always occurred at the lowest point of that gait pattern. On the other hand, in this study, the height of each leg in specific configuration is also adapted utilizing the designed trajectory generator as the gait transition occurs in the idling phase while the leg is not in contact with the ground.

The initial and final states of the idling leg is shown in Table 4.5, where $f(\theta, \mathbf{l})$ represents $\overline{P_1P_8}$ for the angle of the driving link θ and the link dimensions \mathbf{l} . And, the ones for the supporting legs are shown in Table 4.3, where the parameters of a transformed gait is used for the legs upon transition. Figure 4.5 presents the dynamic gait transition from “Obstacle avoidance” to “Jam avoidance” as an example. The binary links of variable dimension and the vertical movement of the grounded revolute joint centers are highlighted in orange-red, dark-blue, and light-green in the presented Figure.

Table – 4.5 The initial and final state of the idling leg in the Transformation in Walking. ($f(\theta, \mathbf{l})$: Length of $\overline{P_1 P_8}$)

	Variables	Initial states	Final states
θ	position[rad]	θ_A	θ'_B
	speed[rad/s]	$\pm\eta/T$	$\pm\eta'/T$
\mathbf{l}	position[%]	$\overline{P_i P_j} : a$	$\overline{P_i P_j} : 0$
		$\overline{P_m P_n} : 0$	$\overline{P_m P_n} : b$
	speed[%/s]	$\mathbf{0}$	$\mathbf{0}$
y	position[m]	0	$f(\theta_A, \mathbf{l}) - f(\theta'_B, \mathbf{l}')$
	speed[m/s]	0	0

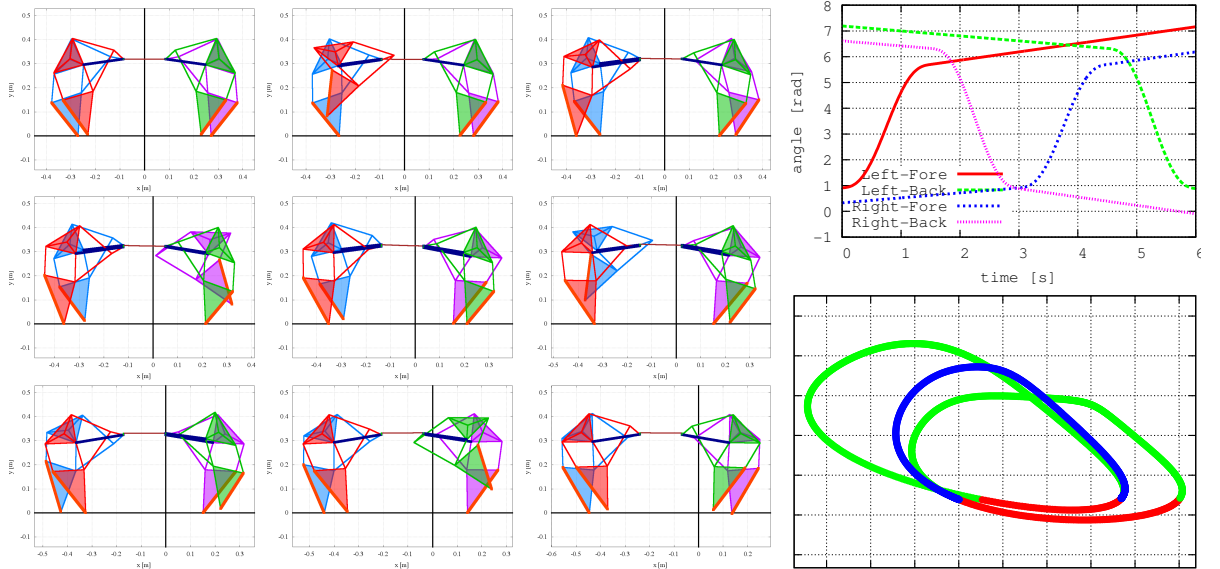


Fig. – 4.5 The transformation from “Obstacle avoidance” to “Jam avoidance” by Transformation in Walking. **Left:** Some steps of the transformation. The binary links of variable dimension are highlighted in orange-red and dark-blue. **Right-Top:** The generated trajectories for the driving link. **Right-Bottom:** The foot trajectory of leg “Left-Fore”. The green and red line represents the trajectory of the idling leg and the support leg, respectively. The blue line represents the foot trajectory under the transformation.

4.6 Stability Analysis of Gait Transition

This Section presents the static stability analysis for all gait transitions synthesized with our reconfigurable Jansen platform. Firstly, we will discuss the stability analysis of

the static gait transitions where the transformation occurs always on the initial state of the PHASE. As shown in Figure 4.2 and Table 4.3, the robot would maintain stability in the case of static gait transitions given that the legs are always in contact with the ground. Also, the use of sliding screw mechanism for achieving structural reconfiguration of the platform prohibits any instantaneous gait transitions and associated stability issues. As for the stability during dynamic gait transition, the relationship between the support legs and COG of the robot for all gait transitions are presented in Table 6. In case of PHASE 1 and PHASE 4, the static stability would be maintained as illustrated in Table 4.4 given that all support legs are in the same configuration before and after gait transition. Hence,

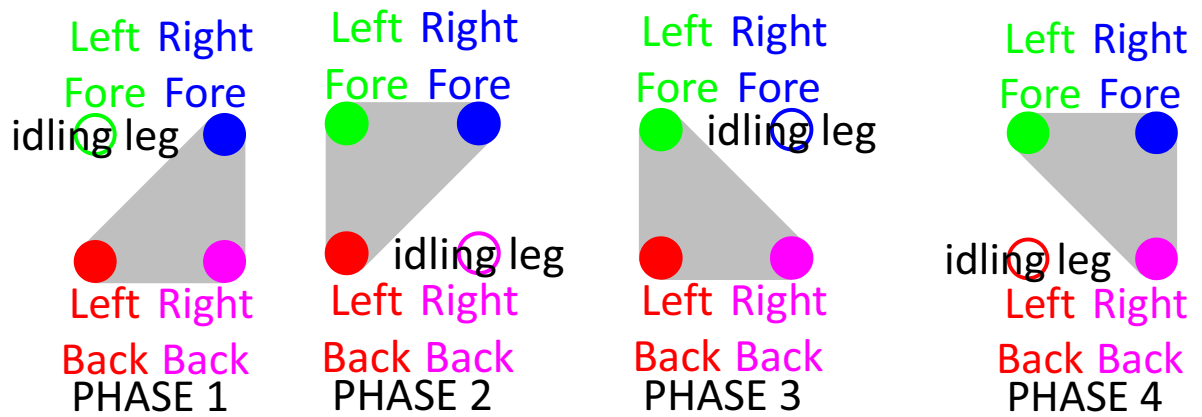


Fig. – 4.6 The variety of the supporting leg polygon of the quadruped robot. The gray area represents the static stability zone.

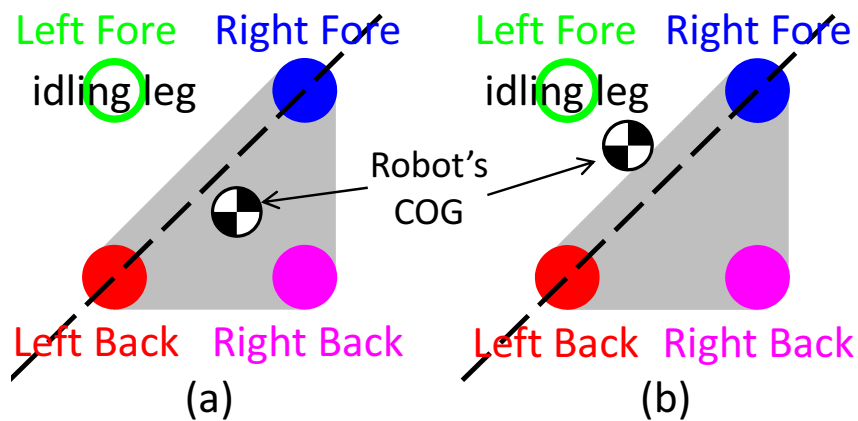


Fig. – 4.7 The positional relationship between a line on the 2 legs in opposing corner and the COG which is relevant to the static stability. If the COG exists in side of the support leg than the line, the robot is static stable.

the focus of our further discussion will be on the static stability analysis in the PHASE 2 and PHASE 3. Table 4.6 presents the stability analysis with respect to PHASE 2 where the black points represents the COG of the robot, whereas red points, blue points, green points and purple points represents the contacting point of the support legs, and gray line represents the static stability zone. From Table 4.6, it can be inferred that the proposed approach ensures stable gait transition in PHASE 2 while walking as the center of gravity always remains within the static stability zone.

Our quadruped robot always walks with three support leg and one idling leg forming a triangular supporting leg polygon. For such a configuration, the stability of the robot would be ensured if the COG falls within the supporting leg polygon. Our case involves four potential variants of triangular polygons as presented in Figure 4.6. When the COG of the robot exists at its center, then the positional relationship between a line connecting the two legs in opposing corners to which the COG is nearest and the COG directly impacts the static stability. In general as shown in Figure 4.7, if the COG exists inside the triangular polygon formed by the supporting legs and the line connecting the two legs in opposing corners to which the COG is nearest, then the robot is statically stable (Figure 4.7(a)) else unstable (Figure 4.7(b)). For situations involving gait transitions as shown in Figure 4.8 from gait *A* to gait *B*, our approach ensures that two of the supporting legs in opposing corners would always have the same configuration. Such an approach ensures

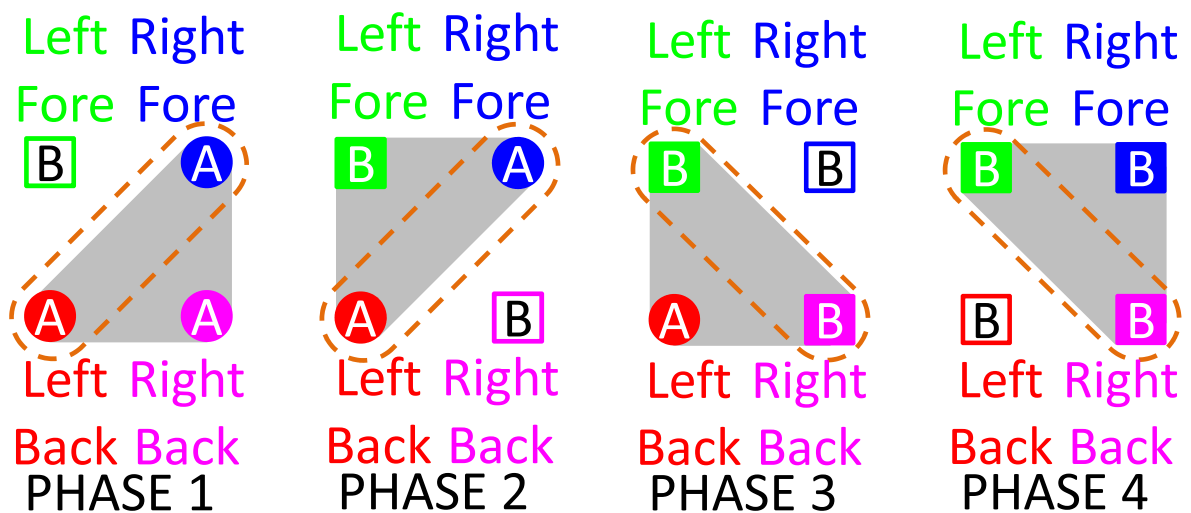
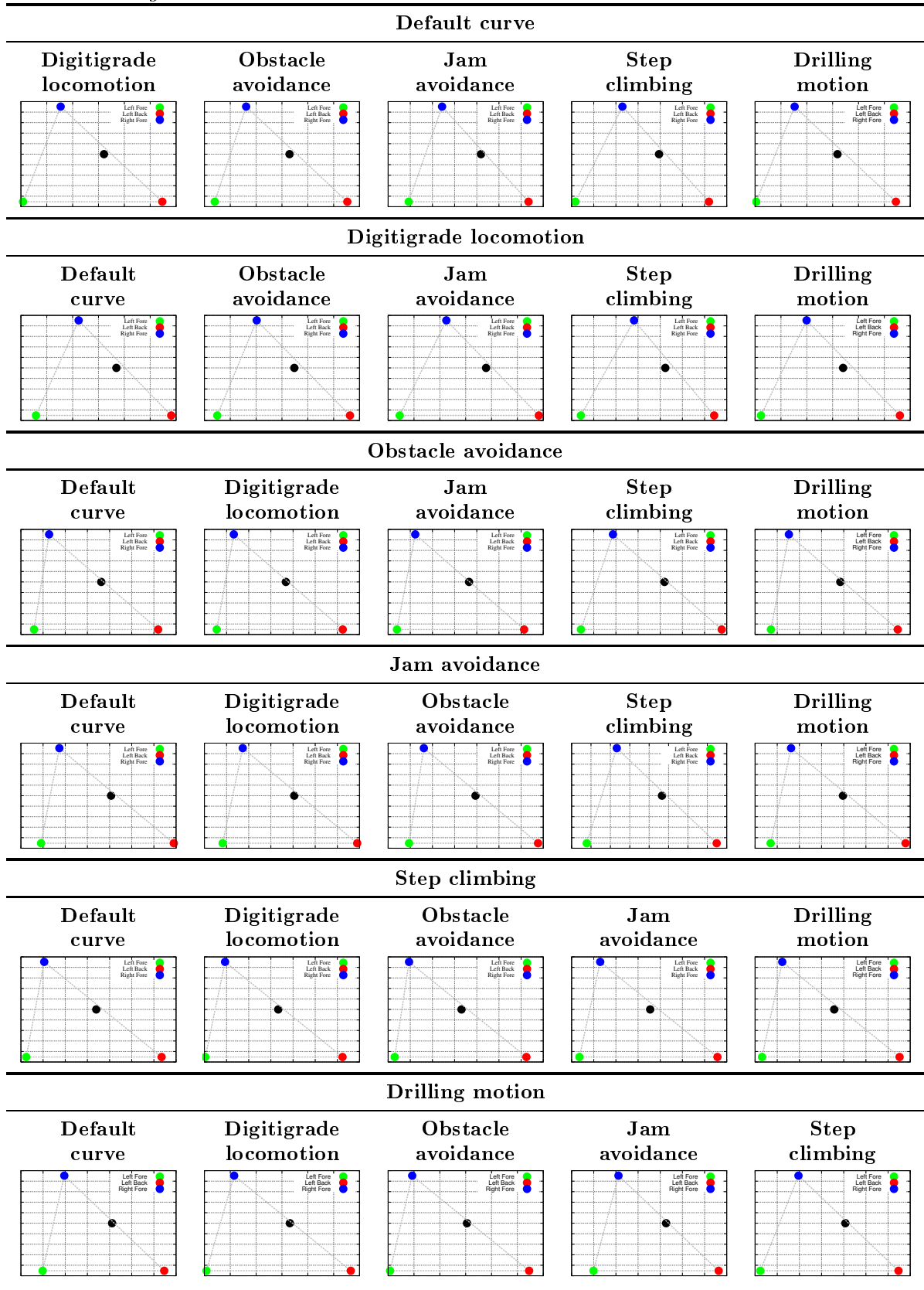


Fig. – 4.8 The variety of combination of the gait pattern. “A” within circle and “B” within square represents a gait pattern A and a gait pattern B, respectively.

Table – 4.6 Results of the static stability analysis of the gait transition II -*Dynamic gait transition-*



static stability while gait transition in motion with respect to PHASE 3. Thus, the static stability of the dynamic gait transition can be achieved by realizing static stability of the realized gaits and the stability in PHASE 1-4 of the gait transition.

4.7 Conclusion

An original design approach has been presented in this chapter towards development of a trajectory generator that realizes a set of stable walking gaits and gait transition for a reconfigurable Jansen platform. We have discussed a novel strategy to address the leg synchronization problem in this reconfigurable design and gait transition. Stability analysis is presented for prospective six gait patterns generated and all gait transitions by the reconfigurable platform and results discussed in view of validating the proposed approach. The ability to adapt to situations and produce appropriate stable gaits and switch between gaits would extend the capabilities of the robot beyond their intended application. A four-legged robot is currently being constructed to validate the robustness of the produced gaits and control approaches for real world deployments.

5 . Dynamic Modeling and Nonlinear Position Control of a Quadruped Robot with Theo Jansen Linkage Mechanisms

The Theo Jansen mechanism is gaining widespread popularity among the legged robotics community due to its scalable design, energy efficiency, low payload-to-machine-load ratio, bio-inspired locomotion, and deterministic foot trajectory. In this chapter, we perform dynamic modeling and analysis on a four-legged robot composed of the Theo Jansen mechanisms which is never done in the literature. The projection method is applied to derive the dynamic model because of its powerfulness in modeling such complicated system. Then a position control strategy is proposed based on energy control. Finally, numerical simulations validate the efficacy of the designed controller.

5.1 Free-Fall Model

The schematic diagram of the quadruped robot is shown in Fig. 5.1. This quadruped robot is composed of four Jansen linkage mechanisms and five gears which is driven by only one input to the bright yellow gear. The colors of red, blue, green, and purple represent legs of Left-Fore, Right-Fore, Left-Back, and Right-Back respectively. As a matter of practical convenience, we define $i = r, l$ and $j = f, b$ in this chapter unless otherwise noted where r, l, f , and b represent the right leg, left leg, fore leg, and back leg, respectively. The robot contacts with the ground on only toes, and x axis represents the ground. Because the four legs are the same Jansen linkage mechanisms, the free-falling model of the whole robot is derived by establishing the dynamic models of the single Jansen linkage and the gear system independently and then integrating the two models.

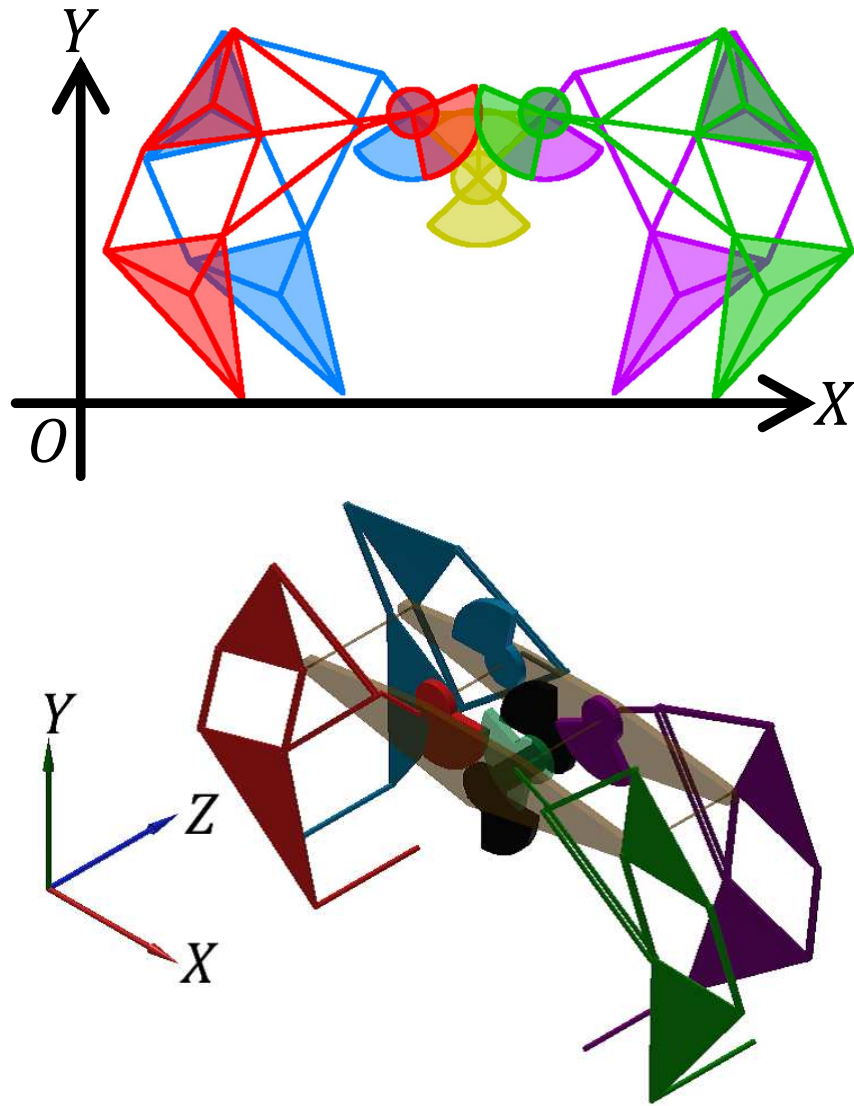


Fig. – 5.1 Schematic diagram of the quadruped robot composed of four Jansen linkage mechanisms and five gears which is driven by only one input to the bright yellow gear. The red, sky blue, green, and purple represent Left-Fore, Right-Fore, Left-Back, and Right-Back respectively.

5.1.1.1 Dynamic Model of Jansen Linkage Mechanism

The schematic diagram and the coordinate system of a single Jansen linkage mechanism are illustrated in Fig. 5.2. The physical parameters of the Jansen linkage mechanisms are tabulated in Table 5.1. The lengths of links adopted for the design in this study are listed in Table 5.3 [18]. It is assumed that the gravity center of every link locates on the center of the specified link, and the gravity center of each triangle locate on vertex of three median lines. The angle between the gravity center and the corners of the triangle, and the length from the gravity center to the corners of the triangle are calculated utilizing

the law of cosines and are given in Table 5.2.

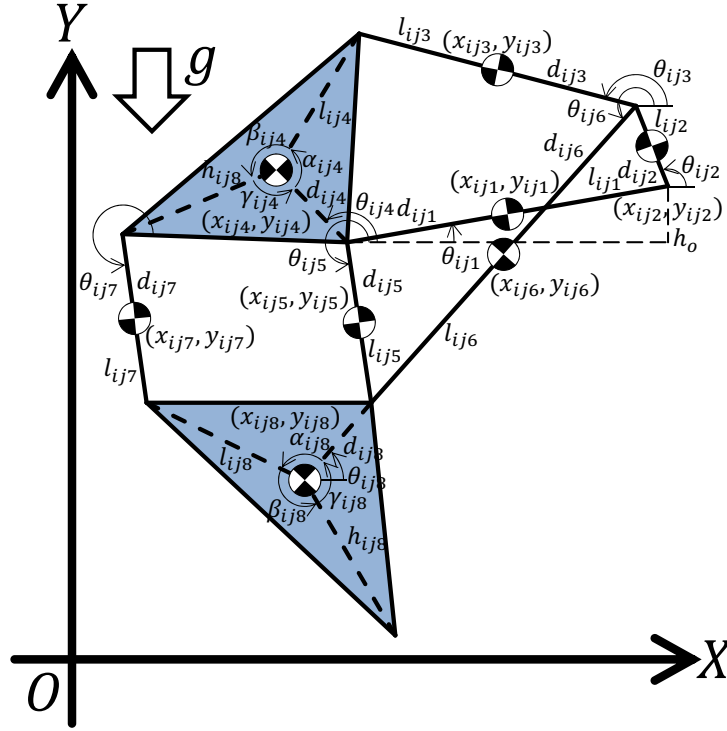


Fig. – 5.2 Schematic diagram of the Theo Jansen linkage mechanism with all parameters defined. The solid lines $l_{ij1}, l_{ij2}, l_{ij3}, l_{ij5}, l_{ij6}, l_{ij7}$ are the links; the two blue triangular parts are treated as the mass components; the dashed lines connect the gravity center of the mass and the corners of the triangle parts.

Table – 5.1 Physical parameters of the Theo Jansen linkage mechanism. ($\zeta, \xi = 1, \dots, 8$)

Parameter	Notation	Value
Inertia moment [kg·m ²]	$J_{ij\zeta}$	0.01
Mass [kg]	$m_{ij\zeta}$	0.1
Viscous friction coefficient [Nm·s/rad]	$C_{ij\zeta\xi}$	0.01
Height of link-1 [m]	h_0	0.02316
Length of link [m]	$L_{1, \dots, 12}$	
Length from extremity to gravity center [m]	$d_{ij\zeta}$	
Length from gravity center to end [m]	$l_{ij\zeta}$	
Length from gravity center to corner of triangle [m]	$d_{ij\{4,8\}}$ $l_{ij\{4,8\}}$ $h_{ij\{4,8\}}$	
Central angle of triangle [m]	$\alpha_{ij\{4,8\}}$ $\beta_{ij\{4,8\}}$ $\gamma_{ij\{4,8\}}$	

To construct the constraint-free dynamic model based on Fig. 5.2, first of all, the

Table – 5.2 Kinematic parameters of the Theo Jansen linkage mechanism

Parameter	Value
d_{ij4}	0.0606657 m
l_{ij4}	0.0844427 m
h_{ij4}	0.0882124 m
d_{ij8}	0.0739384 m
l_{ij8}	0.102658 m
h_{ij8}	0.126316 m
α_{ij4}	1.87097 rad
β_{ij4}	2.4248 rad
γ_{ij4}	1.98742 rad
α_{ij8}	1.57408 rad
β_{ij8}	2.51629 rad
γ_{ij8}	2.19281 rad

Table – 5.3 The lengths of links adopted for the Theo Jansen linkage mechanism of this study

Link	Value (m)
L_1	0.16218
L_2	0.05417
L_3	0.174425
L_4	0.117645
L_5	0.12567
L_6	0.11754
L_7	0.12671
L_8	0.17974
L_9	0.19161
L_{10}	0.16169
L_{11}	0.11967
L_{12}	0.217995

generalized coordinate of this system is defined as

$$\mathbf{x}_{pij} = \left[\theta_{ij1} \quad x_{ij1} \quad y_{ij1} \quad \cdots \quad \theta_{ij8} \quad x_{ij8} \quad y_{ij8} \right]^T, \quad (5.1)$$

where $\theta_{ijk}(k = 1, \dots, 8)$ represents the absolute angle of each link, and $(x_{ijk}, y_{ijk})(k = 1, \dots, 8)$ represents the absolute coordinate of each link. The translational and rotational motions of each constraint-free object that forms the robot are expressed in the vector form with the generalized coordinate (5.1) as presented below,

$$\mathbf{M}_{ij} \ddot{\mathbf{x}}_{pij} = \mathbf{h}_{ij}, \quad (5.2)$$

where the generalized mass matrix \mathbf{M}_{ij} and the generalized force matrix \mathbf{h}_{ij} are defined as

$$\mathbf{M}_{ij} = \text{diag}(J_{ij1}, m_{ij1}, m_{ij1}, \dots, J_{ij8}, m_{ij8}, m_{ij8}),$$

$$\mathbf{h}_{ij} = \begin{bmatrix} C_{ij12}\dot{\phi}_{ij12} + C_{ij14}\dot{\phi}_{ij14} \\ 0 \\ -m_{ij1}g \\ -C_{ij12}\dot{\phi}_{ij12} + C_{ij23}\dot{\phi}_{ij23} \\ 0 \\ -m_{ij2}g \\ -C_{ij23}\dot{\phi}_{ij23} + C_{ij34}\dot{\phi}_{ij34} + C_{ij36}\dot{\phi}_{ij36} \\ 0 \\ -m_{ij3}g \\ -C_{ij14}\dot{\phi}_{ij14} - C_{ij34}\dot{\phi}_{ij34} + C_{ij45}\dot{\phi}_{ij45} + C_{ij47}\dot{\phi}_{ij47} \\ 0 \\ -m_{ij4}g \\ -C_{ij45}\dot{\phi}_{ij45} + C_{ij56}\dot{\phi}_{ij56} + C_{ij58}\dot{\phi}_{ij58} \\ 0 \\ -m_{ij5}g \\ -C_{ij36}\dot{\phi}_{ij36} - C_{ij56}\dot{\phi}_{ij56} + C_{ij68}\dot{\phi}_{ij68} \\ 0 \\ -m_{ij6}g \\ -C_{ij47}\dot{\phi}_{ij47} + C_{ij78}\dot{\phi}_{ij78} \\ 0 \\ -m_{ij7}g \\ -C_{ij68}\dot{\phi}_{ij68} - C_{ij78}\dot{\phi}_{ij78} \\ 0 \\ -m_{ij8}g \end{bmatrix},$$

where $\dot{\phi}_{ij\zeta\xi} = \dot{\theta}_{ij\xi} - \dot{\theta}_{ij\zeta}$, ($\zeta, \xi = 1, \dots, 8$).

In the next step, the constraint matrix \mathbf{C}_{ij} which holds $\mathbf{C}_{ij}\dot{\mathbf{x}}_{pij} = 0$ is derived from constraint conditions. The coordinates of the gravity center and the length of each link satisfy a certain relationship geometrically. By taking into account these geometric rela-

tionships, the holonomic constraints are formulated as follows:

$$\Phi_{hij} = \begin{bmatrix} x_{ij2} - x_{ij1} - l_{ij1} \cos \theta_{ij1} - d_{ij2} \cos \theta_{ij2} \\ y_{ij2} - y_{ij1} - l_{ij1} \sin \theta_{ij1} - d_{ij2} \sin \theta_{ij2} \\ x_{ij3} - x_{ij2} - l_{ij2} \cos \theta_{ij2} - d_{ij3} \cos \theta_{ij3} \\ y_{ij3} - y_{ij2} - l_{ij2} \sin \theta_{ij2} - d_{ij3} \sin \theta_{ij3} \\ x_{ij4} - x_{ij3} - l_{ij3} \cos \theta_{ij3} - l_{ij4} \cos(\theta_{ij4} + \alpha_{ij4}) \\ y_{ij4} - y_{ij3} - l_{ij3} \sin \theta_{ij3} - l_{ij4} \sin(\theta_{ij4} + \alpha_{ij4}) \\ x_{ij4} - x_{ij1} + d_{ij1} \cos \theta_{ij1} - d_{ij4} \cos \theta_{ij4} \\ y_{ij4} - y_{ij1} + d_{ij1} \sin \theta_{ij1} - d_{ij4} \sin \theta_{ij4} \\ x_{ij5} - x_{ij1} + d_{ij1} \cos \theta_{ij1} - d_{ij5} \cos \theta_{ij5} \\ y_{ij5} - y_{ij1} + d_{ij1} \sin \theta_{ij1} - d_{ij5} \sin \theta_{ij5} \\ x_{ij6} - x_{ij5} - l_{ij5} \cos \theta_{ij5} + l_{ij6} \cos \theta_{ij6} \\ y_{ij6} - y_{ij5} - l_{ij5} \sin \theta_{ij5} + l_{ij6} \sin \theta_{ij6} \\ x_{ij6} - x_{ij2} - l_{ij2} \cos \theta_{ij2} - d_{ij6} \cos \theta_{ij6} \\ y_{ij6} - y_{ij2} - l_{ij2} \sin \theta_{ij2} - d_{ij6} \sin \theta_{ij6} \\ x_{ij7} - x_{ij4} + h_{ij4} \cos(\theta_{ij4} - \gamma_{ij4}) - d_{ij7} \cos \theta_{ij7} \\ y_{ij7} - y_{ij4} + h_{ij4} \sin(\theta_{ij4} - \gamma_{ij4}) - d_{ij7} \sin \theta_{ij7} \\ x_{ij8} - x_{ij5} - l_{ij5} \cos \theta_{ij5} + d_{ij8} \cos \theta_{ij8} \\ y_{ij8} - y_{ij5} - l_{ij5} \sin \theta_{ij5} + d_{ij8} \sin \theta_{ij8} \\ x_{ij8} - x_{ij7} - l_{ij7} \cos \theta_{ij7} + l_{ij8} \cos(\theta_{ij8} + \alpha_{ij8}) \\ y_{ij8} - y_{ij7} - l_{ij7} \sin \theta_{ij7} + l_{ij8} \sin(\theta_{ij8} + \alpha_{ij8}) \end{bmatrix} = 0.$$

Then the constraint matrix is defined as

$$C_{ij} := \frac{\partial \Phi_{hij}}{\partial \mathbf{x}_{pij}}. \quad (5.3)$$

The constraint dynamical system can thus be formulated by adding the constraint term (5.3) with Lagrange's multipliers λ_{ij} to (5.2) as

$$\mathbf{M}_{ij} \ddot{\mathbf{x}}_{pij} = \mathbf{h}_{ij} + \mathbf{C}_{ij}^T \lambda_{ij}. \quad (5.4)$$

Moreover, the degrees of freedom of the unconstrained system is found to be 24 from (5.1). The degrees of freedom should be constrained by 20 holonomic constraints in this system. Therefore, the degrees of freedom of the constrained dynamical system (5.4) is 4.

The tangent speed of the constrained system is denoted as,

$$\dot{\mathbf{q}}_{ij} = \begin{bmatrix} \dot{\theta}_{ij1} & \dot{x}_{ij1} & \dot{y}_{ij1} & \dot{\theta}_{ij2} \end{bmatrix}^T.$$

Setting a partition symbolically as $\mathbf{v} = \begin{bmatrix} \dot{\mathbf{q}}_{ij}^T & \mathbf{v}_{Dij}^T \end{bmatrix}^T$ where \mathbf{v}_{Dij} shows dependent velocities with respect to $\dot{\mathbf{q}}_{ij}$. \mathbf{C}_{ij} is decomposed into $\mathbf{C}_{ij} = \begin{bmatrix} \mathbf{C}_{ij1} & \mathbf{C}_{ij2} \end{bmatrix}$ satisfying $\mathbf{C}_{ij}\dot{\mathbf{x}}_{pij} = \mathbf{C}_{ij1}\dot{\mathbf{q}}_{ij} + \mathbf{C}_{ij2}\mathbf{v}_{Dij}$. \mathbf{D}_{ij} is the orthogonal complement matrix to \mathbf{C}_{ij} satisfying $\mathbf{C}_{ij}\mathbf{D}_{ij} = 0$, $\dot{\mathbf{x}}_{pij} = \mathbf{D}_{ij}\dot{\mathbf{q}}_{ij}$, and

$$\mathbf{D}_{ij} = \begin{bmatrix} \mathbf{I}^{4 \times 4} \\ -\mathbf{C}_{ij2}^{-1}\mathbf{C}_{ij1} \end{bmatrix},$$

where $\mathbf{I}^{4 \times 4}$ represents the identity matrix $\mathbf{I} \in \mathbf{R}^{4 \times 4}$.

Finally, multiplying (5.4) by \mathbf{D}_{ij}^T from the left side and substituting the coordinate transformation $\dot{\mathbf{x}}_{pij} = \mathbf{D}_{ij}\dot{\mathbf{q}}_{ij}$ into (5.4) can eliminate the constraint term with λ_{ij} , and the dynamic model of the Jansen Linkage Mechanism is

$$\mathbf{D}_{ij}^T \mathbf{M}_{ij} \mathbf{D}_{ij} \ddot{\mathbf{q}}_{ij} + \mathbf{D}_{ij}^T \mathbf{M}_{ij} \dot{\mathbf{D}}_{ij} \dot{\mathbf{q}}_{ij} = \mathbf{D}_{ij}^T \mathbf{h}_{ij}. \quad (5.5)$$

5.1.2 Dynamic Model of Gear System

After the establishment of the dynamic model of the Jansen Linkage Mechanism, the dynamic model of the gear system [86] is derived following the same steps as Section 5.1.1. Table 5.4 gives the notations and values of the physical parameters of the gear system. Fig. 5.3 illustrates the schematic diagram and coordinate system of the gear system consisting of six gears where the subscripts ι and m represent the frame of the gears and the driving gears including, respectively. The two driving gears are driven by an actuator and rotate synchronously. Meanwhile, the four driven gears are driven by the two driving gears. The frame is used to fix all the gears. All gears are non-circular gears [96–98] which vary their gear ratios during rotation, but the driven gears rotate one revolution with respect to one revolution of the driving gear. In addition, the gear ratio of each gear varies depending on the angle between the driving gear and the gear frame.

Table – 5.4 Physical parameters of the gear system.

Parameter	Notation	Value
Inertia moment [kg·m ²]	J_l	0.01
	J_m	0.01
	J_{ij}	0.01
Mass [kg]	m_l	1.0
	m_m	0.1
	m_{ij}	0.1
Viscous friction coefficient [Nm·s/rad]	C_l	0.01
	C_m	0.01
	C_{ij}	0.01
Center distance of gears [m]	d	0.1
Length of frame [m]	l_m	$d/\sqrt{2}$
	l_{ij}	$d/\sqrt{2}$
Radius of gears [m]	r_{mij}	
	r_{ij}	

Based on these conditions, the gear ratio is defined as:

$$r_{mij} = \begin{cases} d \frac{\theta_B - \theta_A}{\theta_B - \theta_A + \pi/2}, & \text{(High Speed Ratio),} \\ d \frac{\theta_A + 2\pi - \theta_B}{\theta_A + 2\pi - \theta_B + 3\pi/2}, & \text{(Low Speed Ratio),} \end{cases}$$

$$r_{ij} = \begin{cases} d \frac{\pi/2}{\theta_B - \theta_A + \pi/2}, & \text{(High Speed Ratio),} \\ d \frac{3\pi/2}{\theta_A + 2\pi - \theta_B + 3\pi/2}, & \text{(Low Speed Ratio),} \end{cases}$$

where, θ_A and θ_B are with respect to each gait pattern of the Jansen linkage mechanism ($\theta_A = 1.05$ rad and $\theta_B = 5.55$ rad in this chapter).

The constraint-free model is derived according to Fig. 5.3 with parameters defined in Table 5.4. The generalized coordinate of this system is given:

$$\mathbf{x}_{pg} = [\theta_l \quad x_l \quad y_l \quad \theta_m \quad x_m \quad y_m \quad \theta_{ij} \quad x_{ij} \quad y_{ij}]^T, \quad (5.6)$$

where, $\theta_{l,m,ij}$ and $(x_{l,m,ij}, y_{l,m,ij})$ represent the absolute angles and coordinates of the gear frame, the driving and driven gears, respectively. With the generalized coordinate (5.6),

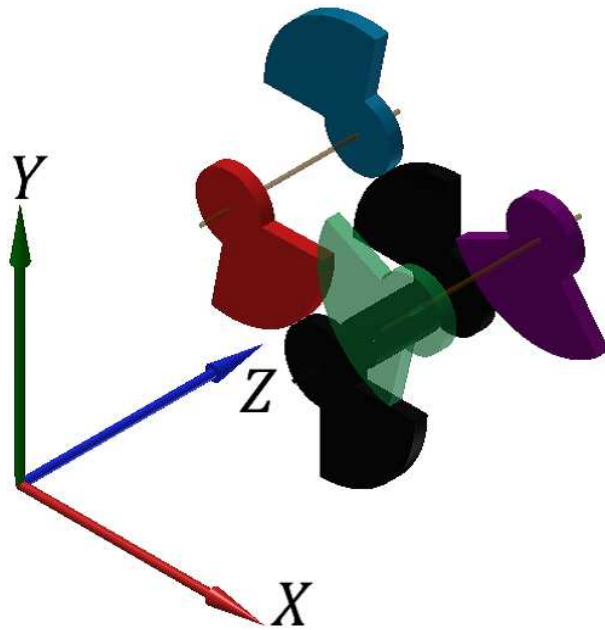
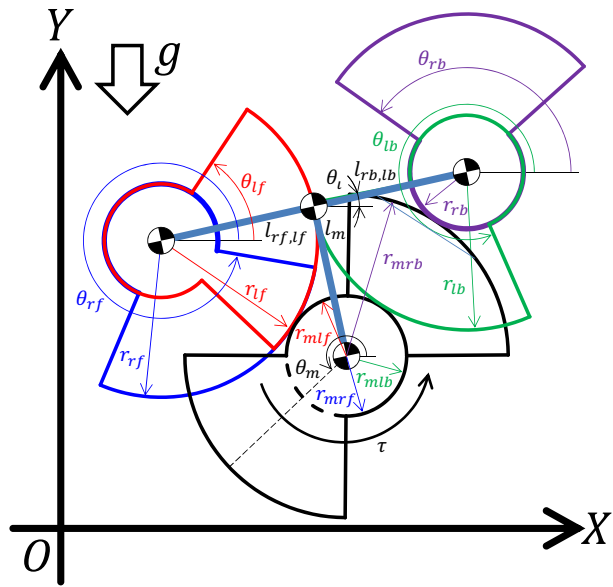


Fig. – 5.3 Schematic diagram of the gear system with parameters defined. The black-margined gear represents the driving gear, and the other gears represent the driven gears.

equations of motion concerned with the gear system are formulated below:

$$M_g \ddot{x}_{pg} = h_g, \quad (5.7)$$

where

$$M_g = \text{diag}(J_l, m_l, m_l, J_m, m_m, m_m, J_{ij}, m_{ij}, m_{ij}),$$

and

$$\mathbf{h}_g = \begin{bmatrix} -\tau + C_m(\dot{\theta}_l - \dot{\theta}_m) + C_{ij}(\dot{\theta}_l - \dot{\theta}_{ij}) \\ 0 \\ -m_l g \\ \tau - C_m(\dot{\theta}_l - \dot{\theta}_m) \\ 0 \\ -m_m g \\ -C_{rf}(\dot{\theta}_l - \dot{\theta}_{rf}) \\ 0 \\ -m_{rf} g \\ -C_{rb}(\dot{\theta}_l - \dot{\theta}_{rb}) \\ 0 \\ -m_{rb} g \\ -C_{lf}(\dot{\theta}_l - \dot{\theta}_{lf}) \\ 0 \\ -m_{lf} g \\ -C_{lb}(\dot{\theta}_l - \dot{\theta}_{lb}) \\ 0 \\ -m_{lb} g \end{bmatrix},$$

with τ representing the input torque.

The coordinates of the gravity center and the length of each link are correlated geometrically. And the rotation angles and radius of gears also conform to some relationship. Based on these relationships, the holonomic constraints are formulated as follows: For the gravity centers and gear ratio, the holonomic constraints are formulated as follows:

$$\Phi_{hg} = \begin{bmatrix} x_m - x_l - l_m \sin \theta_l \\ y_m - y_l - l_m \cos \theta_l \\ \theta_{rf} + \frac{r_{mrf}}{r_{rf}} \theta_m - \frac{r_{mrf} + r_{rf}}{r_{rf}} \theta_l \\ x_{rf} - x_l + l_{rf} \cos \theta_l \\ y_{rf} - y_l + l_{rf} \sin \theta_l \\ \theta_{rb} + \frac{r_{mrb}}{r_{rb}} \theta_m - \frac{r_{mrb} + r_{rb}}{r_{rb}} \theta_l \\ x_{rb} - x_l - l_{rb} \cos \theta_l \\ y_{rb} - y_l - l_{rb} \sin \theta_l \\ \theta_{lf} + \frac{r_{mlf}}{r_{lf}} \theta_m - \frac{r_{mlf} + r_{lf}}{r_{lf}} \theta_l \\ x_{lf} - x_l + l_{lf} \cos \theta_l \\ y_{lf} - y_l + l_{lf} \sin \theta_l \\ \theta_{lb} + \frac{r_{mlb}}{r_{lb}} \theta_m - \frac{r_{mlb} + r_{lb}}{r_{lb}} \theta_l \\ x_{lb} - x_l - l_{lb} \cos \theta_l \\ y_{lb} - y_l - l_{lb} \sin \theta_l \end{bmatrix} = 0.$$

The corresponding constraint matrix \mathbf{C}_g which holds $\mathbf{C}_g \dot{\mathbf{x}}_{pg} = 0$ is defined as

$$\mathbf{C}_g := \frac{\partial \Phi_{hg}}{\partial \mathbf{x}_{pg}}. \quad (5.8)$$

Subsequently, the constraint dynamical model can thus be obtained by adding the constraint matrix with Lagrange's multipliers λ_g to (5.7) as

$$M_g \ddot{\mathbf{x}}_{pg} = \mathbf{h}_g + \mathbf{C}_g^T \lambda_g. \quad (5.9)$$

The degrees of freedom of the unconstrained system are found to be 18 from (5.6) which should be constrained by 14 holonomic constraints in this system. Therefore, the degrees of freedom of the constrained dynamical system is 4. The tangent speed of the constrained system is

$$\dot{\mathbf{q}}_g = \begin{bmatrix} \dot{\theta}_l & \dot{x}_l & \dot{y}_l & \dot{\theta}_m \end{bmatrix}^T.$$

The orthogonal complement matrix \mathbf{D}_g is obtained according to the same steps as Section 5.1.1. Multiplying (5.9) by \mathbf{D}_g^T from the left side and substituting the coordinate transformation $\dot{\mathbf{x}}_{pg} = \mathbf{D}_g \dot{\mathbf{q}}_g$ into (5.9) yield the dynamic model of Fig. 5.3:

$$\mathbf{D}_g^T M_g \mathbf{D}_g \ddot{\mathbf{q}}_g + \mathbf{D}_g^T M_g \dot{\mathbf{D}}_g \dot{\mathbf{q}}_g = \mathbf{D}_g^T \mathbf{h}_g. \quad (5.10)$$

5.1.3 System Integration

Up to now the dynamic models of the Jansen linkage mechanisms and the gear system have already been established. Then the whole constraint-free dynamic model of the quadruped robot can be obtained by integrating (5.5) and (5.10):

$$\mathbf{M} \ddot{\mathbf{x}}_p = \mathbf{h}, \quad (5.11)$$

where

$$\mathbf{x}_p = \begin{bmatrix} \mathbf{q}_g^T & \mathbf{q}_{rf}^T & \mathbf{q}_{lf}^T & \mathbf{q}_{rb}^T & \mathbf{q}_{lb}^T \end{bmatrix}^T,$$

$$\mathbf{M} = \text{diag}(\mathbf{D}_{rf}^T M_{rf} \mathbf{D}_{rf}, \mathbf{D}_{lf}^T M_{lf} \mathbf{D}_{lf}, \mathbf{D}_{rb}^T M_{rb} \mathbf{D}_{rb}, \mathbf{D}_{lb}^T M_{lb} \mathbf{D}_{lb}),$$

$$\mathbf{h} = \begin{bmatrix} \mathbf{D}_{rf}^T \mathbf{h}_{rf} - \mathbf{D}_{rf}^T M_{rf} \dot{\mathbf{D}}_{rf} \dot{\mathbf{q}}_{rf} \\ \mathbf{D}_{lf}^T \mathbf{h}_{lf} - \mathbf{D}_{lf}^T M_{lf} \dot{\mathbf{D}}_{lf} \dot{\mathbf{q}}_{lf} \\ \mathbf{D}_{rb}^T \mathbf{h}_{rb} - \mathbf{D}_{rb}^T M_{rb} \dot{\mathbf{D}}_{rb} \dot{\mathbf{q}}_{rb} \\ \mathbf{D}_{lb}^T \mathbf{h}_{lb} - \mathbf{D}_{lb}^T M_{lb} \dot{\mathbf{D}}_{lb} \dot{\mathbf{q}}_{lb} \end{bmatrix}.$$

Again, given the holonomic constraints of the gravity center of each link,

$$\Phi_{\mathbf{h}} = \begin{bmatrix} \theta_{rf1} - \theta_l - \tan^{-1}(L_1/h_0) \\ x_{rf1} - x_l + l_{rf} \cos \theta_l + l_{rf1} \cos \theta_{rf1} \\ y_{rf1} - y_l + l_{rf} \sin \theta_l + l_{rf1} \sin \theta_{rf1} \\ \theta_{rf2} + \frac{r_{mrf}}{r_{rf}} \theta_m - \frac{r_{mrf} + r_{rf}}{r_{rf}} \theta_l \\ \theta_{rb1} - \theta_l - \tan^{-1}(-L_1/h_0) \\ x_{rb1} - x_l - l_{rb} \cos \theta_l + l_{rb1} \cos \theta_{rb1} \\ y_{rb1} - y_l - l_{rb} \sin \theta_l + l_{rb1} \sin \theta_{rb1} \\ \theta_{rb2} + \frac{r_{mrb}}{r_{rb}} \theta_m - \frac{r_{mrb} + r_{rb}}{r_{rb}} \theta_l \\ \theta_{lf1} - \theta_l - \tan^{-1}(L_1/h_0) \\ x_{lf1} - x_l + l_{lf} \cos \theta_l + l_{lf1} \cos \theta_{lf1} \\ y_{lf1} - y_l + l_{lf} \sin \theta_l + l_{lf1} \sin \theta_{lf1} \\ \theta_{lf2} + \frac{r_{mlf}}{r_{lf}} \theta_m - \frac{r_{mlf} + r_{lf}}{r_{lf}} \theta_l \\ \theta_{lb1} - \theta_l - \tan^{-1}(-L_1/h_0) \\ x_{lb1} - x_l - l_{lb} \cos \theta_l + l_{lb1} \cos \theta_{lb1} \\ y_{lb1} - y_l - l_{lb} \sin \theta_l + l_{lb1} \sin \theta_{lb1} \\ \theta_{lb2} + \frac{r_{mlb}}{r_{lb}} \theta_m - \frac{r_{mlb} + r_{lb}}{r_{lb}} \theta_l \end{bmatrix} = 0,$$

the constraint dynamical system is thus

$$\mathbf{M} \ddot{\mathbf{x}}_p = \mathbf{h} + \mathbf{C}^T \boldsymbol{\lambda}, \quad (5.12)$$

where

$$\mathbf{C} := \frac{\partial \Phi_{\mathbf{h}}}{\partial \mathbf{x}_p}. \quad (5.13)$$

From (5.11) we find that the the degrees of freedom of the unconstraint system are 20 and constrained by 16 holonomic constraints. Hence, the degrees of freedom of the constrained dynamical system is 4.

Finally, by multiplying (5.12) by \mathbf{D}^T (where \mathbf{D} is the orthogonal complement matrix) from the left side and substituting the coordinate transformation $\dot{\mathbf{x}}_p = \mathbf{D} \dot{\mathbf{q}}$ into (5.12),

the dynamic free-falling model is

$$D^T M D \ddot{\mathbf{q}} + D^T M \dot{D} \dot{\mathbf{q}} = D^T \mathbf{h}, \quad (5.14)$$

where

$$\dot{\mathbf{q}} = \begin{bmatrix} \dot{\theta}_l & \dot{x}_l & \dot{y}_l & \dot{\theta}_m \end{bmatrix}^T$$

is the tangent speed of the constrained system which is the same as that of the gear system.

5.2 Plant Model

The derived dynamic model (5.14) is the free-falling model which does not include reaction force from the ground. However, such force exist and can not be neglected in real situation. In this section, the dynamic model including the floor reaction force and the collision with the ground is derived by expanding the free-falling model.

Our previous study has shown that the toes of the Jansen linkage mechanisms slip consistently while walking [81]. Hence, the further dynamic model considering friction is derived in this section by assuming that the coefficient of friction is uniform.

5.2.1 Contact with the Ground

We consider the floor reaction force by expanding the constraint matrix using the projection method [99]. Contacting the toes with the ground can be regarded as constraining the toes on the ground (*i.e.*, on the x axis). Thus, the floor reaction force is derived by including the constraint when y -coordinate of the toe is less than 0 and the constraint force of the toes is greater than 0 (*i.e.*, the force is generated from the ground to the robot). Since this constraint can be described by the position constraint which is the holonomic constraint, the constraint matrix is defined as:

$$\mathbf{C}_p = \begin{bmatrix} \mathbf{C}_{rf}^T & \mathbf{C}_{lf}^T & \mathbf{C}_{rb}^T & \mathbf{C}_{lb}^T \end{bmatrix}^T, \\ \mathbf{C}_{ij} = \frac{\partial t_{ij}}{\partial \mathbf{x}_p}, \quad (t_{ij} \leq 0 \cap \lambda_{fij} > 0),$$

where $t_{ij} = y_{ij8} + h_{ij8} \sin(\theta_{ij8} - \gamma_{ij8})$, and λ_{fij} represents the floor reaction force. Also, by utilizing the constraint matrix, (5.12) is expanded as

$$\mathbf{M}\ddot{\mathbf{x}}_p = \mathbf{h} + \begin{bmatrix} \mathbf{C} \\ \mathbf{C}_p \end{bmatrix}^T \begin{bmatrix} \boldsymbol{\lambda} \\ \boldsymbol{\lambda}_p \end{bmatrix}, \quad (5.15)$$

which can be projected to the tangent speed space using the orthogonal complement matrix \mathbf{D} , and then the motion equations including the contact on the floor are formulated as

$$\mathbf{D}^T \mathbf{M} \mathbf{D} \ddot{\mathbf{q}} + \mathbf{D}^T \mathbf{M} \dot{\mathbf{D}} \dot{\mathbf{q}} = \mathbf{D}^T \mathbf{h} + \mathbf{D}^T \mathbf{C}_p^T \boldsymbol{\lambda}_p. \quad (5.16)$$

Next, the friction force will be included in the model. Some linear/non-linear friction models have been already proposed in refs. [100–103]. In this study, one of the simplest friction models which is composed of only kinetic and viscous frictions is applied because it has been assumed that the coefficient of friction is uniform. The kinetic friction force is generated when the toe has a speed and the viscous friction force is generated in proportion to the speed of the toe. Hence the friction model \mathbf{f} is represented as

$$\mathbf{f} = \begin{bmatrix} \mathbf{f}_{rf}^T \mathbf{D}_{rf} & \mathbf{f}_{rb}^T \mathbf{D}_{rb} & \mathbf{f}_{lf}^T \mathbf{D}_{lf} & \mathbf{f}_{lb}^T \mathbf{D}_{lb} \end{bmatrix}^T, \quad (5.17)$$

where

$$\mathbf{f}_{ij} = \begin{bmatrix} \mathbf{Z}^{21 \times 1} \\ h_{ij8} \sin(\theta_{ij8} - \gamma_{ij8}) (\lambda_{ij} \mu_d \text{sgn} \dot{\theta}_{ij8} + \mu_v \dot{\theta}_{ij8}) \\ \lambda_{ij} \mu_d \text{sgn} \dot{x}_{ij8} + \mu_v \dot{x}_{ij8} \\ 0 \end{bmatrix},$$

with kinetic friction coefficient μ_d , viscous friction coefficient μ_v , and zero matrix $\mathbf{Z}^{m \times n}$. (5.17) is projected to the tangent speed space utilizing the orthogonal complement matrix and then substituted into (5.16). Finally, the motion equation of the quadruped robot with the Jansen linkage mechanisms considering the friction force is obtained:

$$\mathbf{D}^T \mathbf{M} \mathbf{D} \ddot{\mathbf{q}} + \mathbf{D}^T \mathbf{M} \dot{\mathbf{D}} \dot{\mathbf{q}} = \mathbf{D}^T \mathbf{h} + \mathbf{D}^T \mathbf{C}_p^T \boldsymbol{\lambda}_p + \mathbf{D}^T \mathbf{F}. \quad (5.18)$$

5.2.2 Collision with the Ground

As a assumption, the collision between the ground and the toes are non-completely-elastic collision. Based on the projection method, we assume that a impulse is input at the moment when the collision occurs, and the tangent speed after collision can be derived from the one before collision [99, 104]. The tangent speeds before and after collision are defined as $\dot{\mathbf{q}}^-$ and $\dot{\mathbf{q}}^+$ respectively, and their relationship can be expressed as:

$$\dot{\mathbf{q}}^+ = \mathbf{H}(\mathbf{I} - \mathbf{M}^{-1}\mathbf{C}'^T(\mathbf{C}'\mathbf{M}^{-1}\mathbf{C}'^T)^{-1}\mathbf{C}')\mathbf{D}\dot{\mathbf{q}}^-, \quad (5.19)$$

where

$$\mathbf{H} = \begin{bmatrix} \mathbf{I}^{4 \times 4} & \mathbf{Z}^{4 \times 16} \end{bmatrix}$$

and \mathbf{C}' represents the constraint matrix after collision which is defined as

$$\mathbf{C}' = \begin{bmatrix} \mathbf{C} \\ \mathbf{C}_p \end{bmatrix}.$$

5.3 Control System Design

So far we have the dynamic model taking into account the floor reaction and friction forces. However, the coefficient of friction is unknown in general that it is difficult to use the dynamic model into the controller. Therefore, the controller is designed by utilizing the approximate model based on the approximation conditions [105].

5.3.1 Approximate Model

Following two approximation conditions set based on characteristics of the model and the mechanism, the approximate model is derived.

The first approximation condition is the contact with the ground by two legs consistently. The model is a two-dimensional model, and the heights of the legs are not equal generally in different angles of the driving link in a complex linkage mechanism such as the Jansen linkage mechanism in this case [86, 106]. And it is not general to contact the ground by three legs. Hence, the condition of contacting the ground by two legs consistently can be approximated.

The second approximation condition is that one leg does not slip. Such state represents to walk with the highest efficiency. Referring to ref. [28], we know that the Jansen linkage mechanism is able to walk with high efficiency in general. Thus, this condition can also be approximated.

For the first approximation condition, contacting with the ground by two legs can be regarded as constraining the toes on the ground (*i.e.*, on the x axis). For the second approximation condition, one leg does not slip can be regarded as that the toe does not have the speed in x direction. Since these two constraints can be described as the position constraints, they can be treated as the holonomic constraints. The new constraint matrix is defined as follows:

$$\begin{aligned} \mathbf{C}_a &= \begin{bmatrix} \mathbf{C}_{ax}^T & \mathbf{C}_{a1}^T & \mathbf{C}_{a2}^T \end{bmatrix}^T, \\ \mathbf{C}_{ax} &= \frac{\partial(x_{ij8} + h_{ij8} \cos(\theta_{ij8} - \gamma_{ij8}))}{\partial \mathbf{x}_p}, \\ \mathbf{C}_{a1} &= \frac{\partial t_{rj}}{\partial \mathbf{x}_p}, & (t_{rj} \leq t_{lj}), \\ \mathbf{C}_{a2} &= \frac{\partial t_{lj}}{\partial \mathbf{x}_p}, & (t_{lj} < t_{lj}), \end{aligned}$$

where $t_{ij} = y_{ij8} + h_{ij8} \sin(\theta_{ij8} - \gamma_{ij8})$. Using this constraint matrix, (5.12) is expanded as

$$\mathbf{M} \ddot{\mathbf{x}}_p = \mathbf{h} + \begin{bmatrix} \mathbf{C} \\ \mathbf{C}_a \end{bmatrix}^T \begin{bmatrix} \boldsymbol{\lambda} \\ \boldsymbol{\lambda}_a \end{bmatrix}, \quad (5.20)$$

which can be projected to the tangent speed space by using the orthogonal complement matrix \mathbf{D} . Thus we have the motion equation including contact forces on the plane:

$$\mathbf{D}^T \mathbf{M} \mathbf{D} \ddot{\mathbf{q}} + \mathbf{D}^T \mathbf{M} \dot{\mathbf{D}} \dot{\mathbf{q}} = \mathbf{D}^T \mathbf{h} + \mathbf{D}^T \mathbf{C}_a^T \boldsymbol{\lambda}_a. \quad (5.21)$$

5.3.2 Transformation of Dynamic Model

Due to the presence of Lagrange's multiplier $\boldsymbol{\lambda}_a$, model (5.21) which represents the constraint forces occurring on each constraint condition can not be utilized directly to the controller. To do that, (5.21) needs to be transformed into a usable form for the controller.

In the first step, the constraint forces of the system are obtained using the projection method [107, 108]:

$$\boldsymbol{\lambda} = (\mathbf{C}\mathbf{M}^{-1}\mathbf{C}^T)^{-1}\mathbf{C}(\dot{\mathbf{D}}\dot{\mathbf{q}} - \mathbf{M}^{-1}\mathbf{h}).$$

Hence, the constraint forces of the dynamic model (5.15) can be represented as

$$\begin{bmatrix} \boldsymbol{\lambda} \\ \boldsymbol{\lambda}_a \end{bmatrix} = (\hat{\mathbf{C}}\mathbf{M}^{-1}\hat{\mathbf{C}}^T)^{-1}\hat{\mathbf{C}}(\dot{\mathbf{D}}\dot{\mathbf{q}} - \mathbf{M}^{-1}\mathbf{h}), \quad (5.22)$$

where

$$\hat{\mathbf{C}} = \begin{bmatrix} \mathbf{C} \\ \mathbf{C}_a \end{bmatrix}$$

In the second step, the generalized force matrix \mathbf{h} is expressed as the sum of three terms:

$$\mathbf{h} = \mathbf{E}u + \mathbf{F}\dot{\mathbf{q}} + \mathbf{G}g,$$

where u is the input torque, and

$$\begin{aligned} \mathbf{E} &= \frac{\partial \mathbf{h}}{\partial u} = \mathbf{D}_s^T \begin{bmatrix} \mathbf{E}_g^T & \mathbf{E}_{rf}^T & \mathbf{E}_{rb}^T & \mathbf{E}_{lf}^T & \mathbf{E}_{lb}^T \end{bmatrix}^T, \\ \mathbf{F} &= \frac{\partial(\mathbf{h} - \mathbf{E}u)}{\partial \dot{\mathbf{q}}} = \mathbf{D}_s^T (\mathbf{F}_1 - \mathbf{F}_2) \\ &= \mathbf{D}_s^T (\text{diag}(\mathbf{F}_{ij}) - \mathbf{M}_s \text{diag}(\dot{\mathbf{D}}_{ij})) \mathbf{D}, \\ \mathbf{G} &= \frac{\partial(\mathbf{h} - \mathbf{E}u - \mathbf{F}\dot{\mathbf{q}})}{\partial g} \\ &= \mathbf{D}_s^T \begin{bmatrix} \mathbf{G}_g^T & \mathbf{G}_{rf}^T & \mathbf{G}_{rb}^T & \mathbf{G}_{lf}^T & \mathbf{G}_{lb}^T \end{bmatrix}^T, \end{aligned}$$

with the following components:

$$\begin{aligned} \mathbf{D}_s &= \text{diag}(\mathbf{D}_g, \mathbf{D}_{rf}, \mathbf{D}_{rb}, \mathbf{D}_{lf}, \mathbf{D}_{lb}), \\ \mathbf{M}_s &= \text{diag}(\mathbf{M}_g, \mathbf{M}_{rf}, \mathbf{M}_{rb}, \mathbf{M}_{lf}, \mathbf{M}_{lb}), \\ \mathbf{E}_{ij} &= \frac{\partial \mathbf{h}_{ij}}{\partial u}, \\ \mathbf{F}_{ij} &= \frac{\partial(\mathbf{h}_{ij} - \mathbf{E}_{ij}u)}{\partial \dot{\mathbf{q}}_{ij}}, \\ \mathbf{G}_{ij} &= \frac{\partial(\mathbf{h}_{ij} - \mathbf{E}_{ij}u - \mathbf{F}_{ij}\dot{\mathbf{q}}_{ij})}{\partial g}. \end{aligned}$$

Substituting the above terms into (5.21) and (5.22) and further simplification generate the following model for the controller:

$$\mathbf{D}^T \mathbf{M} \mathbf{D} \ddot{\mathbf{q}} + \mathbf{D}^T (\mathbf{M} \dot{\mathbf{D}} - \mathbf{F} - \boldsymbol{\alpha}) \dot{\mathbf{q}} - \mathbf{D}^T (\mathbf{G} + \boldsymbol{\gamma}) \mathbf{g} = \mathbf{D}^T (\mathbf{E} + \boldsymbol{\beta}) \mathbf{u}, \quad (5.23)$$

where,

$$\begin{aligned} \boldsymbol{\alpha} &= \hat{\mathbf{C}}^T (\hat{\mathbf{C}} \mathbf{M}^{-1} \hat{\mathbf{C}}^T)^{-1} \hat{\mathbf{C}} (\dot{\mathbf{D}} - \mathbf{M}^{-1} \mathbf{F}), \\ \boldsymbol{\beta} &= -\hat{\mathbf{C}}^T (\hat{\mathbf{C}} \mathbf{M}^{-1} \hat{\mathbf{C}}^T)^{-1} \hat{\mathbf{C}} \mathbf{M}^{-1} \mathbf{E}, \\ \boldsymbol{\gamma} &= -\hat{\mathbf{C}}^T (\hat{\mathbf{C}} \mathbf{M}^{-1} \hat{\mathbf{C}}^T)^{-1} \hat{\mathbf{C}} \mathbf{M}^{-1} \mathbf{G}. \end{aligned}$$

5.3.3 Control System based on Energy Control

The control system is designed based on the dynamic model and the energy control which was proposed by Åström et al. as a control method focusing on the energy of the system [109–111]. The energy based control is better than state space representation for controlling complicated mechanisms, such as the quadruped robot with the Jansen linkage mechanism in this case. To realize the position control using energy approach, a potential field [112–115] is introduced. As for the potential field, the target position is designed as the point where the potential is the lowest. Hence, the process of motion control is the process that the energy of the robot is converging to the lowest potential, namely the target position. We define the potential field as

$$E_p = k_p (x_l - x_r)^2, \quad (5.24)$$

where the current position of the robot is defined as x_l ; x_r represents the target position and is defined as $x_r = 0$; k_p is the gradient of the potential field. The kinetic energy of the system is defined as

$$E_k = \frac{1}{2} \dot{\mathbf{x}}_p^T \mathbf{M}_s \dot{\mathbf{x}}_p. \quad (5.25)$$

Combining (5.24) and (5.25), the total energy E of the system is

$$E = E_k + E_p. \quad (5.26)$$

Then we design a Lyapunov function

$$V = \frac{1}{2}(E - E_r)^2, \quad (5.27)$$

where E_r is the target energy, that is $E_r = 0$. Solving the differential of (5.27), we have

$$\dot{V} = E\dot{E} = (E_k + E_p)(\dot{E}_k + \dot{E}_p), \quad (5.28)$$

where

$$\begin{aligned} \dot{E}_p &= \frac{d}{dt}k_p(x_l - x_r)^2 \\ &= 2k_px_l\dot{x}_l = 2k_p\dot{\mathbf{q}}^T \begin{bmatrix} 0, x_l, 0, 0 \end{bmatrix}^T \end{aligned} \quad (5.29)$$

and

$$\dot{E}_k = \frac{d}{dt}\frac{1}{2}\dot{\mathbf{x}}_p^T M_s \dot{\mathbf{x}}_p = \dot{\mathbf{x}}_p^T M_s \ddot{\mathbf{x}}_p.$$

Considering $\dot{\mathbf{x}}_p = \mathbf{D}_s \mathbf{D} \dot{\mathbf{q}}$,

$$\begin{aligned} \dot{E}_k &= \dot{\mathbf{q}}^T \mathbf{D}^T \mathbf{D}_s^T M_s (\mathbf{D}_s \mathbf{D} \ddot{\mathbf{q}} + \mathbf{D}_s \dot{\mathbf{D}} \dot{\mathbf{q}} + \dot{\mathbf{D}}_s \mathbf{D} \dot{\mathbf{q}}) \\ &= \dot{\mathbf{q}}^T (\mathbf{D}^T M \mathbf{D} \ddot{\mathbf{q}} + \mathbf{D}^T M \dot{\mathbf{D}} \dot{\mathbf{q}} + \mathbf{D}^T \mathbf{F}_2 \dot{\mathbf{q}}). \end{aligned} \quad (5.30)$$

Transforming (5.23) into

$$\mathbf{D}^T M \mathbf{D} \ddot{\mathbf{q}} + \mathbf{D}^T M \dot{\mathbf{D}} \dot{\mathbf{q}} + \mathbf{D}^T \mathbf{F}_2 \dot{\mathbf{q}} = \mathbf{D}^T (\mathbf{E} + \beta)u + \mathbf{D}^T (\mathbf{F}_1 + \alpha)\dot{\mathbf{q}} + \mathbf{D}^T (\mathbf{G} + \gamma)g$$

and then substituting it into (5.30) yields

$$\dot{E}_k = \dot{\mathbf{q}}^T (\mathbf{D}^T (\mathbf{E} + \beta)u + \mathbf{D}^T (\mathbf{F}_1 + \alpha)\dot{\mathbf{q}} + \mathbf{D}^T (\mathbf{G} + \gamma)g). \quad (5.31)$$

Substituting (5.29) and (5.31) into (5.28), the differential of the Lyapunov function can

be represented as

$$\dot{V} = (E_k + E_p) \dot{\mathbf{q}}^T \left(\mathbf{D}^T (\mathbf{E} + \boldsymbol{\beta}) u + \mathbf{D}^T (\mathbf{F}_1 + \boldsymbol{\alpha}) \dot{\mathbf{q}} + \mathbf{D}^T (\mathbf{G} + \boldsymbol{\gamma}) g + 2k_p [0, x_l, 0, 0]^T \right). \quad (5.32)$$

To ensure the Lyapunov stability (namely to satisfy $\dot{V} \leq 0$), we choose the input torque as

$$u = -(\mathbf{D}^T (\mathbf{E} + \boldsymbol{\beta}))^\dagger \left(k(E_k + E_p) \dot{\mathbf{q}} + \mathbf{D}^T (\mathbf{G} + \boldsymbol{\gamma}) g + 2k_p [0, x_l, 0, 0]^T \right), \quad (5.33)$$

where \dagger denotes the operator of pseudo inverse; k denotes the tuning parameter, and satisfies $k > 0$.

Finally, substituting (5.33) into (5.32), we have

$$\begin{aligned} \dot{V} &= (E_k + E_p) \dot{\mathbf{q}}^T \left(-k(E_k + E_p) \dot{\mathbf{q}} - \mathbf{D}^T (\mathbf{G} + \boldsymbol{\gamma}) g - 2k_p [0, x_l, 0, 0]^T \right. \\ &\quad \left. + \mathbf{D}^T (\mathbf{F}_1 + \boldsymbol{\alpha}) \dot{\mathbf{q}} + \mathbf{D}^T (\mathbf{G} + \boldsymbol{\gamma}) g + 2k_p [0, x_l, 0, 0]^T \right) \\ &= -k(E_k + E_p)^2 \dot{\mathbf{q}}^T \dot{\mathbf{q}} + (E_k + E_p) \dot{\mathbf{q}}^T \mathbf{D}^T (\mathbf{F}_1 + \boldsymbol{\alpha}) \dot{\mathbf{q}}, \end{aligned}$$

where $\dot{\mathbf{q}}^T \mathbf{D}^T (\mathbf{F}_1 + \boldsymbol{\alpha}) \dot{\mathbf{q}} \leq 0$ because $\dot{\mathbf{q}}^T \mathbf{D}^T (\mathbf{F}_1 + \boldsymbol{\alpha}) \dot{\mathbf{q}}$ represents the viscous friction forces; According to (5.24) and (5.25), $(E_k + E_p) \geq 0$. Therefore,

$$\dot{V} \leq 0,$$

is proofed by using (5.33) as the inputting torque. Since $\dot{V} \leq 0$ is satisfied, the equilibrium of (5.27) is proven to be stable. That is, the position of the robot can be converged to the target position by using the energy-based control strategy.

5.4 Numerical Simulations

Effectiveness of the designed position control system utilizing the approximate model is verified by numerical simulations which are performed by MaTX with Visual C++ 2005 version 5.3.37 [116]. The parameters used in simulations are the ones shown in Table 5.1 and Table 5.4. The simulation time is 80 seconds, and the sampling interval is 0.01

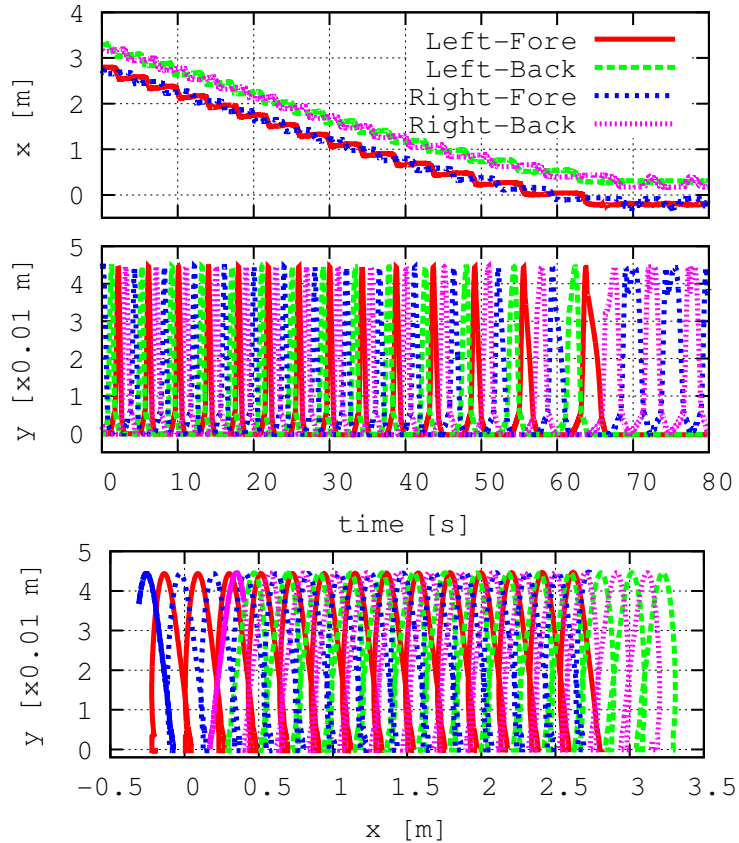


Fig. – 5.4 Time evolutions of x -coordinate (top) and y -coordinate (middle) of the robot's toes, and the trajectory of the feet (bottom).

second. The initial state of the robot is halted on the plane at position $x_l = 3$ m and the Jansen link mechanism is with $\theta_m = -\pi/4$ rad. In addition, the gradient of the potential field $k_p = 1$ and the tuning parameter $k = 0.3$. The coefficient values of kinetic and viscous frictions are given as $\mu_d = 0.1$ and $\mu_v = 0.1$. The numerical simulation results are shown as follows.

From Fig. 5.4 (top), it is confirmed that the robot moves with toes slipping. Fig. 5.4 (bottom) shows that the non-completely-elastic collisions occur at the toes of the robot (*i.e.*, $\dot{t}_{ij} = 0$) when the toes collide with the ground (*i.e.*, $t_{ij} = 0$) and height of the toes is greater than or equal to 0. In addition, in case the toes depart from the ground, the negative floor reaction forces (*i.e.*, the constraint force of $\lambda_{ij} < 0$) is not generated because the position of the toe varies smoothly. Therefore, the dynamic models derived in Section 5.1 and 5.2 represent the dynamics of the robot shown in Fig. 5.1 in two-dimensional surface including the contact and collision with the ground. Meanwhile, the

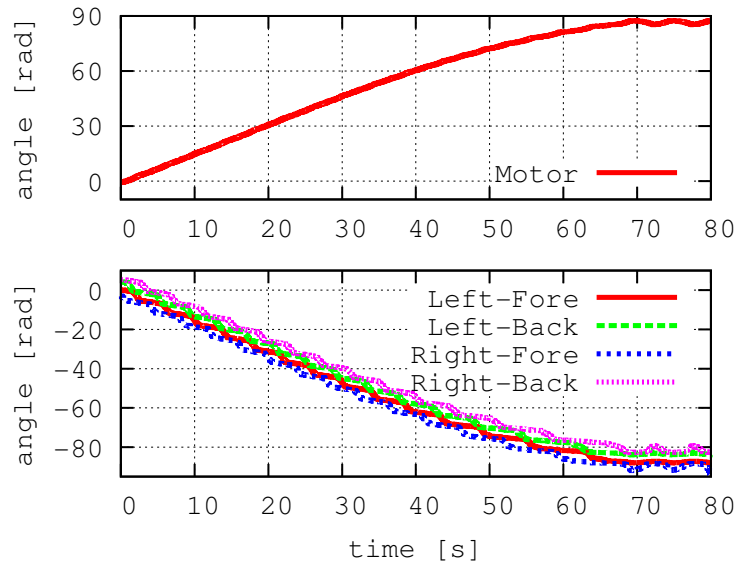


Fig. – 5.5 Time evolution of the angles of the driving gear (top) and driven gears (bottom).

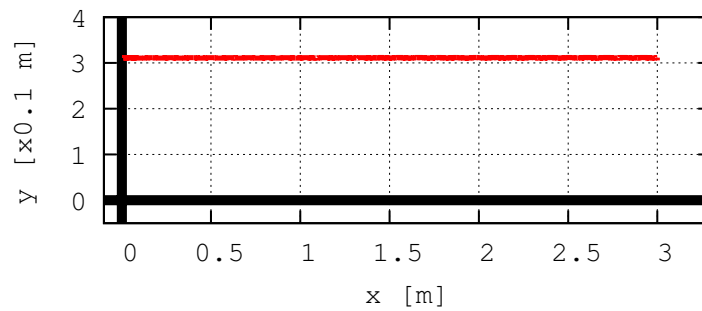


Fig. – 5.6 Trajectory of robot's position.

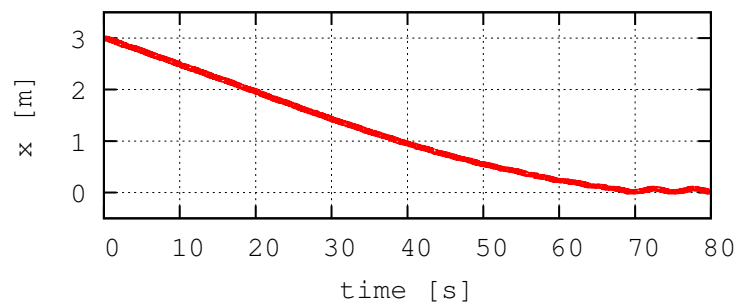


Fig. – 5.7 Time evolution of x-coordinate of the robot.

rotation angle of the driving gear is increasing to from zero to 90° , and those of the four driven gears are varying smoothly to $-80^\circ \sim -90^\circ$ approximately (Fig. 5.5).

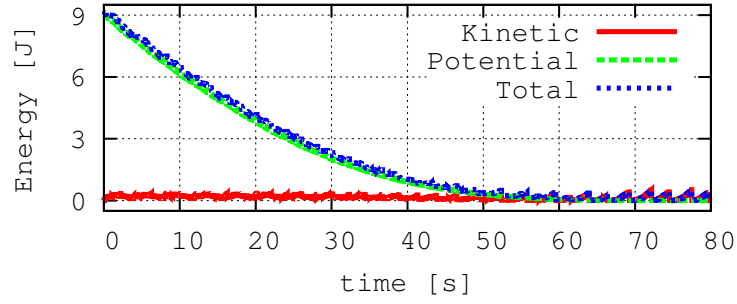


Fig. – 5.8 Time evolutions of the kinetic energy E_k and the potential energy E_p .

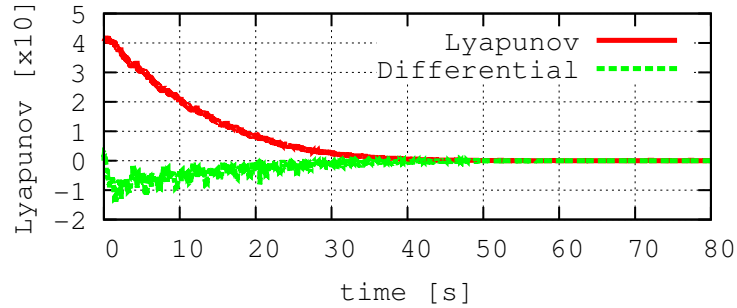


Fig. – 5.9 Time evolutions of the values of the Lyapunov's function V and its differential \dot{V} .

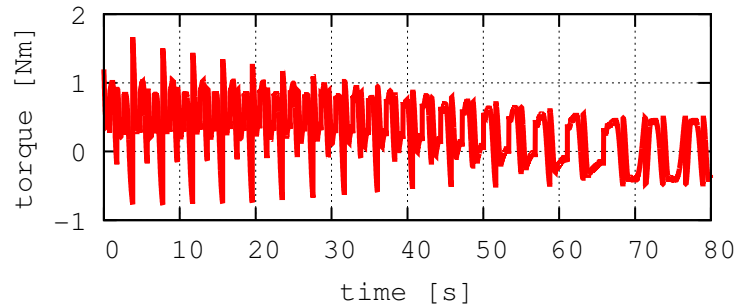


Fig. – 5.10 Time evolution of the input torque u .

From Figs. 5.6 and 5.7, it is confirmed that the position of the robot can be converged to $x = 0$ by the designed position control system. Meanwhile Fig. 5.8 shows that the energy of the system converges to 0. In addition, since the value of the Lyapunov function converges to 0 and its differential is also less than 0 as shown in Fig. 5.9, it is confirmed that the input torque shown in Fig. 5.10 satisfies the Lyapunov's stability theory. Therefore, the position of the quadruped robot with the Jansen linkage mechanism can be

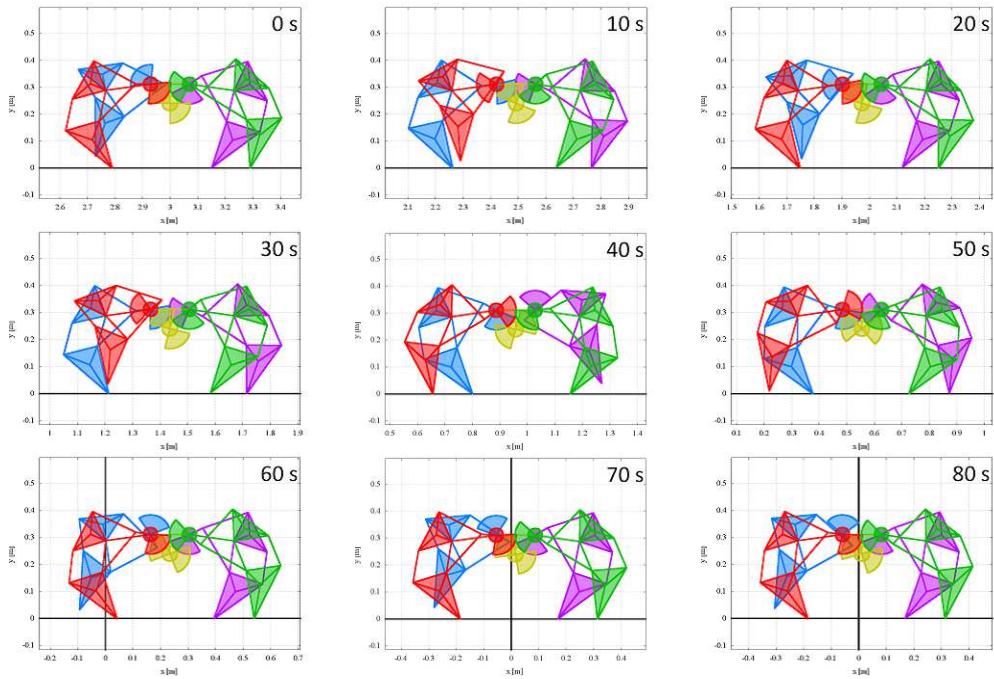


Fig. – 5.11 The snapshots of walking towards the target position based on the energy-based position control.

controlled by applying the position control system based on the energy control. Fig. 5.11 shows that a sequence of the snapshots of walking towards the target position based on the energy-based position control in 80 seconds.

5.5 Conclusion

The chapter presented and analyzed the dynamics of the four-legged robot based on the Theo Jansen linkage mechanism using projection method. The free-falling model of the whole system has been built through integrating the models of Jansen linkage and gear system which are derived respectively. Based on that, the reaction force and friction are taken into account to derive the plant model. The energy control system utilizing the potential field is designed to realize the position control of the Jansen walking robot. Based on the Lyapunov stability theory, the controller is proofed to be able to converge by choosing appropriate input. Effectiveness of the designed controller was verified through the numerical simulations. This research sets a theoretical basis for further investigation, optimization or extension of the Theo Jansen mechanism to develop the legged robot with

reconfigurable Theo Jansen mechanism.

6 . Conclusion

This study aims to formulate the concept of nested reconfiguration which possesses both intra- and inter- reconfiguration, and to develop the robot capable of achieving wide-ranging tasks in highly uncertain environments through providing the nested reconfiguration, and has studied following research topics: development of intra-reconfigurable module robot possessing both the reconfigurable mechanisms and docking system, speed control of toe of the Jansen linkage mechanism, development of the multi-legged nested reconfigurable robot, and the position control of the multi-legged robot with the Jansen linkage mechanisms.

In development of intra-reconfigurable module robot possessing both the reconfigurable mechanisms, the reconfigurable Jansen linkage mechanism has been proposed as the intra-reconfigurable module. The forward kinematics of the Jansen linkage mechanism is derived by utilizing Bilateral problem, and six kind of interesting gait patterns involving Default Curve have been explored. And, the gait transition method of the explored gait patterns has been proposed. Finally, the reconfigurable Jansen linkage mechanism has been implemented indeed, and it has been verified the effectiveness of repeatability and possibility of both the gait patterns and the gait transition method through experiments.

In speed control of toe of the Jansen linkage mechanism, the angle trajectory capable of the constant speed locomotion of the toe of the Jansen linkage mechanism has been generated. In order to realize it, the forward kinematics of the Jansen linkage mechanism which boils down to the problem of the Bilateral has been analyzed. In fact, it has been proven that the norm of the toe speed bears a proportionate relationship to the angular velocity of the driving link. And, the angle trajectory of the driving link capable of the constant speed control of the toe of the Jansen linkage mechanism has been generated by utilizing the relationship. It has been verified that the constant speed control of the toe

of the Jansen linkage mechanism is realized by the generated trajectory via a numerical simulation.

In development of the multi-legged nested reconfigurable robot, the multi-legged robot assembling the developed reconfigurable Jansen linkage mechanisms has been developed. And, synchronization realizing the walking which is most basic locomotion strategy for the multi-legged robot has been presented. As the gait transition method, two types of gait transition methods for the explored gait patterns have been presented. Furthermore, it has been verified that the walking and the gait transitions with stability are realized by the presented synchronization and gait transition methods via numerical simulations.

In the position control of the multi-legged robot with the Jansen linkage mechanisms, the dynamical model of the robot has been derived utilizing Projection Method by integrating the model of both the Jansen linkage mechanism and the gear system. The floor reaction forces and the friction forces have been formulated by expanding the constraint matrix of Projection Method. The appropriate model for the control system has been derived, and the position control system based on the energy control has been designed utilizing the appropriate model. It has been verified that the position of the robot can be controlled by the designed control system through the numerical simulation.

Through these studies, the concept of nested reconfiguration which possesses both intra- and inter-reconfiguration has been formulated. And application of nested reconfigurability and its design and control strategy have been proposed. In addition, each Chapter concludes as follows.

6.1 A Reconfigurable Jansen Leg with Multiple Gait Patterns

An original design approach has been presented in this chapter to achieve adaptive gait patterns in legged robots for which Theo Jansen linkage forms the core. This one degree-of-freedom linkage, that is very efficient and widely adopted in walking platforms, has been modified to produce a wide variety of gait cycles using the reconfiguration principle of variable allocation of joint positions. We have discussed novel approaches to address the position analysis problem and to characterize leg transformation in this

reconfigurable design. Five gait patterns of interest have been identified, analyzed and discussed in relation to potential future applications. These exemplary gait variations considerably extend the capabilities of the original design not only to produce novel gait patterns but also to realize behaviors beyond locomotion. A fully-functional design has been presented, which enables all single-link transformations, and experimental results with a working prototype have been reported.

A four-legged robot is currently being assembled with reconfigurable Jansen legs based on the design herein presented. The objective with this robot is to test different reconfiguration scenarios and control strategies for limb specialization and graceful degradation. Our long-term aim is to develop systematic methods to design reconfigurable robots capable of transforming in response to needs associated with environment, task, or failures.

6.2 Speed Control of Jansen Linkage Mechanism for Exquisite Tasks

This chapter has reported the toe speed control to achieve more complex tasks with the Jansen linkage mechanism. It has been proven that the norm of the toe speed bears a proportionate relationship to the angular velocity of the driving link. And, the angle trajectory of the driving link capable of the constant speed control of the toe of the Jansen linkage mechanism is generated by utilizing the relationship. In addition, it has been verified that the constant speed control of the toe can be realized by utilizing the derived angle trajectory through numerical simulation.

The angle trajectory capable of the speed control of the toe in horizontal direction has been derived as an application of the proposed method. By utilizing the application method, in the case of the multi-legged robot as an example, since the velocity of the all supporting legs can be controlled arbitrarily, the walking control considering the stability of the robot can be realized.

6.3 An Approach to Gait Synchronization and Transition for Reconfigurable Walking Platforms

An original design approach has been presented in this chapter towards development of a trajectory generator that realizes a set of stable walking gaits and gait transition for a reconfigurable Jansen platform. We have discussed a novel strategy to address the leg synchronization problem in this reconfigurable design and gait transition. Stability analysis is presented for prospective six gait patterns generated and all gait transitions by the reconfigurable platform and results discussed in view of validating the proposed approach. The ability to adapt to situations and produce appropriate stable gaits and switch between gaits would extend the capabilities of the robot beyond their intended application. A four-legged robot is currently being constructed to validate the robustness of the produced gaits and control approaches for real world deployments.

6.4 Dynamic Modeling and Nonlinear Position Control of a Quadruped Robot with Theo Jansen Linkage Mechanisms

The chapter presented and analyzed the dynamics of the four-legged robot based on the Theo Jansen linkage mechanism using projection method. The free-falling model of the whole system has been built through integrating the models of Jansen linkage and gear system which are derived respectively. Based on that, the reaction force and friction are taken into account to derive the plant model. The energy control system utilizing the potential field is designed to realize the position control of the Jansen walking robot. Based on the Lyapunov stability theory, the controller is proved to be able to converge by choosing appropriate input. Effectiveness of the designed controller was verified through the numerical simulations. This research sets a theoretical basis for further investigation, optimization or extension of the Theo Jansen mechanism to develop the legged robot with reconfigurable Theo Jansen mechanism.

Reference

- [1] M. Fujita, H. Kitano, and K. Kageyama, “A reconfigurable robot platform,” *Robotics and Autonomous Systems*, vol. 29, no. 2-3, pp. 119 – 132, 1999.
- [2] F. Michaud, M. Arsenault, Y. Bergeron, R. Cadrin, F. Gagnon, M. Legault, M. Millette, J. Paré, M. Tremblay, D. Létoumeau, P. lepage, Y. Morin, S. Caron, and J. Bisson, “Co-design of azimuth: A multi-modal robotic platform,” *ASME 2003 International Design Engineering Technical Conferences and Computers and Information in Engineering Conference*, vol. 1, pp. 801 – 810, 2003.
- [3] Y. Sun and S. Ma, “epaddle mechanism: Towards the development of a versatile amphibious locomotion mechanism,” *Intelligent Robots and Systems (IROS), 2011 IEEE/RSJ International Conference on*, pp. 5035 – 5040, 2011.
- [4] J. Yoon and J. Ryu, “A novel reconfigurable ankle/foot rehabilitation robot,” *Robotics and Automation, 2005. ICRA 2005. Proceedings of the 2005 IEEE International Conference on*, pp. 2290 – 2295, 2005.
- [5] K. Low and J. Yu, “Development of modular and reconfigurable biomimetic robotic fish with undulating fin,” *Robotics and Biomimetics, 2007. ROBIO 2007. IEEE International Conference on*, pp. 274 – 279, 2007.
- [6] H. Xu, D. Tan, Z. Zhang, Y. Ma, and G. Peng, “An innovative reconfigurable mobile robot with multi-maneuver modes,” *Robotics and Biomimetics, 2008. ROBIO 2008. IEEE International Conference on*, pp. 1659 – 1664, 2009.
- [7] A. Siddiqi, O. Deweck, and K. Iagemma, “Reconfigurability in planetary surface vehicles: Modelling approaches and case study,” *JBIS: Journal of the British Interplanetary Society*, vol. 59, pp. 450 – 460, 2006.

- [8] M. Yim, D. Duff, and K. Roufas, “Polybot: a modular reconfigurable robot,” *Robotics and Automation, 2000. Proceedings. ICRA '00. IEEE International Conference on*, vol. 1, pp. 514 – 520, 2000.
- [9] J. Bishop, S. Burden, B. Klavins, R. Kerisverg, N. Napp, and T. Nguyen, “Programmable parts: a demonstration of the grammatical approach to self-organization,” *Intelligent Robots and Systems, 2005. (IROS 2005). 2005 IEEE/RSJ International Conference on*, pp. 3684 – 3691, 2005.
- [10] B. Salemi, M. Moll, and S. Wei-Min, “Superbot: A deployable, multi-functional, and modular self-reconfigurable robotic system,” *Intelligent Robots and Systems, 2006 IEEE/RSJ International Conference on*, pp. 3636 – 3641, 2006.
- [11] K. Gilpin, K. Kotay, D. Rus, and I. Vasilescu, “Miche: Modular shape formation by self-disassembly,” *The international journal of Robotics research*, vol. 27, no. 3-4, pp. 345–372, 2008.
- [12] R. Gross, M. Bonani, F. Mondada, and M. Dorigo, “Autonomous self-assembly in swarm-bots,” *Robotics, IEEE Transactions on*, vol. 22, no. 6, pp. 1552–3098, 2006.
- [13] A. Kamimura, H. Kurokawa, E. Yoshida, S. Murata, K. Tomita, and S. Kokaji, “Automatic locomotion design and experiments for a modular robotic system,” *IEEE/ASME Transactions on Mechatronics*, vol. 10, no. 3, pp. 314–325, 2005.
- [14] C. Paul, J. W. Roberts, H. Lipson, and F. V. Cuevas, “Gait production in a tensegrity based robot,” in *12th IEEE International Conference on Advanced Robotics*, 2005, pp. 216–222.
- [15] K. Tsujita, T. Kobayashi, T. Inoura, and T. Masuda, “Gait transition by tuning muscle tones using pneumatic actuators in quadruped locomotion,” in *IEEE/RSJ International Conference on Intelligent Robots and Systems*, 2008, pp. 2453–2458.
- [16] C. Paul, “Morphological computation: A basis for the analysis of morphology and control requirements,” *Robotics and Autonomous Systems*, vol. 54, no. 8, pp. 619–630, 2006.

- [17] J. G. Cham, J. K. Karpick, and M. R. Cutkosky, “Stride period adaptation of a biomimetic running hexapod,” *The International Journal of Robotics Research*, vol. 23, no. 2, pp. 141–153, 2004.
- [18] S. Nansai, N. Rojas, R. E. Mohan, and R. Sosa, “Exploration of adaptive gait patterns with a reconfigurable linkage mechanism,” *The 2013 IEEE/RSJ International Conference on Intelligent Robots and Systems (IROS)*, pp. 4661–4668, 2013.
- [19] G. C. Haynes and A. A. Rizzi, “Gaits and gait transitions for legged robots,” *Proceedings 2006 IEEE International Conference on Robotics and Automation, 2006 (ICRA2006)*, pp. 1117–1122, 2006.
- [20] C. P. Santos and V. Matos, “Gait transition and modulation in a quadruped robot: A brainstem-like modulation approach,” *Robotics and Autonomous Systems*, vol. 59, no. 9, pp. 620–634, 2011.
- [21] H. Kimura, S. Akiyama, and K. Sakurama, “Realization of dynamic walking and running of the quadruped using neural oscillator,” *Autonomous Robots*, vol. 7, no. 3, pp. 247–258, 1999.
- [22] S. Bartsch, T. Birnschein, M. Langosz, J. Hilljegerdes, D. Kühn, and F. Kirchner, “Development of the six-legged walking and climbing robot spaceclimber,” *J. Field Rob.*, vol. 29, no. 3, pp. 506–532, 2012.
- [23] J. Estremera, J. A. Cobano, and P. G. de Santos, “Continuous free-crab gaits for hexapod robots on a natural terrain with forbidden zones: An application to humanitarian demining,” *Rob. Autom. Syst.*, vol. 58, no. 5, pp. 700–711, 2010.
- [24] F. L. Moro, A. Spröwitz, A. Tuleu, M. Vespignani, N. G. Tsagarakis, A. J. Ijspeert, and D. G. Caldwell, “Horse-like walking, trotting, and galloping derived from kinematic motion primitives (kMPs) and their application to walk/trot transitions in a compliant quadruped robot,” *Biol. Cybern.*, vol. 107, no. 3, pp. 1–12, 2013.
- [25] D. Sanz-Merodio, E. Garcia, and P. G. de Santos, “Analyzing energy-efficient configurations in hexapod robots for demining applications,” *Ind. Robot*, vol. 39, no. 4, pp. 357–364, 2012.

- [26] P. G. de Santos, R. P. E. Garcia, and M. Armada, “Minimizing energy consumption in hexapod robots,” *Adv. Robotics*, vol. 23, no. 6, pp. 681–704, 2009.
- [27] S. S. Roy and D. K. Pratihar, “Dynamic modeling, stability and energy consumption analysis of a realistic six-legged walking robot,” *Rob. Comput. Integr. Manuf.*, vol. 29, no. 2, pp. 400–416, 2013.
- [28] T. Jansen, *The Great Pretender*. 010 Publishers, Rotterdam, 2007.
- [29] D. Giesbrecht, “Design and optimization of a one-degree-of-freedom eight-bar leg mechanism for a walking machine,” *Master thesis, Department of Mechanical and Manufacturing Engineering, The University of Manitoba*, 2010.
- [30] D. Giesbrecht, C. Q. Wu, and N. Sepehri, “Design and optimization of an eight-bar legged walking mechanism imitating a kinetic sculpture, “wind best”,” *Transactions of the Canadian Society for Mechanical Engineering*, vol. 36, no. 4, pp. 343–355, 2012.
- [31] D. Giesbrecht and C. Q. Wu, “Dynamics of legged walking mechanism “wind best”,” *Department of Mechanical and Manufacturing Engineering, University of Manitoba*, 2010.
- [32] D. Giesbrecht, C. Q. Wu, and N. Sepehri, “Synthesis of a legged walking mechanism “wind best” using theory of mechanism design,” *Department of Mechanical and Manufacturing Engineering, University of Manitoba*, 2010.
- [33] F. Moldvan, V. Dolga, and C. Sticlaru, “A new type of walking robot based upon jansen mechanism,” *Advanced Materials Research*, vol. 463, no. 464, pp. 997 – 1001, 2012.
- [34] F. Moldvan, V. Dolga, and C. Pop, *Kinetostatic Analysis an Articulated Walking Mechanism*, ser. Mechanisms, Transmissions and Applications, 2012.
- [35] F. Moldovan and V. Dolga, “Analysis of jansen walking mechanism using cad,” *Solid State Phenomena*, vol. 166-167, pp. 297–302, 2010.

- [36] F. Moldva, V. Dolga, and A. Dobra, “Mechatronic approach of analyzing one dof leg mechanism in order to construct a walking robot system,” *Applied Mechanisc and Materials*, vol. 162, pp. 559 – 566, 2012.
- [37] F. Moldvan, V. Dolga, and C. Pop, “Synthesis of an articulated ten bar mechanism for building a walking robot,” *8th IEEE International Symposium on Applied Computational Intelligence and Informatics*, pp. 365 – 370, 2013.
- [38] K. Komoda and H. Wagatsuma, “A study of availability and extensibility of theo jansen mechanism toward climbing over bumps,” in *Proceedings of the 21st Annual Conference of the Japanese Neural Network Society, Paper No. P3-28*, December 2011.
- [39] —, “A proposal of the extended mechanism for theo jansen linkage to modify the walking elliptic orbit and a study of cyclic base function,” in *Dyn. Walk. Conf.*, 2012.
- [40] W. Khalil and S. Guegan, “Inverse and direct dynamic modeling of gough-stewart robots,” *IEEE Trans. Robot*, vol. 20, no. 4, pp. 754–762, 2004.
- [41] X. Wang and J. K. Mills, “Dynamic modeling of a flexible-link planar parallel platform using a substructuring approach,” *Mech. Mach. Theory*, vol. 41, no. 6, pp. 671–687, 2006.
- [42] S. Mahil, “On the application of lagrange’s method to the description of dyanmic system,” *IEEE Trans. Syst., Man, Cybern.*, vol. 12, no. 6, pp. 877–889, 1982.
- [43] K. Arczewski and W. Blajer, “A unified approach to the modelling of holonomic and nonholonomic mechanical systems,” *Math. Comput. Modell. Dyn. Syst.*, vol. 2, no. 3, pp. 157–174, 1996.
- [44] W. Blajer, “A geometrical interpretation and uniform matrix formulation of multi-body systems dynamics,” *Z. Angew. Math. Mech.*, vol. 81, no. 4, pp. 247–259, 2004.
- [45] H. Ohsaki, M. Iwase, and S. Hatakeyama, “A consideration of nonlinear system modeling using the projection method,” in *SICE Annual Conference*, 2007, pp. 1915–1920.

- [46] H. Ohsaki, M. Iwase, T. Sadahiro, and S. Hatakeyama, “A consideration fo human- unicycle model for unicycle operation analysis based on moment balancing point,” in *IEEE Int. Conf. Syst, Man, Cybern.*, 2009, pp. 2468–2473.
- [47] Y. Itoh, K. Higashi, and M. Iwase, “Ukf-based estimation of indicated torque for ic engines utilizing nonlinear tow-inertia model,” in *51st IEEE Conf. Decis. Control.*, 2012, pp. 4077–4082.
- [48] L. Zhang, J. Dai, and T. Yang, “Reconfiguration techniques and geometric constraints of metamorphic mechanisms,” in *Proceedings of the ASME 2009 International Design Engineering Technical Conferences & Computers and Information in Engineering Conference, Paper No. DETC2009-87345*. ASME, August 30 - September 2 2009, pp. 559–575.
- [49] H. Yan and C. Kang, “Configuration synthesis of mechanisms with variable topologies,” *Mechanism and Machine Theory*, vol. 44, no. 5, pp. 896 – 911, 2009.
- [50] S. and J. i, “Structure synthesis of single-driven metamorphic mechanisms based on the augmented assur groups,” *Journal of Mechanisms and Robotics*, vol. 4, no. 3, p. 031004, 2012.
- [51] V. Singh, S. Skiles, J. Krager, K. Wood, D. Jensen, and R. Sierakowski, “Innovations in design through transformation: A fundamental study of transformation principles,” *Journal of Mechanical Design*, vol. 131, no. 8, p. 081010, 2009.
- [52] J. McCarthy and G. S. Soh, *Geometric Design of Linkages*. Springer, 2011.
- [53] G. Gogate and S. Matekar, “Optimum synthesis of motion generating four-bar mechanisms using alternate error functions,” *Mechanism and Machine Theory*, vol. 54, no. 0, pp. 41 – 61, 2012.
- [54] L. Burmester, *Lehrbuch der Kinematik*. Verlag Von Arthur Felix, Leipzig, Germany, 1888.
- [55] A. Rubel and R. Kaufman, “Kinsyn iii: A new human-engineered system for interactive computer-aided design of planar linkages,” *Journal of Engineering for Industry*, vol. 99, no. 2, pp. 440 – 448, 1977.

- [56] E. Lee and C. Mavroidis, “Solving the geometric design problem of spatial 3r robot manipulators using polynomial homotopy continuation,” *Journal of Mechanical Design*, vol. 124, no. 4, pp. 652 – 661, 2002.
- [57] H. Su, L. Watson, and J. McCarthy, “Generalized linear product homotopy algorithms and the computation of reachable surfaces,” *Journal of Computing and Information Science in Engineering*, vol. 4, no. 3, pp. 226 – 234, 2004.
- [58] J. Mariappan and S. Krishnamurty, “A generalized exact gradient method for mechanism synthesis,” *Mechanism and Machine Theory*, vol. 31, no. 4, pp. 413 – 421, 1996.
- [59] S. Coros, B. Thomaszewski, G. Noris, S. Sueda, M. Forberg, R. Sumner, W. Matusik, and B. Bickel, “Computational design of mechanical characters,” *ACM Transactions on Graphics*, vol. 32, no. 4, pp. 83:1–83:12, July 2013.
- [60] E. Lee and C. Mavroidis, “An elimination procedure for solving the geometric design of spatial 3r manipulators,” *Journal of Mechanical Design*, vol. 128, no. 1, pp. 142 – 145, 2005.
- [61] M. Pucheta, “Computational methods for the design and synthesis of planar mechanisms,” Ph.D. dissertation, Universidad Nacional del Litoral, Argentina, 2008.
- [62] J. McCarthy, *21st Century Kinematics: The 2012 NSF Workshop*. Springer, 2013.
- [63] N. Rojas, “Distance-based formulations for the position analysis of kinematic chains,” Ph.D. dissertation, Institut de Robòtica i Informàtica Industrial (CSIC-UPC), Universitat Politècnica de Catalunya, 2012.
- [64] M. Ceccarelli and T. Koetsier, “Burmester and allievi: A theory and its application for mechanism design at the end of 19th century,” *Journal of Mechanical Design*, vol. 130, p. 072301, 2008.
- [65] S. Song and K. K.J. Waldron, *Machines That Walk -The Adaptive Suspension Vehicle*. The MIT press Cambridge, Massachusetts, USA, 1989.

- [66] G. Carbone and M. Ceccarelli, “Legged robotic systems,” in *Cutting Edge Robotics*, V. Kordic, A. Lazinica, and M. Merdan, Eds. InTech, 2005, ch. 33.
- [67] I. Artobolovskiy, *Mechanisms in Modern Engineering Design - A Handbook for Engineers, Designers, and Inventors, Volume 1*. MIR Publishers, 1975.
- [68] J. Klann. (2009) Jansen linkage - klann linkage comparison. [Online]. Available: <http://www.mechanicalspider.com/comparison.html>
- [69] L. Tsai, *Mechanism Design: Enumeration of Kinematic Structures According to Function*, ser. Mechanical and Aerospace Engineering Series. Taylor & Francis, 2000.
- [70] C. Wampler, “Solving the kinematics of planar mechanisms by dixon determinant and a complex-plane formulation,” *Journal of Mechanical Design*, vol. 123, no. 3, pp. 382–387, 2001.
- [71] N. Rojas and F. Thomas, “On closed-form solutions to the position analysis of baranov trusses,” *Mechanism and Machine Theory*, vol. 50, pp. 179 – 196, 2012.
- [72] ———, “Application of distance geometry to tracing coupler curves of pin-jointed linkages,” *ASME Journal of Mechanisms and Robotics*, vol. 5, no. 2, p. 021001, 2013.
- [73] S.-W. Kim, S.-H. Han, and D. H. Kim, “Analysis of a crab robot based on jansen mechanism,” in *2011 11th International Conference on Control, Automation and Systems (ICCAS)*, 2011, pp. 858–860.
- [74] C. Heng and R. de Leon, “Treadmill training enhances the recovery of normal stepping patterns in spinal cord contused rats,” *Experimental Neurology*, vol. 216, no. 1, pp. 139 – 147, 2009.
- [75] C. Kuo, J. Dai, and H. Yan, “Reconfiguration principles and strategies for reconfigurable mechanisms,” in *1st ASME/IFTOMM International Conference on Reconfigurable Mechanisms and Robots*, June 2009, pp. 1 – 7.

- [76] N. Rojas, R. Mohan, and R. Sosa, “Reconfiguration in linkages by variable allocation of joint positions: A modular design approach,” in *3rd IFToMM International Symposium on Robotics and Mechatronics*, October 2-4 2013.
- [77] T. Li and M. Ceccarelli, “An experimental analysis of human straight walking,” *Frontiers of Mechanical Engineering*, vol. 8, no. 1, pp. 95–103, 2013.
- [78] J. Johnson and J. Burton, *Animal Tracks and Signs: Track Over 400 Animals From Big Cats to Backyard Birds*. National Geographic Society, 2008.
- [79] F. Lacquaniti, R. Grasso, and M. Zago, “Motor patterns in walking,” *Physiology*, vol. 14, no. 4, pp. 168–174, 1999.
- [80] N. Rojas and F. Thomas, “A coordinate-free approach to tracing the coupler curves of pin-jointed linkages,” in *2011 ASME International Design Engineering Technical Conferences & Computers and Information in Engineering Conference, Paper No. DETC2011-48147*, 2011.
- [81] S. Nansai, R. Mohan, and M. Iwase, “Dynamic analysis and modeling of jansen mechanism,” *Procedia Engineering*, vol. 64, pp. pp.1562–1571, 2013.
- [82] K. Ting, J. Zhu, and D. Watkins, “The effects of joint clearance on position and orientation deviation of linkages and manipulators,” *Mechanism and Machine Theory*, vol. 35, no. 3, pp. 391 – 401, 2000.
- [83] K. Erbatur, A. Okazaki, K. Obiya, T. Takahashi, and A. Kawamura, “A study on the zero moment point measurement for biped walking robots,” *The 7th International Workshop on Advanced Motion Control*, pp. 431–436, 2002.
- [84] S. Kajita, F. Kanehiro, K. Kaneko, K. Fujiwara, K. Harada, K. Yokoi, and H. Hirukawa, “Biped walking pattern generation by using preview control of zero-moment point,” *The 2003 IEEE International Conference on Robotics and Automation*, pp. 1620–1626, 2003.
- [85] P. Sardain and G. Bessonnet, “Forces acting on a biped robot. center of pressure–zero moment point,” *IEEE Transaction on Systems, Man, and Cybernetics*, vol. 34, no. 5, pp. 630–637, 2004.

- [86] A. J. Ingram, “A new type of mechanical walking machine,” *Rand Afrikaans University*, 2004.
- [87] Y. Okazaki, M. Yamamoto, M. Komatsu, Y. Tsusaka, and Y. Adachi, “Development of a human safe, multi-degree-of-freedom robot arm technology using pneumatic muscles (in japanese),” *Journal of the Robotics Society of Japan*, vol. 28, no. 3, pp. 62–70, 2010.
- [88] Y. Noguchi, M. Iwase, S. Hatakeyama, and M. Izutsu, “A yoyo trick realized by parallel-link manipulator,” *The 39th Annual Conference of the IEEE Industrial Electronics Society*, pp. 4049–4054, 2013.
- [89] Y. Takeda and M. Okada, “Development of a jumping robot with a non-circular gear,” *The 2012 JSME Conference on Robotics and Mechatronics*, no. 12-3, 2012.
- [90] H. Nagashiro, Y. Nomura, and Y. Kinouchi, “A neural network model for quadruped gait generation and transitions,” *Neurocomputing*, no. 38-40, pp. 1469–1475, 2001.
- [91] K. Yoneda and S. Hirose, “Tumble stability criterion of a walking machine (in japanese),” *Journal of the Robotics Society of Japan*, vol. 14, no. 4, pp. 517–522, 1996.
- [92] S. Hirise, H. Tsukakoshi, and K. Yoneda, “Static stability criterion for walking robots on irregular terrairings (in japanese),” *Journal of the Robotics Society of Japan*, vol. 16, no. 8, pp. 1076–1082, 1998.
- [93] D. A. Messuri and C. A. Klein, “Automatic body regulation for maintaining stability of a legged vehicle during rough-terrain locomotion,” *IEEE Journal of Robotics and Automation*, vol. RA-1, no. 3, pp. 132–141, 1985.
- [94] S. Y. Shen, C. H. Lin, C. C. Cheng, J. C. Lu, S. F. Wang, and P. C. Lin, “Design of a leg-wheel hybrid mobile platform,” *The 2009 IEEE/RSJ International Conference on Intelligent Robots and Systems (IROS)*, pp. 4682–4687, 2009.
- [95] G. Endo and S. Hirose, “Study on roller-walker (system integration and basic experiments),” *The 1999 IEEE International Conference on Robotics & Automation (ICRA)*, pp. 2032–2037, 1999.

- [96] D. Mundo, G. Gatti, and D. B. Dooner, “Optimized five-bar linkages with non-circular gears for exact path generation,” *Mech. Mach. Theory*, vol. 44, no. 4, pp. 751–760, 2009.
- [97] E. Ottaviano, D. Mundo, G. A. Danieli, and M. Ceccarelli, “Numerical and experimental analysis of non-circular gears and cam-follower systems as function generators,” *Mech. Mach. Theory*, vol. 43, no. 8, pp. 996–1008, 2008.
- [98] D. Mundo, “Geometric design of a planetary gear train with non-circular gears,” *Mech. Mach. Theory*, vol. 41, no. 4, pp. 456–472, 2006.
- [99] H. Ohta, M. Yamakita, and K. Furuta, “From passive to active dynamic walking,” *Int. J. Robust Nonlin.*, vol. 11, no. 3, pp. 287–303, 2001.
- [100] C. C. D. Wit and P. Lischinsky, “Adaptive friction compensation with partially known dynamic friction model,” *Int. J. Adapt Control Signal Process.*, vol. 11, no. 1, pp. 65–87, 1997.
- [101] J. Swevers, F. Al-Bender, C. G. Ganseman, and T. Prajogo, “An integrated friction model structure with improved presliding behavior for accurate friction compensation,” *IEEE Trans. Automat. Contr.*, vol. 45, no. 4, pp. 675–686, 2000.
- [102] H. Olsson, K. Åström, C. C. de Wit, M. Göfvert, and P. Lischinsky, “Friction models and friction compensation,” *Eur. J. Control*, vol. 4, no. 3, pp. 176–195, 1998.
- [103] V. Lampeart, J. Swevers, and F. Al-Bender, “Modification of the leuven integrated friction model structure,” *IEEE Trans. Automat. Contr.*, vol. 47, no. 4, pp. 683–687, 2002.
- [104] A. Ohta, A. Sugiki, Y. Ohta, S. Suzuki, and K. Furuta, “Engine modeling based on projection method and conservation laws,” in *IEEE Int. Conf. Control Applications*, vol. 2, 2004, pp. 1420–1424.
- [105] S. Nansai, M. Iwase, and M. R. Elara, “Energy based position control of jansen walking robot,” in *IEEE Int. Conf. Syst, Man, Cybern.*, 2013, pp. 1241–1246.

- [106] F. Moldovan, V. Dolga, and C. Pop, “Kinetostatic analysis of an articulated walking mechanism,” *Mech. Mach. Science*, vol. 3, pp. 103–110, 2012.
- [107] K. Watanabe, M. Iwase, S. Hatakeyama, and T. Maruyama, “Control strategy for a snake-like robot based on constraint force and verification by experiment,” in *IEEE/RSJ Int. Conf. Intell. Robots Syst.*, 2008, pp. 1618–1623.
- [108] K. Furuta, “Super mechano-systems: Fusion of control and mechanism,” *15th Triennial World Congress of IFAC*, vol. 15, pp. 1635–1635, 2002.
- [109] K. J. Åström and K. Furuta, “Swing up a pendulum by energy control,” *Automatica*, vol. 36, no. 2, pp. 287–295, 2000.
- [110] K. J. Åström, J. Aracil, and F. Gordillo, “A new family of smooth strategies for swinging up a pendulum,” *Automatica*, vol. 44, no. 7, pp. 1841–1848, 2007.
- [111] J. Aracil, F. Gordillo, and K. J. Åström, “A new family of pumping-dumping smooth strategies for swinging up a pendulum,” in *16th IFAC World Congress*, 2005.
- [112] Y. K. Hwang and N. Ahuja, “A potential field approach to path planning,” *IEEE Trans. Robot. Automat.*, vol. 8, no. 1, pp. 23–32, 1992.
- [113] E. Rimon and D. E. Koditschek, “Exact robot navigation using artificial potential functions,” *IEEE Trans. Robot. Automat.*, vol. 8, no. 5, pp. 501–518, 1992.
- [114] J. Barraquand, B. Langlois, and J. C. Latombe, “Numerical potential field techniques for robot path planning,” *IEEE Trans. Syst., Man, Cybern.*, vol. 22, no. 2, pp. 224–241, 1992.
- [115] Y. Koren and J. Borenstein, “Potential field methods and their inherent limitations for mobile robot navigation,” in *IEEE Int. Conf. Robot. Autom.*, 1991, pp. 1398–1404.
- [116] M. Koga, “Matx/rmatx: A freeware for integrated cacsds,” in *IEEE Int. Sym. Computer Aided Control System Design*, 1999, pp. 452–456.

Acknowledgment

Author of this study, Shunsuke Nansai, have been given a lot of helping and tutelage at writing of this study. I want to take this opportunity to show my big appreciation. Professor Masami Iwase, Tokyo Denki University, has given the author multiplicity of advices and tutelage to advance the study. When the author almost lost the author's destination and have faced difficult issues, he has kindly always given the author appropriate advices. The author would like to offer my heartfelt thanks. Professor Mohan Rajesh Elara, Singapore University of Technology and Design, has indicated some important ideas of this study, and shown most basic direction of this study. In addition, he has given the author a lot of chance for the author's career up as a researcher, and the author could spend a fulfilling research life. The author would like to offer the author's heartfelt thanks. Professor Shoshiro Hatakeyama, Tokyo Denki University, has taught the author right way to do a research as well as professional attitude to research and humanity as researcher. The author would like to offer the author's heartfelt thanks. Professor Ricardo Sosa, Singapore University of Technology and Design, has indicated and helped the author to write some theses. The author would like to offer the author's heartfelt thanks. Dr. Nicolas Rojas, Yale University, has taught the author requisite theory in this study, and has helped the author to write some theses. The author would like to offer the author's heartfelt thanks. Professor Masaki Izutsu, Tokyo Denki University, has taught the author basic strategy of many control theory and issues, and has always encouraged the author. The author would like to offer the author's heartfelt thanks. Professor Jun Ishikawa and Professor Norihiro Kamamichi, Tokyo Denki University, has given the author a lot of fine suggestions for this study. The author would like to offer the author's heartfelt thanks. Professor Akio Nakamura, Tokyo Denki University, has taught the author an existence of a member of society as well as attitude of mind of a researcher. The author would like

to offer the author's heartfelt thanks. Dr. Hiroshi Osaki, NF Corporation, and Mr. Yuta Suzuki, Ebara Corporation, has given the author a lot of advices and encouragements for research life as well as laboratory life since the author was an under graduate student. The author would like to offer the author's heartfelt thanks. The author was able to spend fulfilling laboratory life by grace of both all laboratory members of Hatakeyama-Iwase Lab commencing with Mr. Takuma Nemoto and all members in Singapore University of Technology and Design. The author would like to offer the author's heartfelt thanks. Finally, the author really appreciate to the parents who allow the author's selfish decision and always help the author.

本研究をまとめるに当たり、多くの方々よりご指導・ご助力を賜りました。この場を借りて感謝の意を示させていただきます。東京電機大学 岩瀬将美准教授には、研究を進めるうえで数えきれないほどのご指導・ご助言をいただきました。著者が目標を見失いそうになった際や難しい問題に直面した際には、常に適切なアドバイスをいただきました。心より深く感謝申し上げます。Singapore University of Technology and Design Mohan Rajesh Elara 講師には、本研究のアイディアを示唆していただき、また基本的な方向性を示していただきました。さらには、研究者としてのキャリアアップの機会を数多くいただき、充実した研究生活を送ることができました。心より感謝申し上げます。東京電機大学 畠山省四朗教授には、研究の進め方だけでなく、物事に取り組む姿勢や考え方、研究者としてあるべき人間性など、多くのことをご指導いただきました。心より深く感謝申し上げます。Singapore University of Technology and Design Ricardo Sosa 助教には、論文の執筆に当たり、重要な示唆および助力をいただきました。感謝いたします。Yale University Nicoral Rojas 氏には、本研究において必要不可欠な技術・知識をご教示いただき、また、論文の執筆において、多大な助力をいただきました。心より感謝いたします。東京電機大学 井筒正義助教には、問題のとらえ方や制御理論のもととなる考え方など多くのご助言、多くの激励をいただきました。心より深く感謝申し上げます。東京電機大学 石川潤教授、釜道紀浩准教授には、本研究に対して数多くの貴重なアドバイスをいただきました。心より感謝申し上げます。東京電機大学 中村明生准教授には、研究者としての心構えや社会人としての在り方をご教示いただきました。感謝申し上げます。現：エヌエフ回路設計ブロック 大崎大氏および現：株式会社荏原製作所 鈴木佑多氏には、研究だけでなく研究室生活の面でも多くのご助言、激励をいただきました。心より深く感謝申し上げます。岩瀬研究室 根本琢磨氏をはじめとする、畠山研究室、岩瀬研究室の皆様、さらには Singapore University of Technology and Design の皆様のおかげで、有意義な研究室生活を過ごすことができました。感謝申し上げます。最後に、私のわがママを聞き入れてくれ、さらに惜しめない援助をいただいた両親に感謝申し上げます。